This is to certify that the

dissertation entitled

LOCAL HEATING OF BIOLOGICAL BODIES

WITH HF ELECTRIC AND MAGNETIC FIELDS

presented by

Manochehr Kamyab Hessary

has been accepted towards fulfillment
of the requirements for

Ph.D. degree in Elec. Engr.

Major professor

Date 6/7/82

LOCAL HEATING OF BIOLOGICAL BODIES WITH HF ELECTRIC AND MAGNETIC FIELDS

By

Manochehr Kamyab Hessary

A DISSERTATION

Submitted to
Michigan State University
in partial fulfillment of the requirements
for the degree of

DOCTOR OF PHILOSOPHY

Department of Electrical Engineering and Systems Science

1982

ABSTRACT

LOCAL HEATING OF BIOLOGICAL BODIES
WITH HF ELECTRIC AND MAGNETIC FIELDS

BY

Manochehr Kamyab Hessary

In this research the schemes of utilizing HF electric and magnetic fields to locally heat a biological body are investigated, with the application to hyperthermia cancer therapy or other medical purposes. The HF electric field maintained by a capacitor-plate applicator and the HF magnetic field produced by a current disk are used to heat biological bodies locally.

Rigorous theoretical analysis for such applicators are presented in this thesis. First the problem of a capacitor consisting of a pair of flat-plate electrodes of arbitrary dimensions in free space is studied. The distributions of the electric charges on the plates are obtained numerically for variety of cases and the electric fields at various points in free space are calculated. Following this study, the heating pattern induced by a capacitor-plate applicator inside a body is analyzed theoretically. Numerical results obtained on the basis of the solutions of two coupled integral equations are presented for several cases. After this a current disk applicator (pancake applicator) is studied. The electric field and the heating pattern induced in a body by a current disk placed on the body surface are obtained numerically.

Theoretical schemes are developed to synthesize the voltage distribution on a capacitor-plate applicator and the current distribution on a current disk to obtain a desired heating pattern inside a body. The electric fields inside a simulated body induced by different applicators are measured for several cases and are compared with the theoretical values.

ACKNOWLEDGMENTS

I would like to express my gratitude to Dr. K.M. Chen, my major Professor, for his assistance, encouragement and support throughout the course of this research.

Special thanks are extended to Dr. D.P. Nyquist, a member of my guidance committee, for his many helpful suggestions, especially during the experimental part of this work.

I also appreciate the help I received from the other members of my guidance committee, Dr. B. Ho, Dr. D. Reinhard and Dr. B. Drachman.

Finally, I am grateful to my brother, Iradj, whose help and support played a big part in completion of my Ph.D. degree.

TABLE OF CONTENTS

TABLE OF CONTENTS (continued)

LIST OF TABLES

LIST OF FIGURES

LIST OF FIGURES (continued)

LIST OF FIGURES (continued)

LIST OF FIGURES (continued)

LIST OF FIGURES (continued)

LIST OF FIGURES (continued)

LIST OF FIGURES (continued)

CHAPTER I

INTRODUCTION

Since its early days of discovery, electromagnetic radiation and propagation has been utilized to benefit human societies and the everincreasing impact of the EM waves on different aspects of human life has been enormous.

Constant efforts by scientists and engineers to utilize the potential usefulness of EM waves to enhance the quality of life and their incredible achievements has made it possible for many man's dreams to become reality. Intercontinental satellite communication, radar detection systems, microwave technology, and using EM energy for medical purposes in recent years are only few examples to mention.

The idea of using EM energy to induce hyperthermia in biological bodies for the purpose of cancer therapy has become the center of attention of many medical researchers over the past decade. It has been found that when the temperture of a tumor is raised a few degrees above that of the surrounding tissues, accompanying chemo or radiotherapy becomes more effective in treating tumors [1-3]. In the combined therapy of malignancies, the objective is to find a noninvasive method by which to heat the tumor without overheating other parts of the body. EM radiation has been found by many researchers to be a convenient agent to heat a tumor locally.

Significant progress was made in the hyperthermia cancer therapy when Leveen, et al. [4] used 13.56 MHz EM radiation to eradicate tumors in cancer patients. Holt [5] has used 433 MHz EM radiation in combination with X-rays to cure many cancer patients. Antich, et al. [6] used 27.12 MHz EM radiation to heat cutaneous human tumors. Jaines, et al. [7] combined microwave with X-rays to treat tumors in the bodies of terminal cancer patients. Many other researchers [8-13] have used EM radiation of 2450 MHz, 918 MHz or HF range to heat tumors in animal bodies and reported significant tumor regressions.

However, in order to improve the efficiency of applicators, in-depth theoretical study of the EM fields inside biological bodies induced by the applicators, as well as the heating pattern or power deposition in the tumor and other parts of the body is needed.

In the present research the methods of local heating of a biological body with HF electric field (capacitor-plate applicator) and HF magnetic field (current disk applicator) are studied theoretically and experimentally.

In Chapter II a theoretical analysis of flat-plate capacitors of arbitrary dimenisons and arrangements in free space is presented. The distribution of the electric charge on the plates is found numerically, and the three components of the electric field at various points in free space are calculated for variety of cases.

In Chapter III a capacitor-plate applicator is analyzed. Two flat plate electrodes located across a biological body with properly applied voltage distributions are used to heat the body locally. Based on the tensor integral equation method (TIEM) developed by Chen, et al. [16], two coupled integral equations are established from which the induced electric field inside the body and the density of the electric charge on the electrodes are obtained numerically. Then, the specific absorption rate (SAR) of the EM energy in the body is calculated for both homogeneous and heterogeneous bodies. In this chapter, a theoretical scheme is also developed for synthesizing the voltage distribution on the plates in order to obtain a desired heating pattern in the body, and some numerical examples for such a synthesis are given.

In Chapter IV the shortcoming of the capacitor-plate applicators relating to the overheating of the fat layer in biological bodies is explained. The main subject of this chapter is the theoretical study of a current disk applicator (or a pancake applicator). The electric field inside a biological body induced by a current disk applicator placed on the surface of the body is calculated numerically for different current distributions, and various results are presented. A theoretical scheme for synthesizing the current distribution on the disk to obtain a selective heating pattern is developed and some numerical examples are given.

In order to verify the theoretical results, a series of experiments was conducted where the electric fields inside a biological body and in free space induced by applicators were measured. The experimental results are compared with theoretical results at the end of each chapter. The decriptions of the experimental setup and related problems are given in Chapter V.

Chapter VI contains a brief description of the computer programs used to obtain the numberical results. The lists of programs and numerical examples for each program are also included in this chapter.

CHAPTER II

ANALYSIS OF FLAT-PLATE CAPACITORS OF ARBITRARY DIMENSIONS AND ARRANGEMENTS IN FREE-SPACE

In this chapter,a numerical method is developed to analyze the problem of a capacitor which consists of two flat parallel electrodes of arbitrary dimensions and seperated by a distance, and with two different potentials applied to the electrodes. The distribution of induced electric charges on the surfaces of the electrodes are determined first. After that, the electric field maintained between the electrodes, and the capacitance between the electrodes are determined.

2.1 Discription of Problem

Consider a capacitor with two conducting parallel electrodes, S_1 and S_2, as shown in Figure 2.1. Two a.c. potentials of V_{S_1} and V_{S_2} are applied to the electrodes, and a harmonic time variation of $e^{j\omega t}$ is assumed for those potentials.

At any point $\vec{r}$ in free space the vector and scalar potentials, $\vec{A}(\vec{r})$ and $\varphi(\vec{r})$, maintained by the current and charge on S_1 and S_2 can be shown to satisfy the following differential equations.

$$\nabla^2\varphi(\vec{r}) + \beta_0^2\varphi(\vec{r}) = -\frac{\eta_S(\vec{r})}{\epsilon_0} \tag{2.1.1}$$

$$\nabla^2\vec{A}(\vec{r}) + \beta_0^2\vec{A}(\vec{r}) = -\mu_0\,\vec{J}(\vec{r}) \tag{2.1.2}$$

Equations (2.1.1) and (2.1.2) can be solved easily by the Green's function technique resulting in the following integral equations in

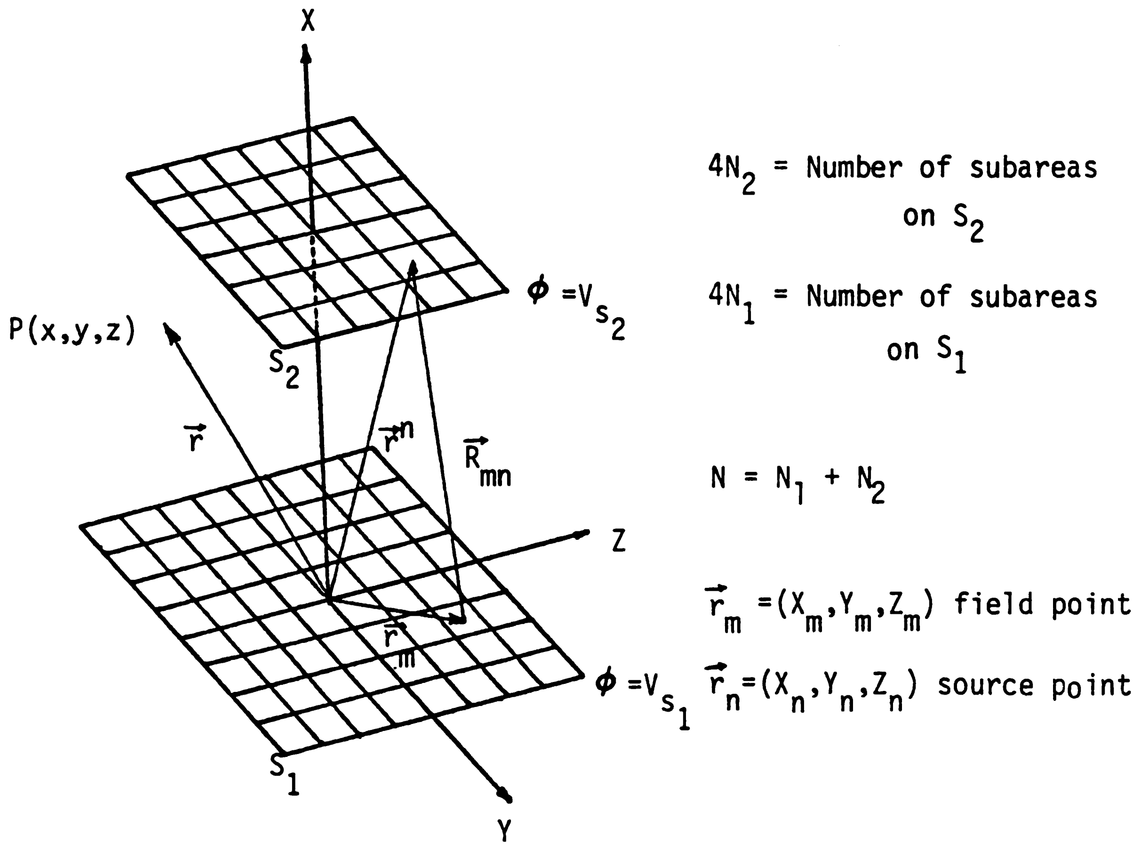

Figure 2.1. A pair of flat, parallel electrodes partitioned into subareas.

terms of η_S and $\vec{J}_S$:

$$\varphi(\vec{r}) = \frac{1}{\epsilon_0} \int_{S_1+S_2} \eta_S(\vec{r}\,')G(\vec{r},\vec{r}\,')ds' \qquad (2.1.3)$$

$$\vec{A}(\vec{r}) = \mu_0 \int_{S_1+S_2} \vec{J}_S(\vec{r}\,')G(\vec{r},\vec{r}\,')ds' \qquad (2.1.4)$$

where $G(\vec{r},\vec{r}\,') = \dfrac{e^{-j\beta_0|\vec{r}-\vec{r}\,'|}}{4\pi|\vec{r}-\vec{r}\,'|}$ is the free space Greens' function.

Equation (2.1.3) may be solved for η_S subject to the condition of vanishing of the tangential component of electric field, i.e.

$$\vec{E}_t = -\nabla_t\varphi(\vec{r}) - j\omega\vec{A}_t(\vec{r}) = 0$$

at low frequencies $|j\omega\vec{A}_t| << |\nabla_t\varphi(\vec{r})|$, thus, $\vec{E}_t \approx -\nabla_t\varphi(\vec{r}) = 0$. For $\vec{r} \in S_1$ and S_2, which implies that $\varphi(\vec{r} \in S_1,S_2)$ = constant.

2.2. Moment Solution of Integral Equation

The induced electric charge $\eta_S(\vec{r})$ is difficult if not impossible to determine in closed form. However, there are numerical techniques available by means of which the solution can be found. One such method is the well known "Method of Moment" which is briefly discussed here. More detailed descriptions can be found in other sources [14].

The moment method is one of the convenient ways of solving integral equations by converting them into a set of simultaneous linear equations in terms of the discretized values of the unknown. The latter can be solved by digital computers with desired accuracy.

To solve equation (2.1.3), S_1 and S_2 are divided into a number of subareas which hereafter are referred to as cells. The charge density on the n^{th} cell is represented by η_n, and the potential at an arbitrary point $P(\vec{r})$ in free space due to the charge on the n^{th} cell is given as

$$\varphi_n(\vec{r}) = \frac{1}{\epsilon_o}\int_{\Delta s_n} \eta_n(\vec{r}\,')G(\vec{r},\vec{r}\,')ds' \tag{2.2.1}$$

where Δs_n represents the surface of n^{th} cell. If Δs_n is chosen small enough, $\eta_n(\vec{r}\,')$ varies insignificantly over s_n, thus (2.2.1) becomes

$$\varphi_n(\vec{r}) = \frac{\eta_n}{\epsilon_o}\int_{\Delta s_n} G(\vec{r},\vec{r}\,')ds' \tag{2.2.2}$$

The total potential at point $\vec{r}$ is

$$\varphi(\vec{r}) = \sum_{n=1}^{4N} \varphi_n(\vec{r}) = \frac{1}{\epsilon_o}\sum_{n=1}^{4N} \eta_n \int_{\Delta s_n} G(\vec{r},\vec{r}\,')ds' \tag{2.2.3}$$

where $4N$ is the total number of surface cells.

Next we require that (2.2.3) be satisfied at the center of each cell with position vector $\vec{r}_m$

$$\varphi_m = \varphi(\vec{r}_m) = \frac{1}{\epsilon_o}\sum_{n=1}^{4N} \eta_n \int_{\Delta s_n} G(\vec{r}_m,\vec{r}\,')ds' \tag{2.2.4}$$

$$m = 1,2,\ldots,4N$$

when $m \neq n$, we can assume that $\vec{r}\,' \simeq \vec{r}_n$, where $\vec{r}_n$ represents the position vector for the center of n^{th} cell, thus (2.2.3) becomes

$$\varphi_m = \frac{1}{\epsilon_o}\Big[\sum_{\substack{n=1\\ n\neq m}}^{4N} \eta_n G(\vec{r}_m,\vec{r}_n)\Delta s_n + \sum_{n=1}^{4N} \delta_{mn}\eta_n \int_{\Delta s_n} G(r_m,r')ds'\Big]$$

$$m = 1,2,\ldots,4N \tag{2.2.5}$$

$$\delta_{mn} = \begin{cases} 0 & m \neq n \\ 1 & m = n \end{cases}$$

The second term on the right is the contribution to the potential at the center of a cell due to the charge on the same cell.

Equation (2.2.5) comprises a set of 4N linear equations in terms of η's and may be written in the matrix form as follows

$$\underset{4N\times 1}{\begin{bmatrix} \varphi_1 \\ \varphi_2 \\ \cdot \\ \cdot \\ \cdot \\ \varphi_{4N} \end{bmatrix}} = \underset{4N\times 4N}{\begin{bmatrix} \\ \\ & G & \\ \\ \\ \end{bmatrix}} \underset{4N\times 1}{\begin{bmatrix} \eta_1 \\ \eta_2 \\ \cdot \\ \cdot \\ \cdot \\ \eta_{4N} \end{bmatrix}} \tag{2.2.5}$$

with $G_{mn} = \frac{1}{\epsilon_o} \Delta S_n G(\vec{r}_m, \vec{r}_n)$

As explained earlier, at low frequencies the vanishing of the tangential component of electric field on the electrodes requires that the potential on the surface of each electrode should be constant. Thus, we have.

$$\varphi_m = \text{constant} = \begin{cases} V_{S_1} & \text{for} \quad m \leq 4N_1 \\ V_{S_2} & \text{for} \quad 4N_1 < m \leq 4(N_1 + N_2) \end{cases}$$

where N_1 and N_2 are the number of cells on ¼ of S_1 and S_2 respectively.

2.3. Calculation of Matrix Elements

In this section the expressions for the matrix elements G_{mn} will be developed. Two different cases of grounded and floating potentials are treated seperately.

2.3.1 Grounded Case: This case is commonly used in practice where one electrode is grounded (S_1 for example) and an a.c. potential is applied to the other electrode. For this case $V_{S_1} = 0$ and $V_{S_2} = V$, where V is the amplitude of the applied voltage. Substituting these values for φ_m into equation (2.2.5), we have

$$\underset{4N\times 1}{\begin{bmatrix} \eta_1 \\ \eta_2 \\ \cdot \\ \cdot \\ \cdot \\ \cdot \\ \cdot \\ \eta_{4N} \end{bmatrix}} = V \underset{4N\times 4N}{\begin{bmatrix} \\ \\ & & G & & \\ \\ \\ \end{bmatrix}}^{-1} \underset{4N\times 1}{\begin{bmatrix} 0 \\ \cdot \\ \cdot \\ \cdot \\ 0 \\ 1 \\ \cdot \\ 1 \end{bmatrix}} \begin{matrix} \\ 4N_1 \\ \\ \\ \\ 4N_2 \\ \\ \end{matrix} \qquad (2.3.1)$$

To make the problem more general, and at the same time to keep the cost of computation down, we assume a four quadrant symmetry for the problem. In other words, the geometry of electrodes is symmetric about the planes $z = 0$ and $y = 0$ (Figure 2.2). The planes of symmetry divide the space and two electrodes into four quadrants labled by

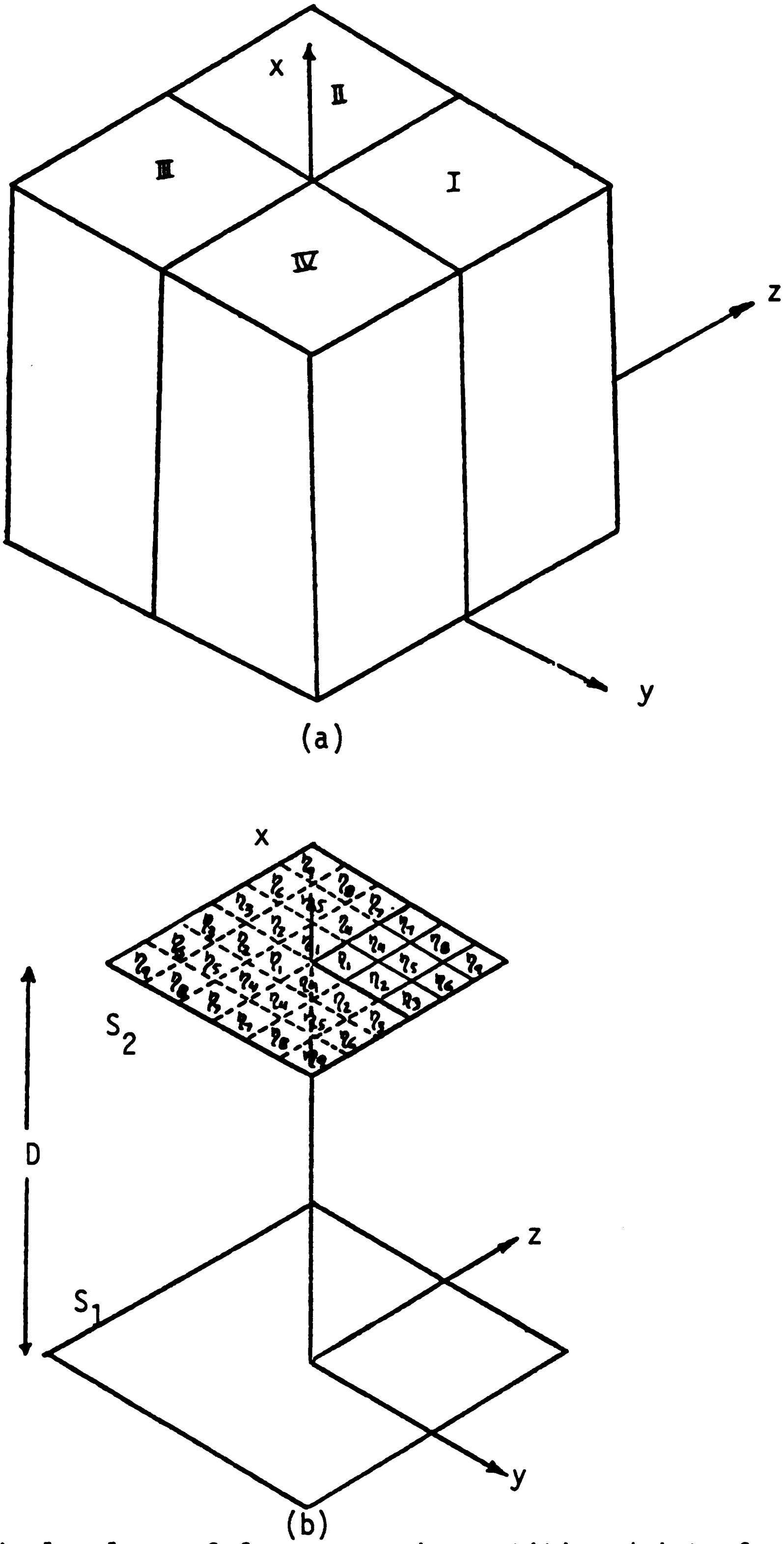

Figure 2.2. A cubical volume of free space is partitioned into four symmetrical quadrants (a), and (b) the geometry of two parallel electrodes with S_2 partitioned and the charge densities on the subareas.

Roman numerals I through IV. It is noted that the cases where no symmetry is present in the geometry the problem can be handled as well, but they are of little value in practical applications.

Under the stated conditions we need only to compute the charge density, and later in this chapter the electric field, only in one quadrant. The desired quantities in the other quadrants can be obtained by utilizing the symmetry. The charge densities on various cells on the first quadrant of S_2 and that of their counterparts on other quadrants are shown in Figure 2.2.b.

Now we proceed with the computation of the matrix elements. The off-diagonal elements will be computed first.

If $m \neq n$, by symmetry and refer to Figure 2.2.b, we have

$$\eta_n^{I} = \eta_n^{II} = \eta_n^{III} = \eta_n^{IV}$$

which reduces the size of G matrix in (2.3.1) to $\frac{1}{4}$ of that when there is no symmetry present. With this symmetry, (2.3.1) reduces to

$$\underset{NX1}{\begin{bmatrix} \eta_1 \\ \eta_2 \\ \cdot \\ \cdot \\ \cdot \\ \cdot \\ \cdot \\ \eta_N \end{bmatrix}} = V \underset{NXN}{\begin{bmatrix} \\ \\ \\ & G^S & \\ \\ \\ \end{bmatrix}^{-1}} \underset{NX1}{\begin{bmatrix} 0 \\ \cdot \\ \cdot \\ \cdot \\ 0 \\ 1 \\ \cdot \\ 1 \end{bmatrix}} \begin{array}{l} \\ N_1 \\ \\ \\ \\ N_2 \\ \end{array}$$

where

$$G^S_{mn} = \frac{\Delta S_n}{\epsilon_o}[G(\vec{r}_m,\vec{r}_n^{\;I}) + G(\vec{r}_m,\vec{r}_n^{\;II}) + G(\vec{r}_m,\vec{r}_n^{\;III}) + G(\vec{r}_m,\vec{r}_n^{\;IV})] \tag{2.3.3}$$

with $$G(\vec{r}_m,\vec{r}_n) = \frac{e^{-j\beta_o|\vec{r}_m-\vec{r}_n|}}{4\pi|\vec{r}_m-\vec{r}_n|}, \text{ and}$$

$$\vec{r}_m = X_m\hat{x} + Y_m\hat{y} + Z_m\hat{z}$$

$$\vec{r}_n^{\;I} = X_n\hat{x} + Y_n\hat{y} + Z_n\hat{z} \qquad \vec{r}_n^{\;II} = X_n\hat{x} - Y_n\hat{y} + Z_n\hat{z}$$

$$\vec{r}_n^{\;III} = X_n\hat{x} - Y_n\hat{y} - Z_n\hat{z} \qquad \vec{r}_n^{\;IV} = X_n\hat{x} + Y_n\hat{y} - Z_n\hat{z}$$

where (X_m,Y_m,Z_m) and (X_n,Y_n,Z_n) are the cartesian coordinates of the centers of the m^{th} cell (field point), and the n^{th} cell (source point), respectively. Thus, G^S_{mn} can be written as

$$G^S_{mn} = \frac{\Delta S_n}{4\pi\epsilon_o}\left[\frac{e^{-j\beta_o R^I_{mn}}}{R^I_{mn}} + \frac{e^{-j\beta_o R^{II}_{mn}}}{R^{II}_{mn}} + \frac{e^{-j\beta_o R^{III}_{mn}}}{R^{III}_{mn}} + \frac{e^{-j\beta_o R^{IV}_{mn}}}{R^{IV}_{mn}}\right] \tag{2.3.4}$$

where

$$R^I_{mn} = [(X_m - X_n)^2 + (Y_m - Y_n)^2 + (Z_m - Z_n)^2]^{1/2}$$

$$R^{II}_{mn} = [(X_m - X_n)^2 + (Y_m + Y_n)^2 + (Z_m - Z_n)^2]^{1/2}$$

$$R^{III}_{mn} = [(X_m - X_n)^2 + (Y_m + Y_n)^2 + (Z_m + Z_n)^2]^{1/2}$$

$$R^{IV}_{mn} = [(X_m - X_n)^2 + (Y_m - Y_n)^2 + (Z_m + Z_n)^2]^{1/2}$$

and

$$X_m = \begin{cases} D & \text{for } m > N_1 \\ 0 & \text{otherwise} \end{cases}, \quad X_n = \begin{cases} D & \text{for } n > N_1 \\ 0 & \text{otherwise} \end{cases}$$

D = The distance between the electrodes.

For diagonal elements, $m = n$ and as a result $\vec{r}_m = \vec{r}_n$, which makes the first term on the right hand side of (2.3.3) become infinite. Since this term represents the contribuiton to the potential at the center of a cell due to the charge on the same cell, it is easy to avoid the singularity by evaluating this term analytically. For this purpose, we approximate the square cell by a cicular one of the same area as shown in Figure 2.3. The potential at the center of the circular disk with uniform charge density η is.

$$\varphi = \frac{\eta}{4\pi\epsilon_o} \int_{S_c} \frac{e^{-j\beta_o r}}{r} \, r dr d\theta = \frac{\eta}{2j\beta_o\epsilon_o} \left(e^{-j\beta_o\sqrt{\frac{D_S}{\pi}}} - 1\right) \tag{2.3.5}$$

Therefore, the diagonal elements can be obtained by substituting (2.3.5) into (2.3.3) for $\Delta S_n\, G(\vec{r}_m, \vec{r}_n)$ and setting $m = n$:

$$G^S_{mm} = \frac{1}{2j\beta_o\epsilon_o} \left(e^{-j\beta_o\sqrt{\frac{D_S}{\pi}}} - 1\right) + \frac{\Delta S_m}{4\pi\epsilon_o} \left[\frac{e^{-j\beta_o R^{II}_{mn}}}{R^{II}_{mn}} + \frac{e^{-j\beta_o R^{III}_{mn}}}{R^{III}_{mn}} + \frac{e^{-j\beta_o R^{IV}_{mn}}}{R^{IV}_{mn}}\right] \tag{2.3.6}$$

This concludes the evaluation of the matrix elements for the grounded potential case.

2.3-2 Floating Potential Case: When the potentials of the electrodes are floating, V_{S_1} and V_{S_2} are not known, except for the special case

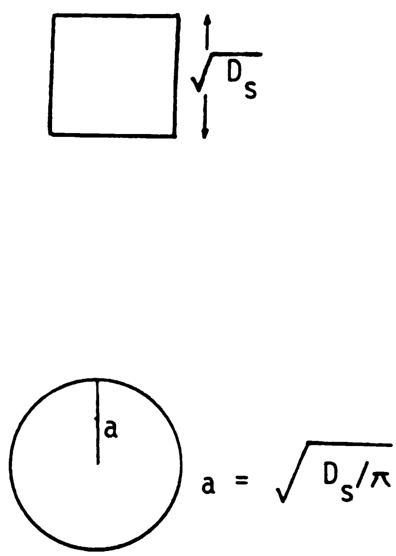

Figure 2.3. A square cell is approximated by a circular one for the calculation of the diagonal elements of matrix G^s

of $S_1 = S_2$, for which $V_{S_2} = -V_{S_1} = \frac{V}{2}$. However, it is noted that once the voltage on one of the electrodes is obtained, that of the other is determined from

$$V_{S_1} - V_{S_2} = V \tag{2.3.7}$$

This means that one extra unknown is introduced into the equations (2.2.5). Therefore an additional equation is required in order that the equation system (2.2.5) can be uniquely solved. This extra equation can be derived from the continuity equation.

$$\nabla \cdot \vec{J} = -j\omega\rho \tag{2.3.8}$$

If we integrate (2.3.8) over the volume enclosed by surface S surrounding electrode S_1 as illustrated in Figure 2.4 , and apply the divergence theorem we obtain

$$q_1 = \frac{-I}{j\,\omega} \tag{2.3.9}$$

where q_1 is the total induced charge on S_1 and I is the current flowing out from electrode. Similarly for S_2 we have

$$q_2 = \frac{I}{j\,\omega} \tag{2.3.10}$$

with q_2 being the total charge on S_2. Adding (2.3.9) and (2.3.10) and noting that $q_1 + q_2 = \sum_{n=1}^{N} \eta_n \, \Delta S_n$, leads to the following relation .

$$\sum_{n=1}^{N} \eta_n \, \Delta S_n = 0 \tag{2.3.11}$$

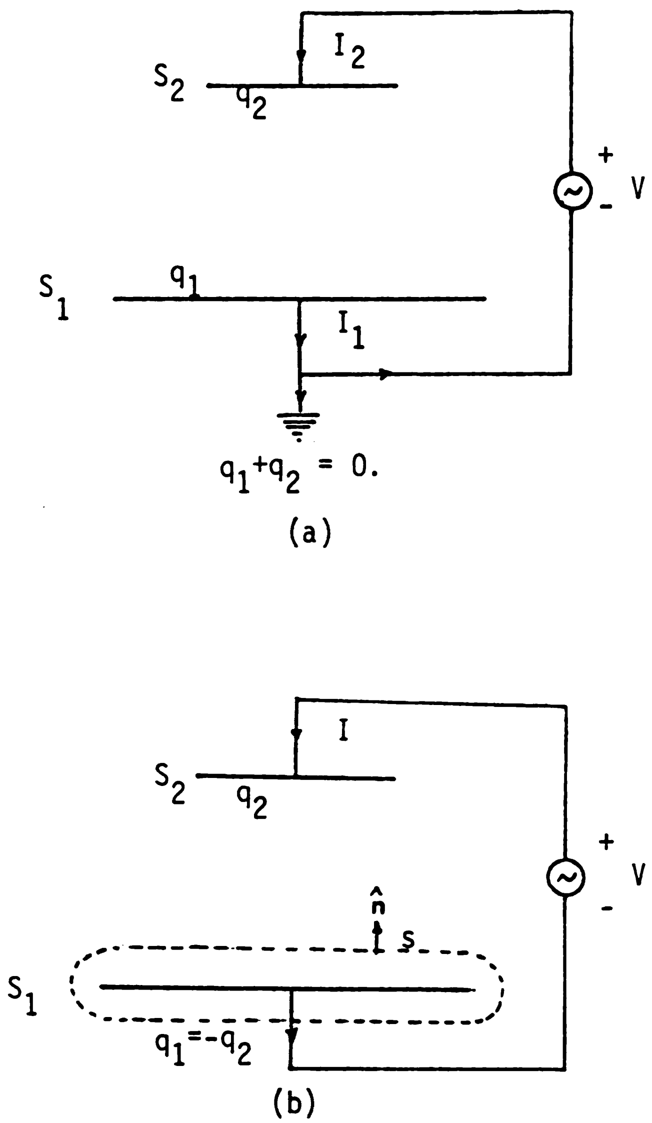

Figure 2.4. Relation between the charge on and the current flowing into the electrodes. (a) grounded potential case (b) floating potential case.

Equation (2.3.11) in conjunction with the equation (2.2.5) gives the following matrix representation of N + 1 equations in terms of charge densities and the potential of S_1 .

$$\left[\begin{array}{ccc:c} & & & -1 \\ & & & -1 \\ & & & \vdots \\ & G^s & & \vdots \\ & & & -1 \\ \hdashline \Delta S_1 & \cdots & \Delta S_n & 0 \end{array}\right] \left[\begin{array}{c} \eta_1 \\ \vdots \\ \vdots \\ \eta_N \\ \hdashline V_{s_1} \end{array}\right] = V \left[\begin{array}{c} 0 \\ \vdots \\ 0 \\ 1 \\ \vdots \\ 1 \\ \hdashline 0 \end{array}\right] \begin{array}{l} \left.\vphantom{\begin{array}{c} 0 \\ \vdots \\ 0 \end{array}}\right\} N_1 \\ \left.\vphantom{\begin{array}{c} 1 \\ \vdots \\ 1 \end{array}}\right\} N_2 \\ \vphantom{0} \end{array} \tag{2.3.12}$$

2.4 Numerical Results

A computer program has been developed for solving (2.2.5) and (2.3.12), and the induced charge density has been obtained for several cases. The capacitance between the electrodes of the same dimension was calculated as the ratio of the total induced charge and the applied voltage for several values of the seperation between electrodes, and the results are depicted in Figure 2.4. (the solid curve). The dashed curve on Figure 2.4. is obtained from the formula for the electrostatic capacitance of

$$C = \epsilon_0 \frac{A}{D} \tag{2.4.1}$$

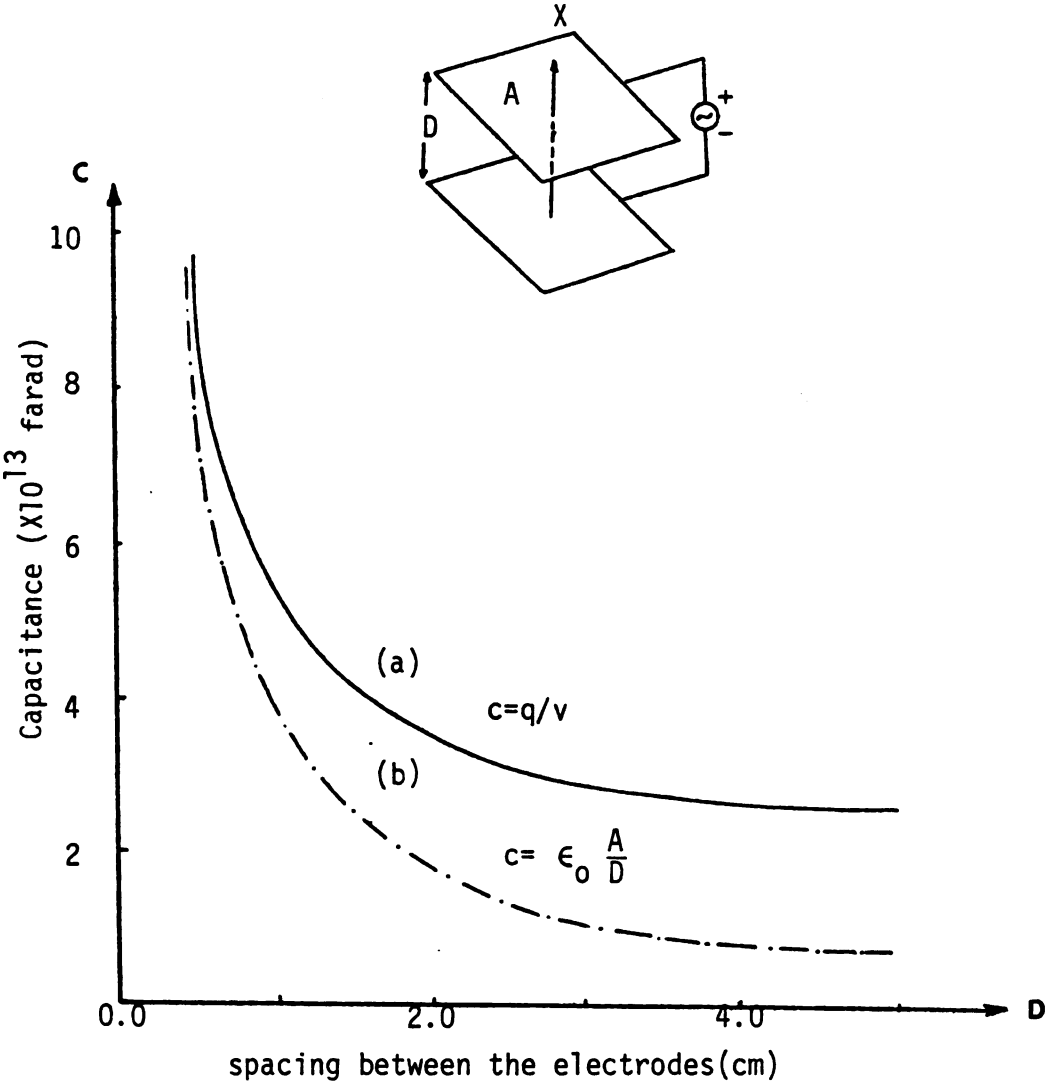

Figure 2.5. The capacitance Vs spacing of two parallel plates of equal size. (a) using the methode of subareas, (b) using $c = \epsilon_0 A/D$.

The closeness of the two curves for small values of the seperation between electrodes suggests that the value for capacitance obtained from (2.4.1) is close to the exact value of capacitance obtained numerically. For a large seperation between the electrodes the expression (2.4.1) does not give accurate results for the capacitance, the numerical method should be employed instead for exact evaluation of the capacitance between the electrodes.

Figure 2.6. shows the distribution of the induced electric charge on the upper electrode S_1 and lower electrode S_2 along the edge (Z-axis), and the diagonal (Z_d axis) of the electrodes. The electrodes are of equal dimension (6 x 6 cm). The solid curves are obtained for $D = 2.$ cm, while the dashed curves are for the case when $D = 4.$ cm. A floating voltage of 2. volts at 15 MH_z is applied between the electrodes. It is noted that the charges on the upper and lower electrodes have equal magnitude, but they are 180^o out of phase. It is observed that the charge is distributed almost uniformly on the middle section of each electrode and increases rapidly towards the edges, and at the corners of electrodes the magnitude of charge is maximum.

In Figure 2.7. the lower electrode S_1 of Figure 2.6. is grounded and D is kept constant at 4. cm. The distributions of the electric charge on the electrodes are shown along Z, and Z_d (solid curves). The charge distributions for floating potential case are also included for the purpose of comparison (dashed curves). It is noted that for the grounded potential case the magnitude of the charge on the upper electrode is noticeably larger than that on the lower grounded electrode.

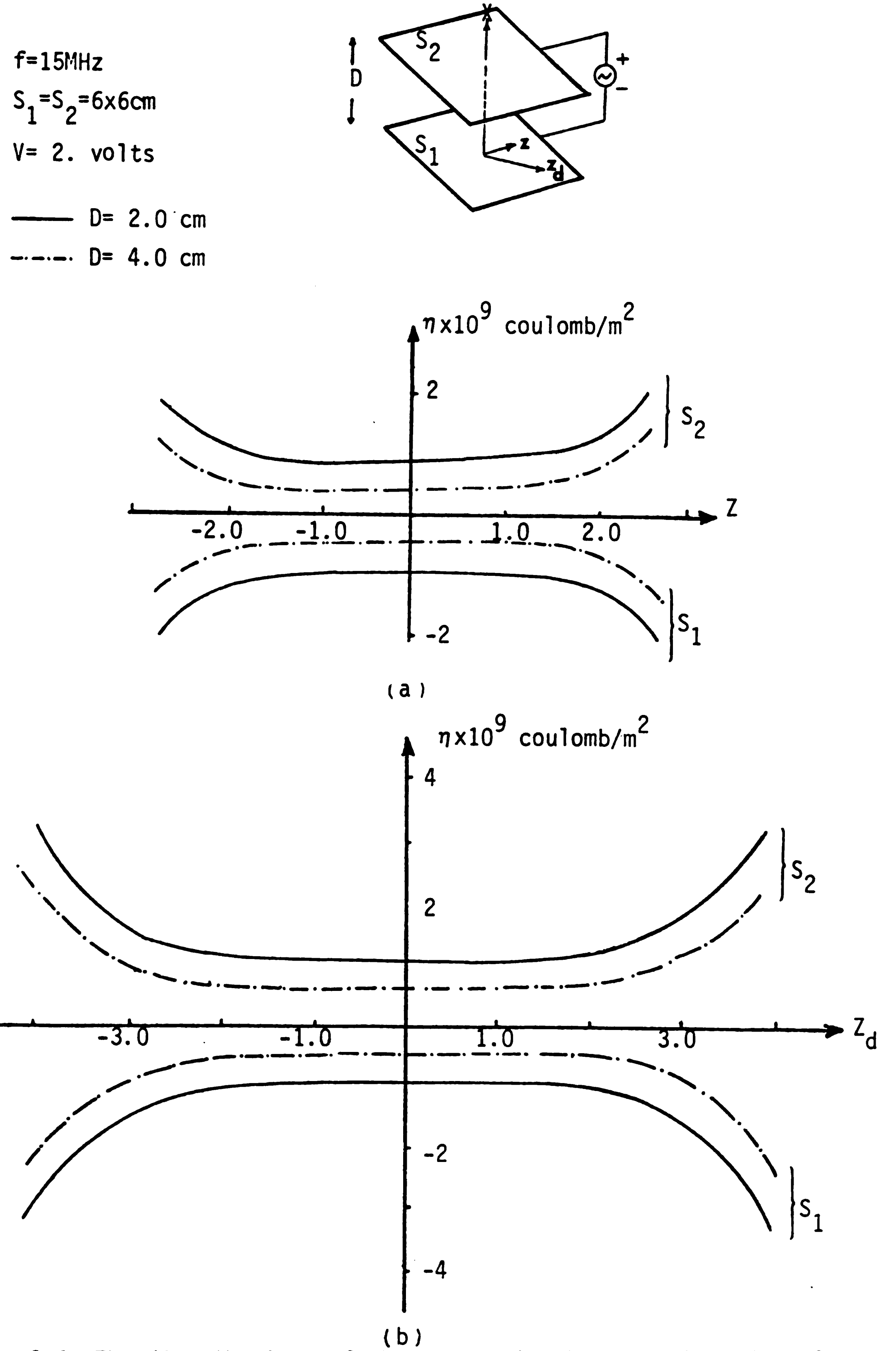

Figure 2.6. The distributions of the charge densities on S_1 and S_2 for two cases of D=2.(solid curves),and D=4.(dashed curves);(a)along Z (b) along Z_d

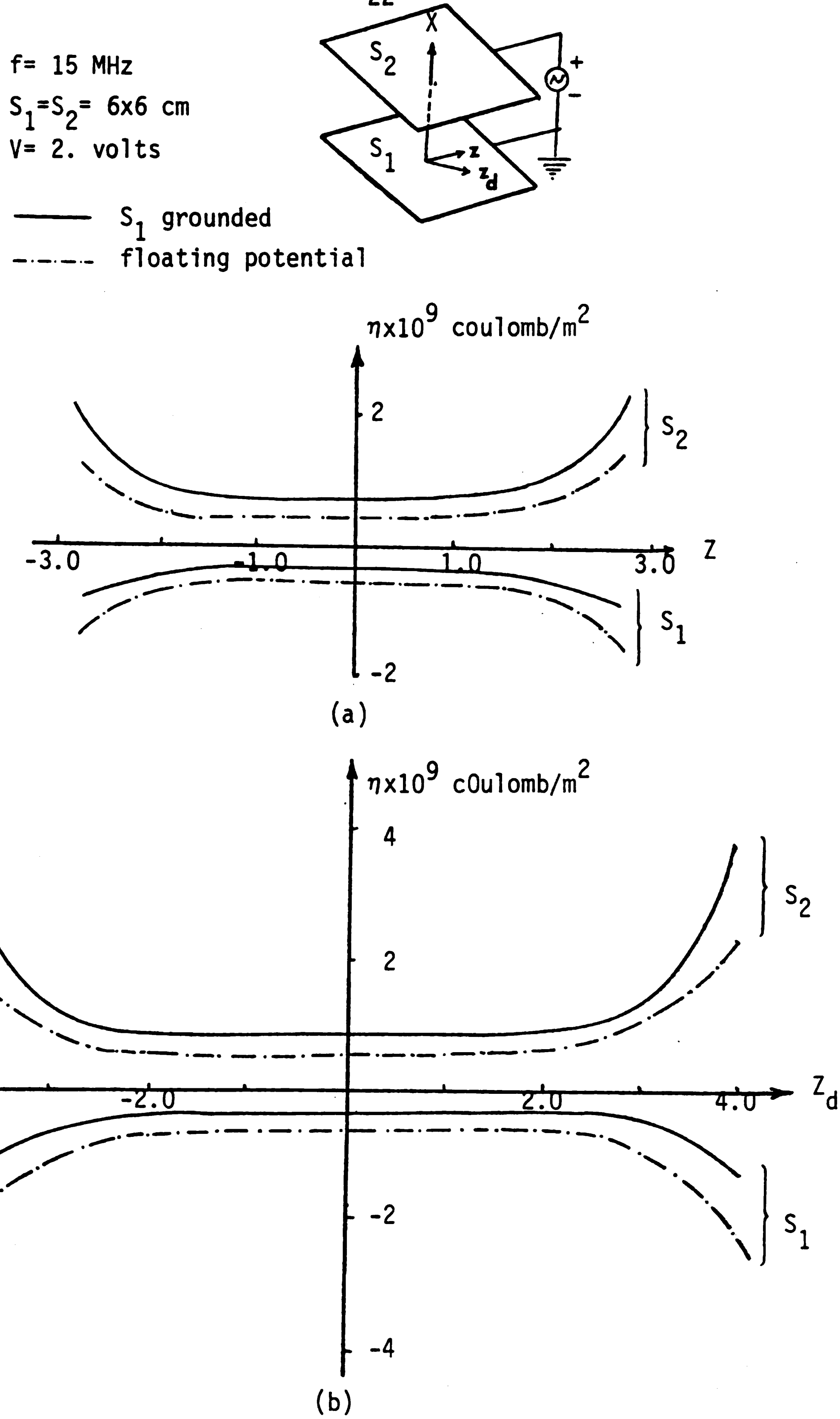

Figure 2.7. The distributions of the charge densities on S_1 and S_2 (same dimension) (a) along Z. (b) along Z_d

Figure 2.8. shows the distribution of the electric charge on the surface of two electrodes with different dimensions. The solid curves represent the case when the larger lower electrode is grounded, and the dashed curves are obtained for the case of floating potentials.

2.5. Computation of the Electric Field

This section is devoted to the calculation of the electric field in free space maintained by the charge and current on the surfaces of the parallel electrodes. If $\varphi(\vec{r})$ and $\vec{A}(\vec{r})$ are the scalar and vector potentials at point $\vec{r}$ in free space, the electric field at that point is

$$\vec{E}(\vec{r}) = -\nabla\varphi(\vec{r}) - j\omega\vec{A}(\vec{r}) \tag{2.5.1}$$

At low frequencies and in the near zone, the first term on the right hand side of (2.5.1) predominates. In other words, in the near-zone the electric field is mainly due to the charge on the surfaces of the electrodes. Thus, the electric field can be expressed as;

$$\vec{E}(\vec{r}) = -\nabla \int_{S_1+S_2} \eta_S(\vec{r}\,') \frac{e^{-j\beta_0|\vec{r}-\vec{r}\,'|}}{|\vec{r}-\vec{r}\,'|} dS' \tag{2.5.2}$$

Taking the differential operator inside the integral, and after some straightforward manipulation we get

$$\vec{E}(\vec{r}) = \frac{1}{4\pi\epsilon_0} \int_{S_1+S_2} \eta_S(\vec{r}\,') \frac{(1+j\beta_0|\vec{r}-\vec{r}\,'|)(\vec{r}-\vec{r}\,')}{|\vec{r}-\vec{r}\,'|^3} e^{-j\beta_0|\vec{r}-\vec{r}\,'|} dS' \tag{2.5.3}$$

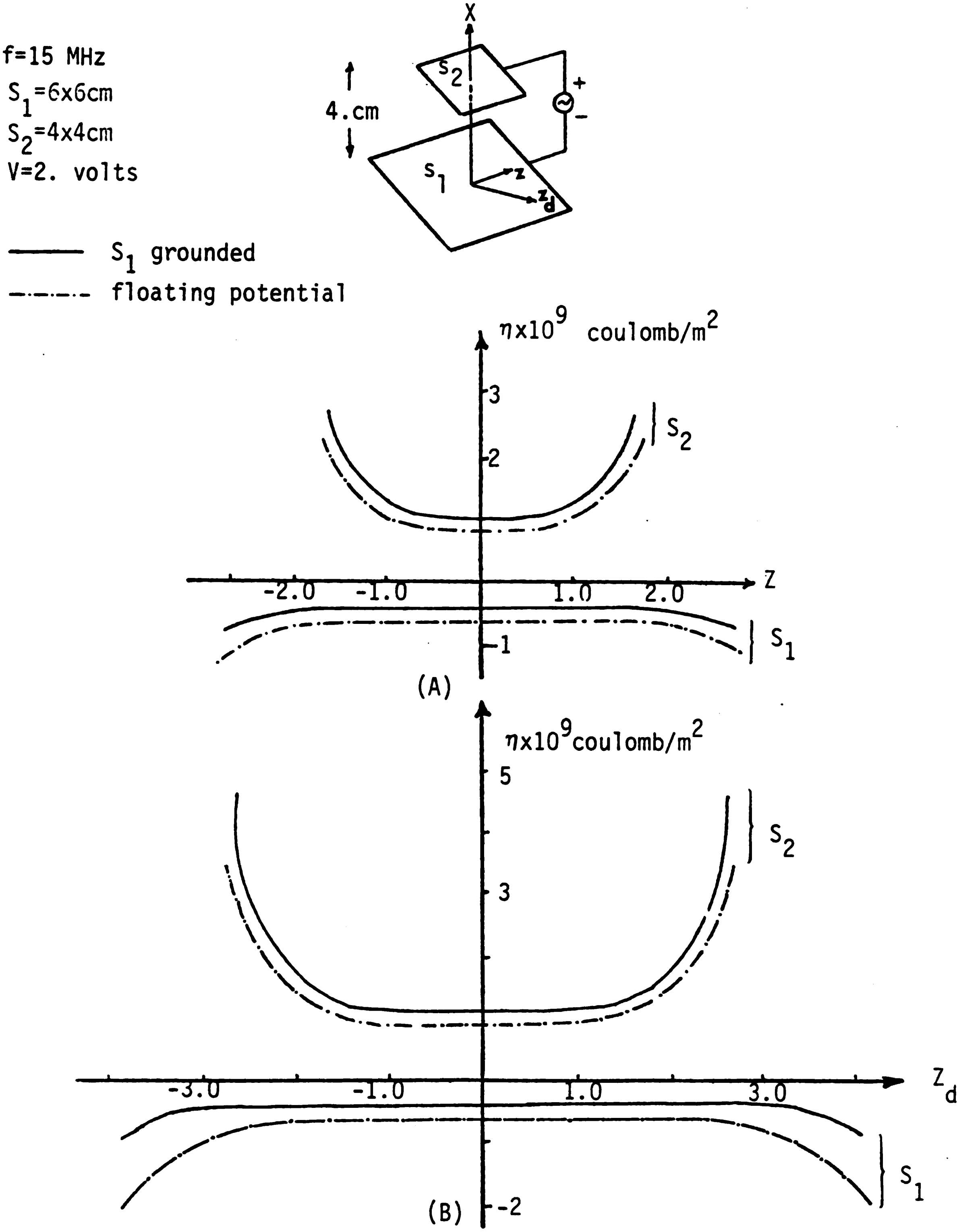

Figure 2.8. The distribution of charge densities on S_1 and S_2 (different dimensions) for grounded(solid lines) and floating potential cases: (A) along Z, (B) along Z_d

The electric field at point $\vec{r}$ in free space due to the charge on the n^{th} subarea is approximately equal to

$$\vec{E}_n(\vec{r}) = \frac{\Delta S_n \eta_n}{4\pi\epsilon_o} \frac{(1+j\beta_o|\vec{r}-\vec{r}_n|)(\vec{r}-\vec{r}_n)}{|\vec{r}-\vec{r}_n|^3} e^{-j\beta_o|\vec{r}-\vec{r}_n|}$$

The total electric field is then

$$\vec{E}(\vec{r}) = \sum_{n=1}^{4N} \vec{E}_n(\vec{r}) = \sum_{n=1}^{4N} \frac{\Delta S_n \eta_n}{4\pi\epsilon_o} \frac{(1+j\beta_o|\vec{r}-\vec{r}_n|)(\vec{r}-\vec{r}_n)}{|\vec{r}-\vec{r}_n|^3} e^{-j\beta_o|\vec{r}-\vec{r}_n|} \qquad (2.5.4)$$

The three scalar components of $\vec{E}$ in the first quadrant can be written as

$$E_X^I = \sum_{n=1}^{N} \eta_n (C_n^I + C_n^{II} + C_n^{III} + C_n^{IV})(X-X_n) \qquad (2.5.5)$$

$$E_Y^I = \sum_{n=1}^{N} \eta_n (C_n^I + C_n^{IV})(Y-Y_n) + (C_n^{II} + C_n^{III})(Y+Y_n) \qquad (2.5.6)$$

$$E_Z^I = \sum_{n=1}^{N} \eta_n (C_n^I + C_n^{II})(Z-Z_n) + (C_n^{III} + C_n^{IV})(Z+Z_n) \qquad (2.5.7)$$

where

$$C_n^k = \frac{\Delta S_n}{4\pi\epsilon_o} \frac{1+j\beta_o R_n^k}{(R_n^k)^3} e^{-j\beta_o R_n^k} \qquad k = I, II, III, IV$$

and (X,Y,Z) are the coordinates of the field point $\vec{r}$, and

$$R_n^k = |\vec{r} - \vec{r}_n^{\,k}|$$

where $\vec{r}_n^{\,k}$ is the position vector for the source point in the k^{th} quadrant. The numerical results for the electric field components are shown for various cases in Figures 2.9 to 2.12.

Figure 2.9. shows the distirubiton of the three components of the electric fields, maintained by the charges on the electrodes, at the centers of the partitioned subvolumes ($1\ cm^3$) between the electrodes of equal dimension (6 x 6 cm) when the potentials of the electrodes are left floating. The applied voltage between the electrodes is 2. volt and the frequency is 15 MHz. Due to symmetry only the fields in one quarter of the free space between the electrodes are shown in the Figure. It is seen that the X-component of the electric field predominates as expected. Also the field is rather uniform with a slight decrease in the middle portion between electrodes.

Figure 2.10. shows the distribution of the X-component (dominant component) of the electric field in free space between two electrodes of equal diminsions (6 x 6 cm) seperated by a distance of 4. cm. A voltage of 2. volts at 15 MHz is applied between the electrodes while the lower electrode is grounded. For this case weaker electric fields are maintained near the grounded electrode, even though the electric field in the free space between electrodes is still rather uniform. Figure 2.11. shows the similar distribution of electric fields maintained in the free space between two electrodes of different dimensions, the upper electrode is 4 x 4 cm, and the lower one is 6 x 6 cm. The potentials of the electrodes are left floating and the applied voltage is 2. volts at 15 MHz. The most noteworthy phenomenon in Figure 2.11

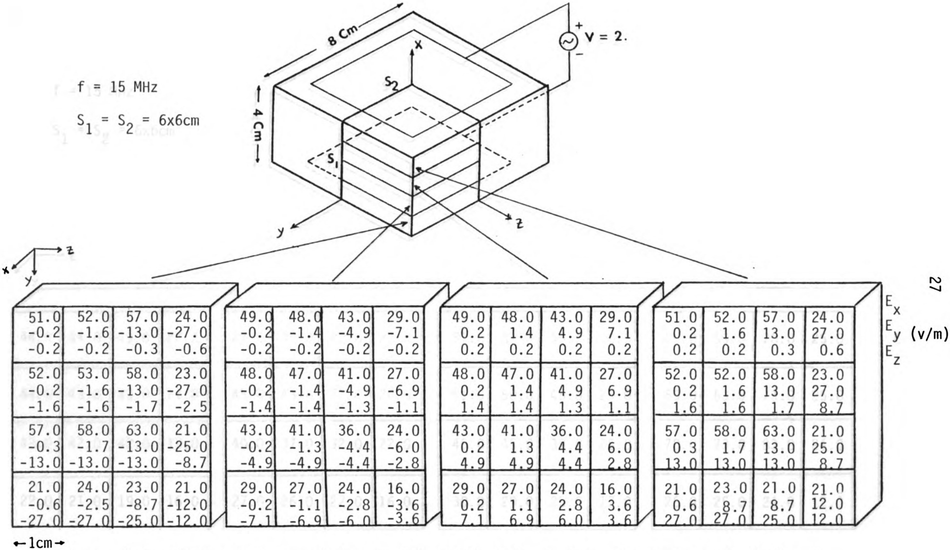

Figure 2.9. Three components of the electric field at the centers of subvolumes in different layers in ¼ of free space between two electrodes of equal dimension for floating potential case.

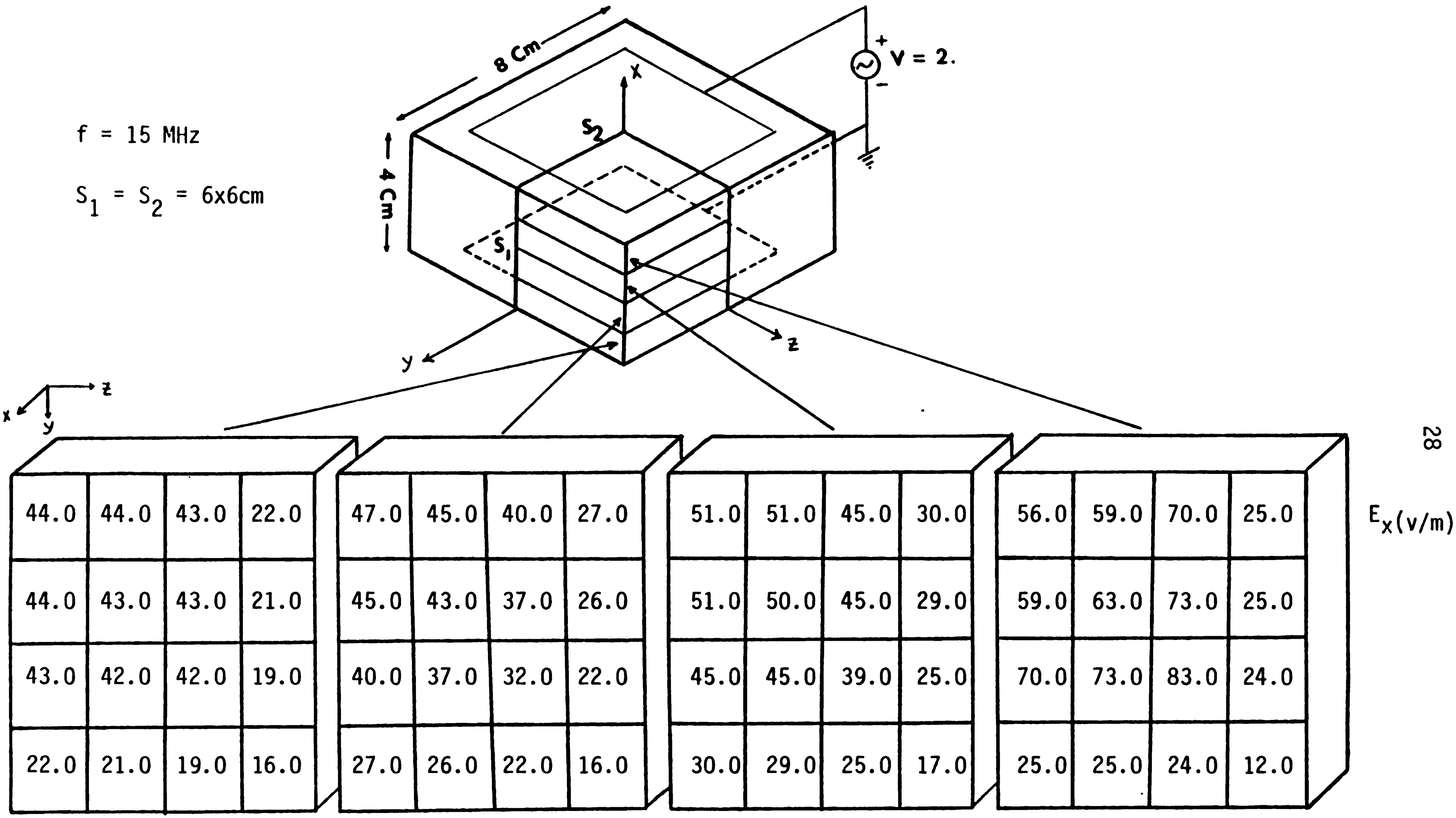

Figure 2.10. The X-component of the electric field at the centers of subvolumes in different layers in ¼ of free space between two electrodes of equal size with S_1 grounded.

f = 15 MHz

S_1 = 6x6cm

S_2 = 4x4cm

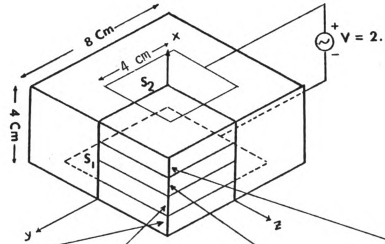

Layer 1 (E_x, E_y, E_z (v/m))

41.0 0.2 0.2	41.0 0.2 0.1	42.0 8.0 0.0	17.0 18.0 0.2
40.0 0.1 0.2	40.0 0.4 0.4	42.0 8.0 0.6	16.0 18.0 1.4
42.0 0.0 8.0	42.0 0.6 8.0	44.0 8.5 8.5	15.0 17.0 5.6
17.0 0.2 18.0	16.0 1.4 18.0	15.0 5.6 17.0	8.0 8.0 8.0

Layer 2

43.0 1.4 1.4	40.0 2.4 0.9	32.0 0.2 0.5	20.0 2.9 0.2
40.0 0.9 2.4	37.0 1.8 1.8	30.0 0.5 0.9	19.0 3.3 0.1
32.0 0.5 0.2	30.0 0.9 0.5	25.0 1.3 1.3	15.0 3.4 1.2
20.0 0.2 2.9	19.0 0.1 3.3	15.0 1.2 3.4	10.0 2.3 2.3

Layer 3

51.0 2.8 2.8	46.0 10.0 2.5	32.0 12.0 1.8	18.0 8.0 0.9
46.0 2.5 10.0	42.0 8.0 8.0	28.0 10.0 5.5	16.0 6.5 2.9
32.0 1.8 12.0	28.0 5.5 10.0	21.0 6.5 6.5	13.0 4.0 2.9
18.0 0.9 8.0	16.9 2.9 6.5	13.0 2.9 4.0	9.0 2.0 2.0

Layer 4

65.0 2.0 2.0	73.0 18.0 2.0	27.0 37.0 2.0	12.0 17.0 1.6
73.0 2.0 18.0	80.0 18.0 18.0	26.0 34.0 11.0	11.0 14.0 5.0
27.0 2.0 37.0	26.0 11.0 34.0	15.0 16.0 16.0	8.8 9.0 6.3
12.0 1.6 17.0	11.0 5.0 14.0	8.0 6.3 9.0	6.0 5.0 5.0

E_x
E_y (v/m)
E_z

←1cm→

Figure 2.11. Three components of the electric field at the center of subvolumes in different layers in ¼ of free space between two electrodes of different sizes for floating potential case.

is the distribution of the high electric field near the smaller upper electrode. This pehnomenon is expected from physical intuition, and has been used in practical applications to focus the electric field.

Figure 2.12 shows the similar results as that given in Figure 2.11. with two different features: The larger lower electrode is grounded, and only the X-components of electric fields are shown. The interesting point we observe from Figure 2.12. is that when the larger electrode is grounded, the concentration of higher electric fields near the smaller electrode becomes most outstanding. This phenomenon should have practical applications.

Figure 2.13. shows the distribution of the X-component (dominant component) of the electric field along the X-axis maintained between two electrodes of equal dimension. The spacing D between electrodes is kept at 4. cm and the electrode dimension (a) is varied to give four cases of $\frac{D}{a}$: 1.16, 1.75, 2.4, and 3.5. A voltage of 2. volts at 15 MHz is applied to each of the four cases. The lower electrode S_1 is grounded, and the distribution of X-component of the electric field along the X-axis is shown in the Figure for the four cases. It is noted that when the dimension of electrodes is about the same as the spacing between them, the electric field between electrodes is nearly uniform. However when the dimension of electrodes become considerably smaller than the spacing, the distribution of the electric field along the X-axis can be nonuniform; with the intensity of the electric field decreasing quite rapidly from the upper electrode (ungrounded) towards the larger electrode (grounded).

f = 15 MHz

S_1 = 6x6cm

S_2 = 4x4 cm

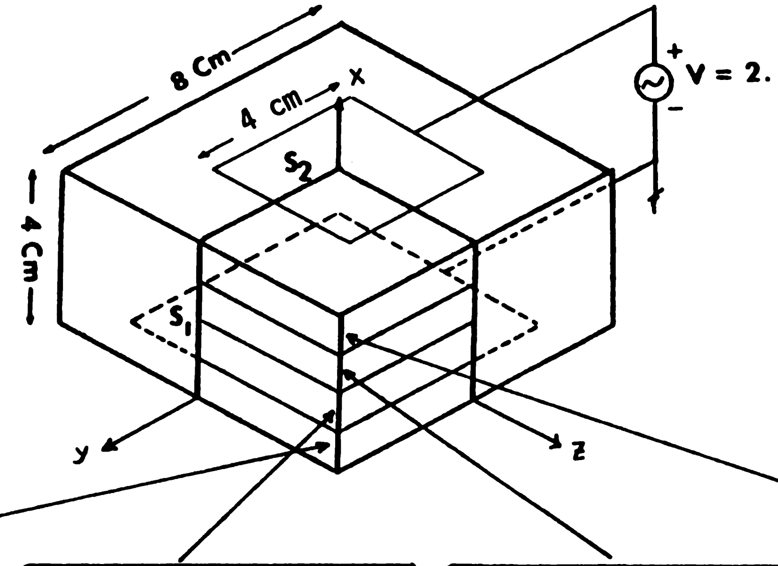

E_x(v/m)

35.0	32.0	30.0	14.0
32.0	30.0	28.0	13.0
30.0	28.0	26.0	11.0
14.0	13.0	11.0	7.4

40.0	36.0	27.0	17.0
36.0	32.0	24.0	15.0
27.0	24.0	19.0	12.0
17.0	15.0	12.0	8.7

53.0	47.0	31.0	16.0
47.0	42.0	27.0	14.0
31.0	27.0	18.0	11.0
16.0	14.0	11.0	7.5

71.0	82.0	31.0	9.7
82.0	92.0	26.0	8.7
31.0	26.0	13.0	6.5
9.7	8.7	6.5	4.5

←1cm→

Figure 2.12. The X-component of the electric field at the center of subvolumes in different layers in ¼ of free space between two electrodes of different sizes, with S_1 grounded.

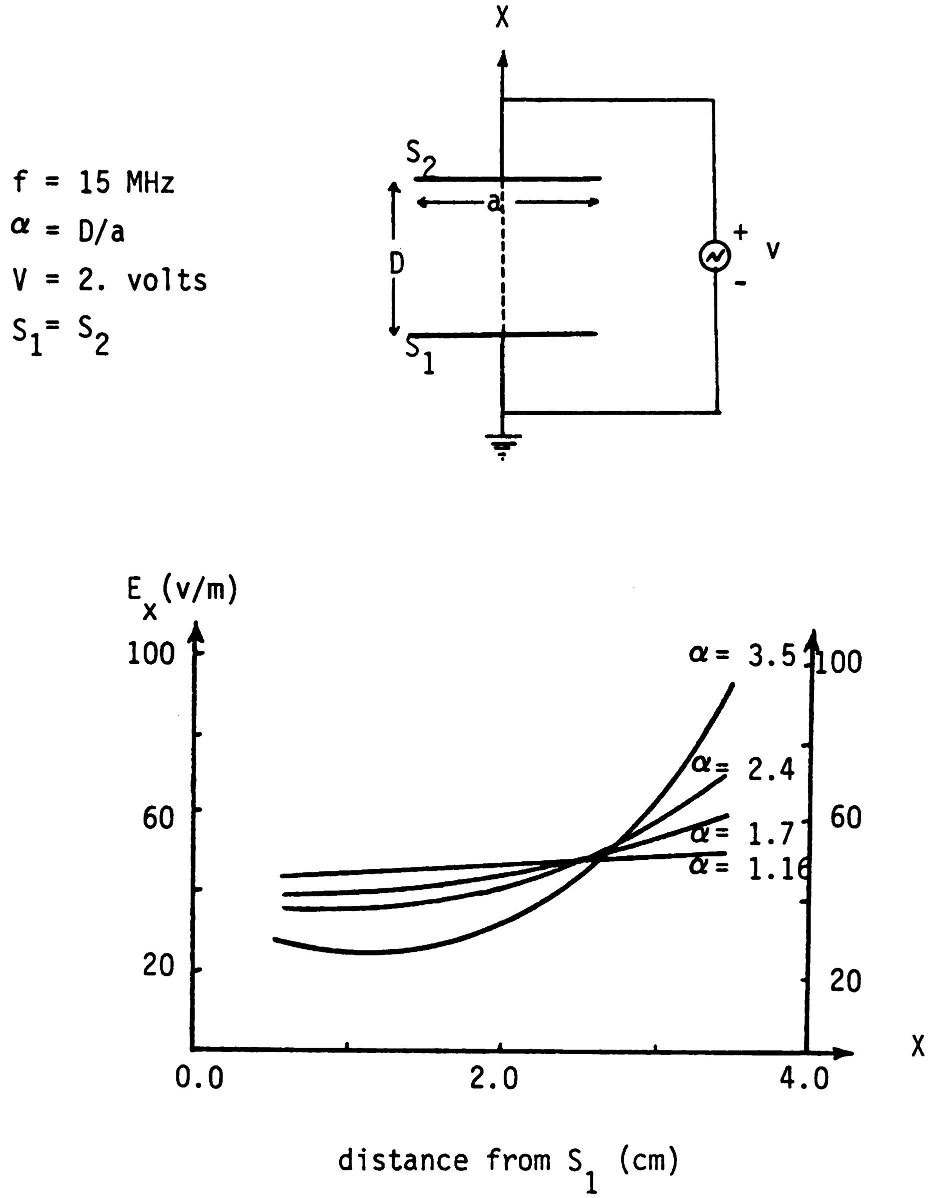

Figure 2.13. Distributions of the X-component of the electric field along the X axis between two electrodes of equal dimension for various ratios of D/a , where D is the spacing between the electrodes and a is the dimension of the electrode. S_1 is grounded.

Figure 2.14. shows the distribution of the X-component of electric field along the X-axis in the free space between two electrodes of different dimensions. A voltage of 2. volts at 15 MHz is applied between electrodes while their potential are left floating. Four cases of different electrode dimensions are considered for different values of β, which is defined as the ratio of the surface areas of the tow electrodes. The spacing between the electrodes, D is kept at 4. cm, it is observed that for $\beta = 1$, the electric field is uniform. For $\beta > 1$, however, the electric field intensity is higher near the smaller electrode S_2, and decreases towards the larger electrodes. It is noted that as the ratio β increases, the electric field intensity decreases more rapidly along the X-axis towards the larger electrode. Similar phenomena are observed for the case when the larger electrode is grounded. The results for this case are shown for four different values of β, in Figure 2.15. comparing Figures 2.14 and 2.15, we observe that for the same value of β if S_1 is grounded the intensity of the electric field increases near the smaller upper electrode S_2 and reduces near the larger lower electrode S_1 as compared with the case of floating potential case. For this reason the grounded potential case has advantage over the floating potential case for the purpose of focusing the electric field.

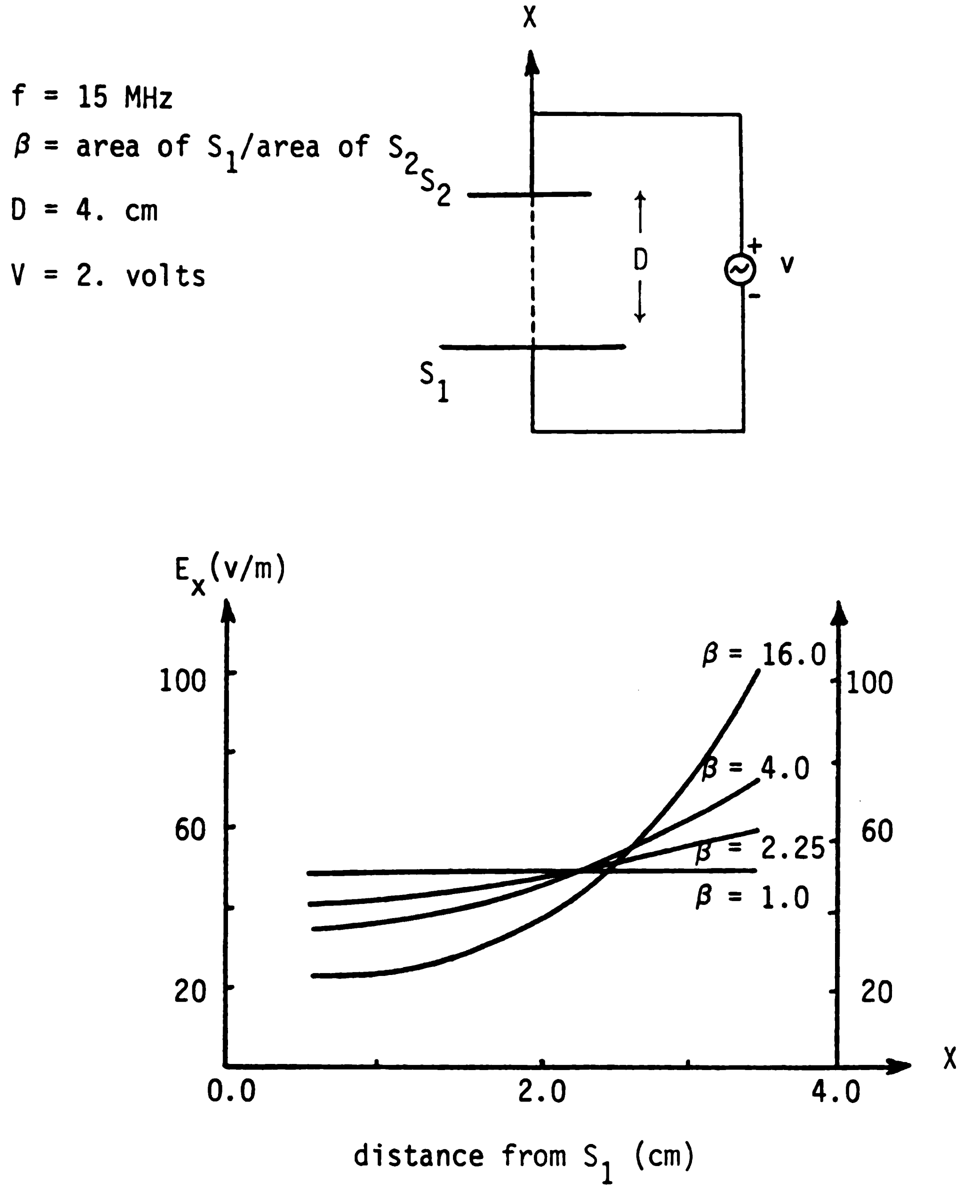

Figure 2.14. Distributions of the X-component of the electric field along the X axis between electrodes of different dimensions for various ratios of S_1/S_2. The potentials of the electrodes are left floating.

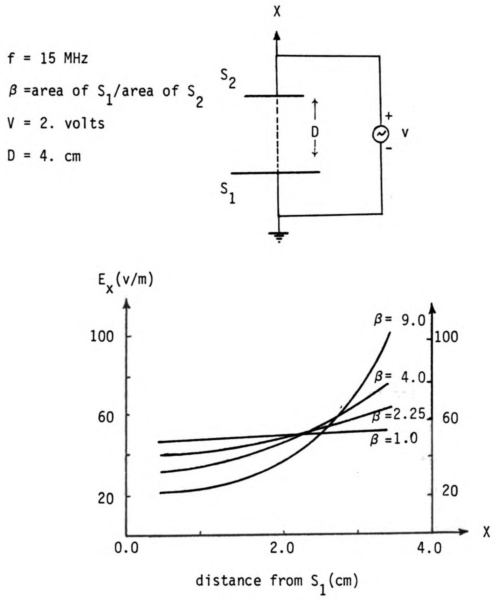

Figure 2.15. Distributions of the X-component of the electric field along the X axis between two electrodes of different dimensions for various ratios of S_1/S_2 where S_1 and S_2 are the surface areas of the two electrodes. (S_1 is grounded)

2.6. Comparison of Numerical Results with Experimental Results

In order to verify the theory and numerical results presented in the preceding sections, a series of experiments was conducted to measure the electric field between the electrodes for various cases of capacitor dimensions and applied voltages. The details of the experimental setup will be given in Chapter V, and only the experimental results will be used to compare with theoretical results in this section.

Figure 2.16. shows the theoretical and experimental results of the electric fields maintained at the inner and outer surfaces of one electrode for three capacitors with various electrode dimensions (a), and seperations D (i) D = 4. cm, and a = 4^{cm}, (ii) D = 8 cm, and a = 6. cm, and (iii) D= 4 cm and a = 6 cm. The electric fields at the inner and at the outer surfaces of one electrode tends to increase towards the edge of the electrode, somewhat proportional to the induced surface charge on the electrode. The electric field at the inner surface of electrode is in general, larger than that at the outer surface. The ratio of the former to the latter becomes larger if the electrode dimension (a) is increased, or the separation between electrodes D is decreased. In the limit of an infinite a and a finite D, there is zero electric field at the outer surface of the electrodes. The agreement between theory and experiment is considered to be good.

In Figure 2.17. the variation of the normalized X-components of the electric field along the X-axis maintained between two electrodes of equal dimension (7 x 7 cm) has been shown for the cases of D = 4 cm (A), and D = 8. cm (B). The solid lines show the theoretical

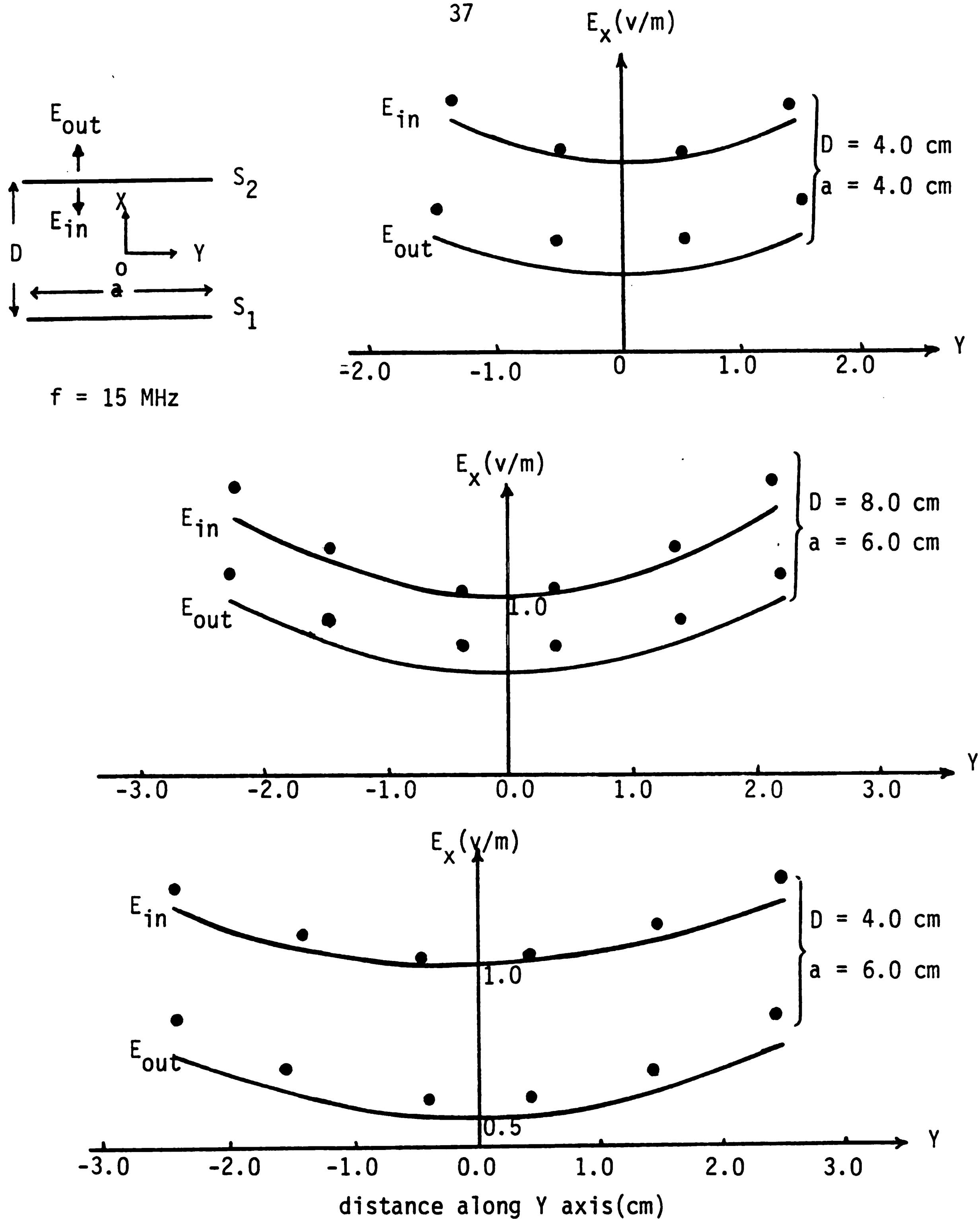

Figure 2.16. Theoretical and experimental results of the electric field at the inner and outer surfaces of one electrode for three capacitors with various electrode dimensions and seperations . Solid lines are the theoretical results and discrete points represent the experimental results.

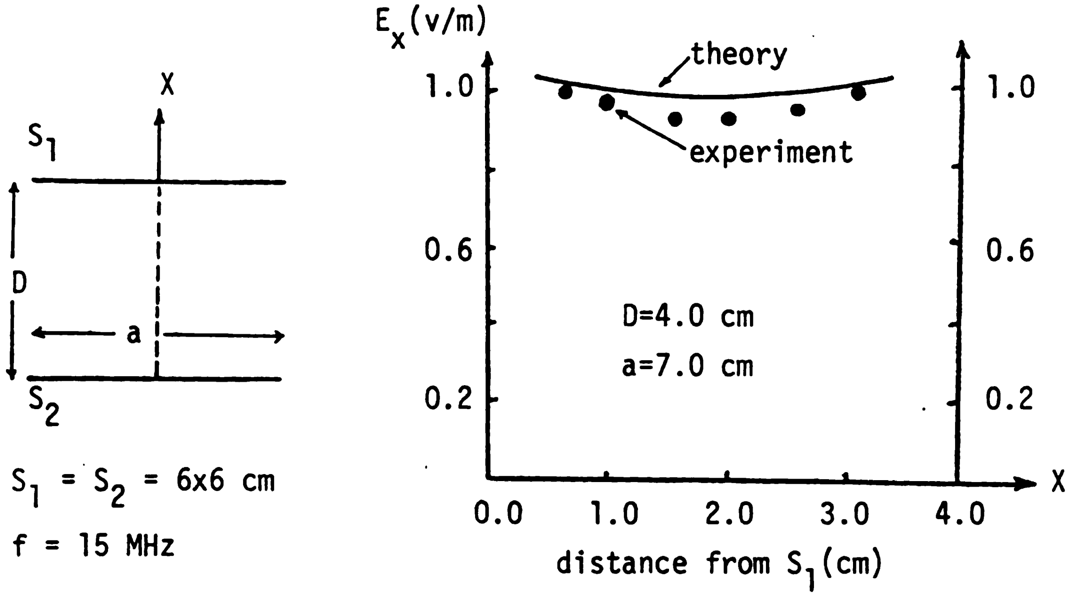

A

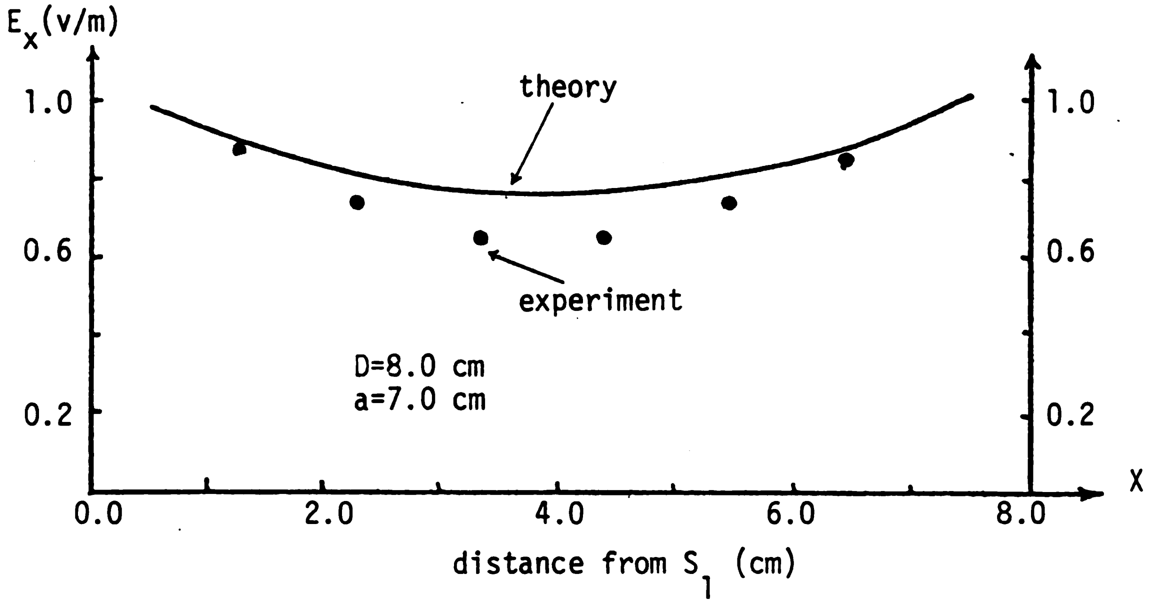

B

Figure 2.17. Theoretical and experimental results for the distribution of the X-component of the electric field along X axis between electrodes of equal dimension. Solid lines show the theoretical results and the discrete points represent the experimental results.

results, while the discrete points represent the experimental values. Again a good agreement between theory and experiment is obtained. In Figure 2.18. the theoretical and experimental results for the variation of the X-component of electric field along the X-axis between two electrodes of different dimensions are shown for the floating potential case (A), and for the grounded potential case (B). In each case the results for 3 different values of β are shown. It is observed that the agreement between theory and experiment is satisfactory.

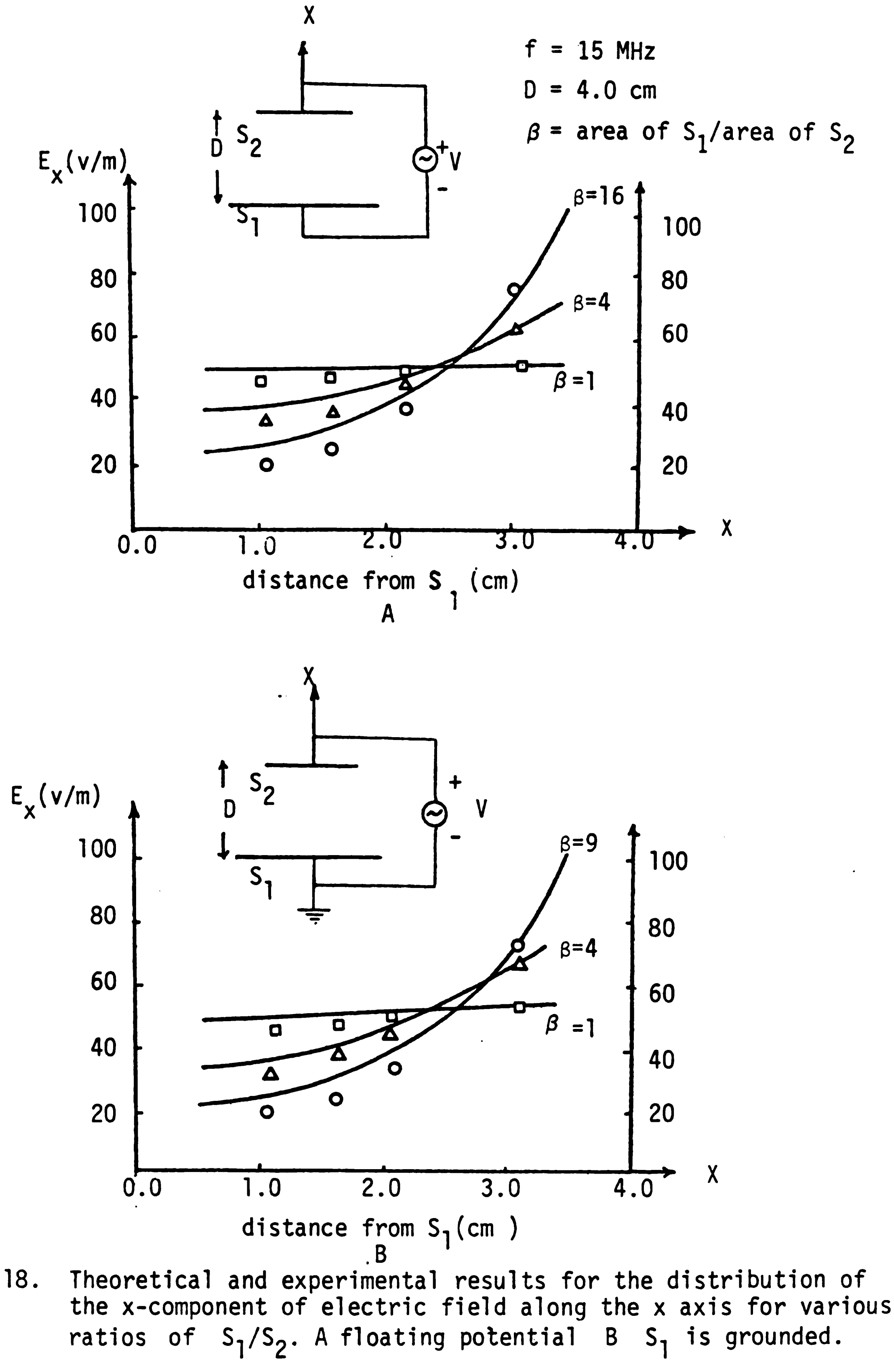

Figure 2.18. Theoretical and experimental results for the distribution of the x-component of electric field along the x axis for various ratios of S_1/S_2. A floating potential B S_1 is grounded.

CHAPTER III

LOCAL HEATING WITH HF ELECTRIC FIELD

The heating effect of nonradiating electromagnetic fields has been utilized over the past decade in order to eradicate the cancerous tumor embedded inside a biological body. A great deal of research has been conducted and successful results have been obtained on tumor-bearing labratory animals and even the human body.

There exist several methods by means of which a biological body can be locally heated. One such method is the local heating with electric field, where the body is placed between two parallel electrodes connected to a RF generator. Although this method has been proven efficient in cancer therapy, very few engineering studies have been conducted to analyze the distribution of the induced electric field and the specific absorption rate of energy (SAR) in the body.

In this chapter we aim to analyze the theoretical aspect of the problem and find the induced electric field in the body for various configurations of the electrodes as shown in Figure 3.1. Also a scheme will be developed to synthesize the potential distribution or the charge distribution on the electrodes in order to obtain a desired heating pattern in the body.

3.1 Problem Discriptions

In the preceding chapter a capacitor consisting of two electrodes

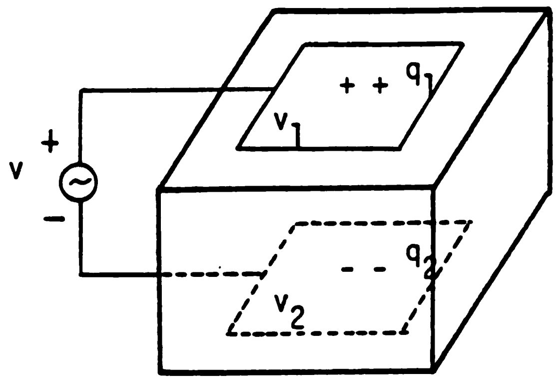

Electrodes of the same size
floating voltage
$v_1 = -v_2 = v/2$ and $q_1 = q_2$

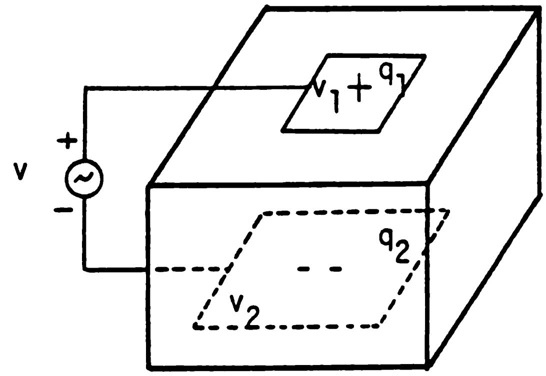

Electrodes of different sizes
floating voltage
$v_1 + v_2 = v$ and $q_1 = q_2$

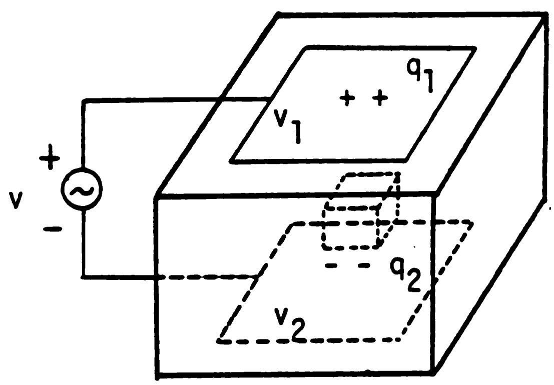

heterogeneous body
$v_1 = -v_2 = v/2$ and $q_1 = q_2$

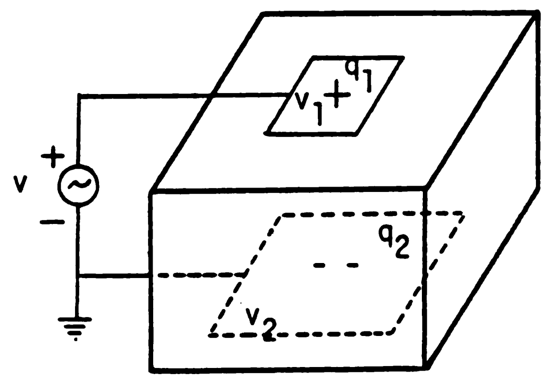

Electrodes of different sizes
one electrode grounded
$v_2 = 0.0$, $v_1 = v$
$q_1 \neq q_2$

Figure 3.1. Different arrangements of capacitor plates placed on the biological body for the purpose of local heating.

of arbitrary dimensions in free space was studied in some detail, and the distributions of the electric charges on the electrodes, as well as the electric field in free space, were obtained.

When a biological body of conductivity σ, permittivity ϵ and permeability μ_o is placed between the electrodes, the problem becomes more complicated in the sense that the charge induced on the electrodes and the induced charge on and the induced current in the body are coupled. This necessitates the establishment of more equations from which more unknown quantities are to be solved as compared with the problem treated in the preceding chapter.

The geometry of the problem is shown in Figure 3.2 where a pair of electrodes are placed across a biological body. The density of charge on the electrodes is denoted by $\eta(\vec{r}')$, and the incident electric field maintained by $\eta(\vec{r}')$ is represented by $\vec{E}^i(\vec{r})$. The total electric field at any point $\vec{r}$ inside the body is the sum of the incident electric field $\vec{E}^i$ and the electric field maintained by the induced current and charge inside the body, or the scattered electric field represented by $\vec{E}^s$.

By using the Maxwells' equations we will obtain two coupled integral equations in terms of the induced charge density on the electrodes and the unknown total electric field inside the body. Then the moment method is employed to solve the integral equations numerically.

3.2 Integral Equation for the Total Electric Field in the Body

The incident EM fields must satisfy the source-free Maxwells' equations in the free space between the electrodes:

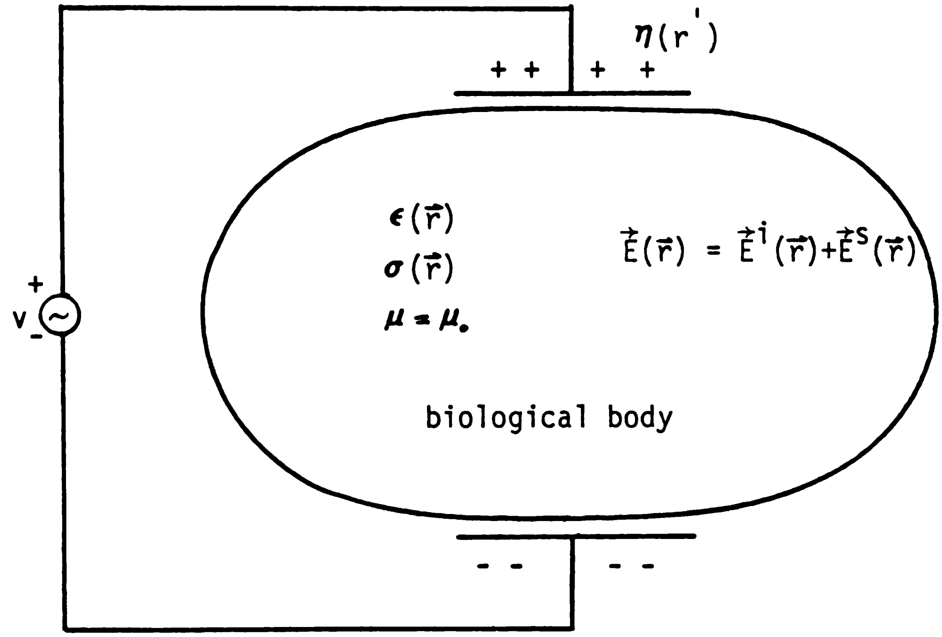

Figure 3.2. A pair of electrodes energized by a HF voltage placed across the biological body for local heating

$$\nabla X \vec{E}^i(\vec{r}) = -j\omega\mu_o \vec{H}^i(\vec{r}) \qquad (3.2.1)$$

$$\nabla X \vec{H}^i(\vec{r}) = j\omega \epsilon_o \vec{E}^i(\vec{r}) \qquad (3.2.2)$$

$$\nabla \cdot \vec{E}^i(\vec{r}) = 0 \qquad (3.2.3)$$

$$\nabla \cdot \vec{H}^i(\vec{r}) = 0 \qquad (3.2.4)$$

where a time variation factor of $e^{j\omega t}$ is assumed for the incident fields.

The total EM fields at any point inside the body can be expressed as the sum of the incident and scattered fields

$$\vec{E}(\vec{r}) = \vec{E}^i(\vec{r}) + \vec{E}^s(\vec{r}) \qquad (3.2.5)$$

$$\vec{H}(\vec{r}) = \vec{H}^i(\vec{r}) + \vec{H}^s(\vec{r}) \qquad (3.2.6)$$

$\vec{E}(\vec{r})$ and $\vec{H}(\vec{r})$ must satisfy the following set of Maxwells' equations.

$$\nabla X \vec{E}(\vec{r}) = -j\omega\mu_o \vec{H}(\vec{r}) \qquad (3.2.7)$$

$$\nabla X \vec{H}(\vec{r}) = [\sigma(\vec{r}) + j\omega \epsilon(\vec{r})]\vec{E}(\vec{r}) \qquad (3.2.8)$$

$$\nabla \cdot [\sigma(\vec{r}) + j\omega \epsilon(\vec{r})]\vec{E}(\vec{r}) = 0 \qquad (3.2.9)$$

$$\nabla \cdot \vec{H}(\vec{r}) = 0 \qquad (3.2.10)$$

substituting (3.2.5) and (3.2.6) into (3.2.7) and (3.2.8) leads to the following equations

$$\nabla X \vec{E}^i(\vec{r}) + \nabla X \vec{E}^s(\vec{r}) = -j\omega\mu_o \vec{H}^i(\vec{r}) - j\omega\mu_o \vec{H}^s(\vec{r}) \qquad (3.2.11)$$

$$\nabla X \vec{H}^i(\vec{r}) + \nabla X \vec{H}^s(\vec{r}) = \sigma(\vec{r})\vec{E}(\vec{r}) + j\omega[\epsilon(\vec{r}) - \epsilon_o]\vec{E}(\vec{r}) + j\omega\epsilon_o[\vec{E}^i(\vec{r}) + \vec{E}^s(\vec{r})] \qquad (3.2.12)$$

If we subtract (3.2.1) and (3.2.2) from the above two equations, the result is

$$\nabla \times \vec{E}^s(\vec{r}) = -j\omega\mu_o \vec{H}^s(\vec{r}) \tag{3.2.13}$$

$$\nabla \times \vec{H}^s(r) = [\sigma(\vec{r}) + j\omega(\epsilon(\vec{r})-\epsilon_o)]\vec{E}(\vec{r}) + j\omega\epsilon_o \vec{E}^s(\vec{r}) \tag{3.2.14}$$

We define an equivalent current density $\vec{J}_{eq}(\vec{r})$ by

$$\vec{J}_{eq}(\vec{r}) = \tau(\vec{r})\vec{E}(\vec{r}) \tag{3.2.15}$$

where $\tau(\vec{r}) = \sigma(\vec{r}) + j\omega\ (\epsilon(\vec{r})-\epsilon_o)$ is called the complex conductivity. Thus, the equation (3.2.14) reduces to

$$\nabla \times \vec{H}^s(\vec{r}) = \tau(\vec{r})\vec{E}(\vec{r}) + j\omega\epsilon_o \vec{E}(\vec{r}) \tag{3.2.16}$$

It is noted that the equivalent current density, $\vec{J}_{eq}$ consists of the conduction current $\sigma\vec{E}$, and the polarization current $j\omega(\epsilon(\vec{r})-\epsilon_o)\vec{E}$.

The appropriate Maxwells' equations for the scattered fields can be summarized as follows

$$\nabla \times \vec{E}^s(\vec{r}) = -j\omega\mu_o \vec{H}^s(\vec{r}) \tag{3.2.17}$$

$$\nabla \times \vec{H}^s(\vec{r}) = \vec{J}_{eq}(\vec{r}) + j\omega\epsilon_o \vec{E}^s(\vec{r}) \tag{3.2.18}$$

$$\nabla \cdot \vec{E}^s(\vec{r}) = \frac{1}{\epsilon_o}\rho_{eq}(\vec{r}) \tag{3.2.19}$$

$$\nabla \cdot \vec{H}^s(\vec{r}) = 0 \tag{3.2.20}$$

ρ_{eq} is the equivalent charge density and is related to $\vec{J}_{eq}$ by the equation of continuity

$$\nabla\cdot\vec{J}_{eq}(\vec{r}) = -j\omega\rho_{eq}(\vec{r}) \tag{3.2.21}$$

$$\rho_{eq}(\vec{r}) = \frac{j\nabla\cdot J_{eq}(\vec{r})}{\omega} \tag{3.2.22}$$

The scattered electric field can be thought of as the field maintained by $\vec{J}_{eq}(\vec{r})$, which flows within the conductive medium. It can be shown that they are related by the following expression [15]

$$\vec{E}^{s}(\vec{r}) = \int_V \vec{J}_{eq}(\vec{r}')\cdot[\text{P.V.}\overleftrightarrow{G}(\vec{r},\vec{r}') - \frac{\overleftrightarrow{I}\,\delta(\vec{r}-\vec{r}')}{3j\omega\epsilon_o}]\,dv' \tag{3.2.23}$$

where $\overleftrightarrow{G}(\vec{r},\vec{r}') = j\omega\mu_o[\overleftrightarrow{I} + \frac{\nabla\nabla}{\beta_o^2}]\,G(\vec{r},\vec{r}')$ is the free space dyadic Greens' function and $G(\vec{r},\vec{r}') = \frac{e^{-j\beta_o|\vec{r}-\vec{r}'|}}{4\pi|\vec{r}-\vec{r}'|}$ is the scalar Greens' function for free space, and

$$\overleftrightarrow{I} = \hat{x}\hat{x} + \hat{y}\hat{y} + \hat{z}\hat{z}$$

is the unit dyadic.

P.V. stands for the principle value and it means that the source point should be excluded while evaluating the integral. With (3.2.23), (3.2.5) becomes

$$(1 + \frac{\tau(\vec{r})}{3j\omega\epsilon_o})\vec{E}(\vec{r}) - \text{P.V.}\int_V \tau(\vec{r}')\vec{E}(\vec{r}')\cdot\overleftrightarrow{G}(\vec{r},\vec{r}')\,dV = \vec{E}^{i}(\vec{r}) \tag{3.2.24}$$

which is an integral equation for the total electric field $\vec{E}(\vec{r})$ inside the body.

3.3 Integral Equation for the Induced Charge on the Electrodes

An integral equation can be derived for the induced charge density on the electrodes by a proceduce similar to that employed for the free space case in Chapter II. The difference however, is that in the present case the charge induced on the surface of the body must be taken into account for evaluating the potentials on the electrodes. Thus, at any point $\vec{r}$ on the surfaces of the electrodes the potential $V(\vec{r})$ can be expressed in terms of the charge induced on the surfaces of the electrodes and that on the body surface.

$$V(\vec{r}) = \frac{1}{\epsilon_o} \int_{S_1+S_2} \eta(\vec{r}\,')G(\vec{r},\vec{r}\,')ds + \frac{1}{\epsilon_o} \int_{S_b} \eta_b(\vec{r}\,")G(\vec{r},\vec{r}\,")ds" \quad (3.3.1)$$

Where S_1 and S_2 represent the surfaces of the electrodes, S_b represents the body surface, $\eta(\vec{r}\,')$, and $\eta_b(\vec{r}\,")$ represent the charge densities on the electrodes and the body surface, respectively. An expression for η_b in terms of $\vec{J}_{eq}$ may be deduced from (3.2.21).

For a homogeneous biological body $\nabla\cdot\vec{J}_{eq}(\vec{r})$ is nonzero only at the body-free space interface, where the induced charge is present. If (3.2.21) is integrated over an infinitesimal volume enclosed by a samll pillbox as shown in Figure 3.3.b, and the divergence theorem is applied, η_b can be obtained as

$$\eta_b(\vec{r}\,') = -\frac{\tau(\vec{r})\ \hat{n}\cdot\vec{E}(\vec{r})}{j\omega} \quad (3.3.2)$$

Where $\hat{n}$ is the outward unit vector normal to the surface of the body. With (3.3.2), (3.3.1) can be rewritten as

$$V(\vec{r}) = \frac{1}{\epsilon_o} \int_{S_1+S_2} \eta(\vec{r}\,')G(\vec{r},\vec{r}\,')ds' + \frac{j}{\epsilon_o\omega} \int_{S_b} \tau(\vec{r}\,")\hat{n}\cdot\vec{E}(\vec{r}\,")G(\vec{r},\vec{r}\,")ds" \quad (3.3.3)$$

where as before $G(\vec{r},\vec{r}\,') = \dfrac{e^{-j\beta_o|\vec{r}-\vec{r}\,'|}}{4\pi|\vec{r}-\vec{r}\,'|}$

Equation (3.3.3) and (3.2.23) constitute a pair of coupled integral equations for the unknowns $\eta(\vec{r}')$ and $\vec{E}(\vec{r})$.

The incident electric field $\vec{E}^i(\vec{r})$ in (3.2.24) is maintained by the charges distributed on S_1 and S_2 only, and can be written in terms of the charge density $\eta(\vec{r}')$ as

$$\vec{E}^i(\vec{r}) = -\frac{1}{\epsilon_o}\int_{S_1+S_2} \eta(r')\nabla_r G(\vec{r},\vec{r}')ds' \qquad (3.3.5)$$

For convenience, (3.2.24) and (3.3.3) are rewritten together.

$$\left(1+\frac{\tau(\vec{r})}{3j\omega\epsilon_o}\right)\vec{E}(\vec{r}) - \text{P.V.}\int \tau(\vec{r}')\vec{E}(\vec{r}')\cdot\overleftrightarrow{G}(\vec{r},\vec{r}')dv = \vec{E}^i(\vec{r}) \qquad (3.2.24)$$

$$\frac{1}{\epsilon_o}\left[\int_{S_1+S_2} \eta(\vec{r}')G(\vec{r},\vec{r}')ds' + \frac{j}{\omega}\int_{S_b} \tau(\vec{r}'')(\hat{n}\cdot\vec{E}(\vec{r}''))G(\vec{r},\vec{r}'')ds''\right] = V(\vec{r}) \qquad (3.3.3)$$

where $$\vec{E}^i(\vec{r}) = -\frac{1}{\epsilon_o}\int_{S_1+S_2} \eta(\vec{r}')\nabla_r G(\vec{r},\vec{r}')ds'$$

3. Moment Solution of Coupled Integral Equations

The two coupled integral equations may be converted into a system of linear equations in terms of the unknowns by using the method of moments. For this purpose, the body and the electrodes are assumed to be symmetric with respect to the $Y = 0$ and $Z = 0$ planes as shown in Figure 3.3. The first quadrant of the body is divided into N subvolume cells, throughout each cell $\tau(\vec{r})$ and $\vec{E}(\vec{r})$ are assumed to be constant. Similarly, the first quadrants of S_1 and S_2 are partitioned into a total number of N' subareas, over each subarea the charge density η is assumed to be constant.

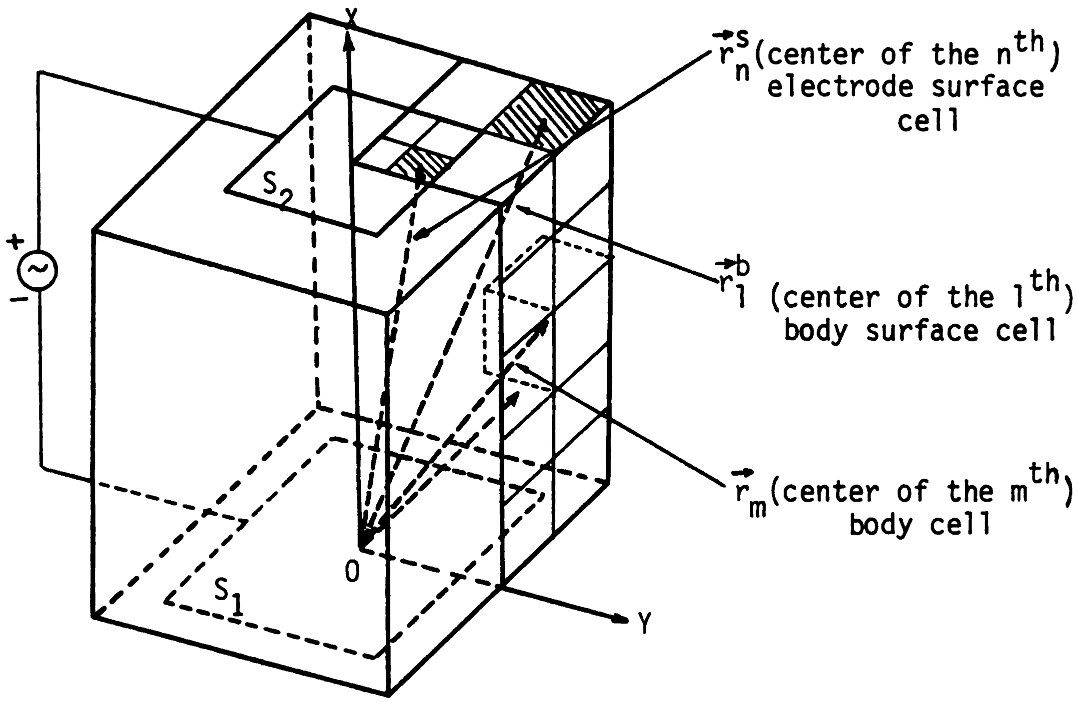

(a)

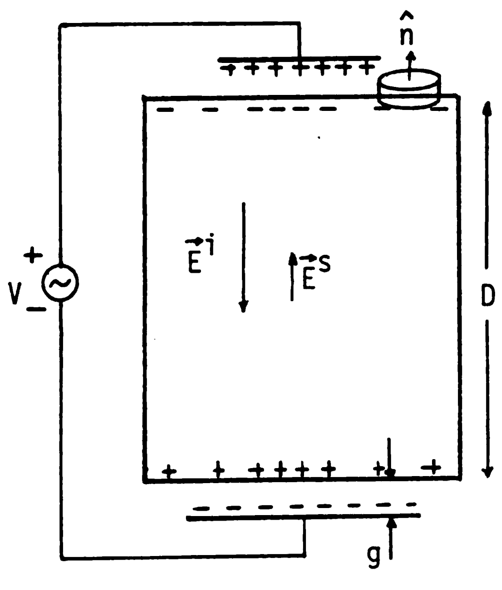

(b)

Figure 3.3. The geometry of a body placed between two electrodes(a).
(b) The side view of the body and the electrodes.

From (3.3.3), the voltage at the center of the m^{th} subarea located in the first quadrant can be written as

$$V(\vec{r}^{\,s}_m) = V^s_m \doteq \frac{1}{\epsilon_o} \sum_{k=1}^{N'} \eta_k \sum_{i=1}^{4} G^i(\vec{r}^{\,s}_m,\vec{r}^{\,s}_k)\Delta S^k_e + j \sum_{\ell=1}^{N_B} \frac{\hat{n}\cdot\vec{E}(\vec{r}^{\,b}_\ell)\tau(\vec{r}^{\,b}_\ell)}{\omega} \cdot \sum_{i=1}^{4} G^i(\vec{r}^{\,s}_m,\vec{r}^{\,b}_\ell)\Delta S^\ell_b \qquad (3.3.4)$$

where i represents the quadrant number and η_k is the charge density on the k^{th} subarea on the electrodes. $\vec{r}^{\,s}_m$, and $\vec{r}^{\,s}_k$ are the position vectors for the centers of the m^{th} cell (field point) and k^{th} cell (source point) on the electrodes.
$\vec{r}^{\,b}_\ell$ represents the position vector of the center of the ℓ^{th} body surface cell, and finally ΔS^k_e, and ΔS^ℓ_b are the areas of the k^{th} cell on the electrode and the ℓ^{th} cell on the body surface, respectively.

The induced electric field inside the body is mainly in the x direction, this implies that $\eta_b = \frac{\tau\hat{x}\cdot E}{j\omega} = \frac{\tau E_X}{j\omega}$.

Therefore, the equation (3.3.4) may be transformed into the following matrix form.

$$\begin{array}{c c} & \begin{array}{cc} N' & N_B \end{array} \\ N' & \left[\begin{array}{c:c} G^S & C \end{array}\right] \end{array} \begin{bmatrix} \eta_1 \\ \vdots \\ \eta_{N'} \\ \hdashline E^1_X \\ \vdots \\ E^{N_B}_X \end{bmatrix} = \begin{bmatrix} V_1 \\ V_2 \\ \vdots \\ V_{N'} \end{bmatrix} \; N' \qquad (3.3.5)$$

Where

$$G^S_{mk} = \frac{1}{\epsilon_o} \sum_{i=1}^{4} \Delta S^k_e G^i_{mk} \quad \text{and} \quad C_{m\ell} = \frac{j\tau_\ell}{\epsilon_o \omega} \sum_{i=1}^{4} G^i_{m\ell} \Delta S^\ell_b \tag{3.3.5a}$$

$$G^i_{mk} \doteq G^i(\vec{r}^S_m, \vec{r}^S_k), \quad G^i_{m\ell} \doteq G^i(\vec{r}^S_m, \vec{r}^b_\ell), \quad \tau_\ell \doteq \tau(r^b_\ell)$$

and N_B is the total number of the subareas on the body surface. The expressions for the elements of the matrices G^S and C will be presented in the next section.

The matrix representation of (3.2.24) is given elsewhere [16], and the result is of the following form:

$$\left[\begin{array}{c:c:c} G_{XX} & G_{XY} & G_{XZ} \\ \hdashline G_{XX} & G_{YY} & G_{YZ} \\ \hdashline G_{ZX} & G_{ZY} & G_{ZZ} \end{array}\right] \left[\begin{array}{c} E_X \\ \hdashline E_Y \\ \hdashline E_Z \end{array}\right] \left[\begin{array}{c} E^i_X \\ \hdashline E^i_y \\ \hdashline E^i_Z \end{array}\right] \tag{3.3.6}$$

Equation (3.3.6) can be written in a more compact form as

$$\Big[\; G \; \Big] \Big[E \Big] = \Big[E^i \Big]$$

where $[G]$ is a $3NX3N$ matrix and $[E]$, and $[E^i]$ are column metrices each with $3N$ elements.

The incident electric field matrix $[E^i]$ can be related to the induced charge densities on the subareas of S_1 and S_2 by the following matrix relation.

$$3N \left[\begin{array}{c} E^i_X \\ \hdashline E^i_Y \\ \hdashline E^i_Z \end{array}\right] = \overset{N'}{\left[\begin{array}{c} A_X \\ \hdashline A_Y \\ \hdashline A_Z \end{array}\right]} \left[\begin{array}{c} \eta_1 \\ \vdots \\ \eta_{N'} \end{array}\right] \tag{3.3.7}$$

With (3.3.7) substituted into (3.3.6), and after some rearrangements, we obtain

$$\begin{array}{cc} & \begin{array}{cccc} \quad & 3N & \quad & N' \end{array} \\ 3N & \left[\begin{array}{c:c:c:c} G_{XX} & G_{XY} & G_{XZ} & A_X \\ \hdashline G_{YX} & G_{YY} & G_{YZ} & A_Y \\ \hdashline G_{ZX} & G_{ZY} & G_{ZZ} & A_Z \end{array}\right] \end{array} \left[\begin{array}{c} E_X \\ \hdashline E_Y \\ \hdashline E_Z \\ \hline \eta_1 \\ \cdot \\ \cdot \\ \eta_{N'} \end{array}\right] \begin{array}{c} 3N \\ \\ \\ N' \end{array} = 0 \tag{3.3.8}$$

For the case when one electrode (S_1) is grounded, equations (3.3.5) and (3.3.8) may be combined into the following matrix representation.

$$\begin{array}{cc} & \begin{array}{cccc} \quad & 3N & \quad & N' \end{array} \\ \begin{array}{c} 3N \\ \\ \\ N' \end{array} & \left[\begin{array}{c:c:c:c} G_{XX} & G_{XY} & G_{XZ} & A_X \\ \hdashline G_{YX} & G_{YY} & G_{YZ} & A_Y \\ \hdashline G_{ZX} & G_{ZY} & G_{ZZ} & A_Z \\ \hdashline C' & 0 & 0 & G^S \end{array}\right] \end{array} \left[\begin{array}{c} E_X \\ \hdashline E_Y \\ \hdashline E_Z \\ \hdashline \eta_1 \\ \cdot \\ \cdot \\ \eta_{N'} \end{array}\right] = V \left[\begin{array}{c} 0 \\ \cdot \\ \cdot \\ \cdot \\ 0 \\ \hdashline 0 \\ \vdots \\ 0 \\ 1 \\ 1 \end{array}\right] \begin{array}{c} \\ \\ \\ \\ \\ \\ N_1 \\ N_2 \\ \\ \end{array} \tag{3.3.9}$$

$$N_1 + N_2 = N'$$

where, N_1 and N_2 are the numbers of subareas on S_1 and S_2, and V is the applied voltage.

The matrix C' is related to the matrix C as

$$\begin{array}{cc} & N \\ N' & \left[\begin{array}{ccc} \quad & C' & \quad \end{array}\right] \end{array} = \begin{array}{cc} & \begin{array}{cc} N & N-N_B \end{array} \\ N' & \left[\begin{array}{c:c} \quad C \quad & \quad 0 \quad \end{array}\right] \end{array}$$

3.4 Calculation of the Matrices Elements

In this section the expressions for the elements of the matrices G, A, G^S, and C will be developed. The elements of the matrix G have been given by Livesay and Chen [16], and only the results will be presented here.

3.4.1 G Matrix

For a four quadrant symmetry it is shown that

$$G^{mn}_{X_pX} = G^{mn_1}_{X_pX} + G^{mn_2}_{X_pX} + G^{mn_3}_{X_pX} + G^{mn_4}_{X_pX} \tag{3.4.1}$$

$$G^{mn}_{X_pY} = G^{mn_1}_{X_pY} - G^{mn_2}_{X_pY} + G^{mn_3}_{X_pY} - G^{mn_4}_{X_pY} \tag{3.4.2}$$

$$G^{mn}_{X_pZ} = G^{mn_1}_{X_pZ} - G^{mn_2}_{X_pZ} - G^{mn_3}_{X_pZ} + G^{mn_4}_{X_pZ} \tag{3.4.3}$$

$$P = 1,2,3$$

$$X_1 = X,\ X_2 = Y,\ X_3 = Z$$

In the above expressions the numbers 1 to 4 in the superscripts represent the quadrant number.

For the diagonal elements we have $m = n$, and

$$G^{nn_1}_{X_pX_q} = \frac{j\omega\mu_o\delta_{Pq}}{3\beta_o^2}\ \{3[\tau(\vec{r}_n) + j\omega\epsilon_o]-2\tau(\vec{r}_n)e^{-j\beta_o a_n}(1+j\beta_o a_n)\} \tag{3.4.4}$$

where

$$q = 1,2,3$$

$$\delta_{Pq} = \begin{cases} 1 & \text{for} \quad P = q \\ 0 & \text{for} \quad P \neq q \end{cases}$$

and

$$a_n = \left(\frac{3\Delta V_n}{3\pi}\right)^{\frac{1}{3}}$$

where ΔV_n is the volume of the n^{th} volume cell.

For $m \neq n$, we have

$$G^{mn^i}_{X_p X_q} = -j\omega\mu_o \beta_o \tau(\vec{r}_{n_1}) \Delta V_{n_i} e^{-j\alpha^i_{mn}} \{[(\alpha^i_{mn})^2 - 1 - j\alpha^i_{mn}]\delta_{pq}$$

$$+ \text{Cos}\, \theta^{mn^i}_{X_p} \text{Cos}\, \theta^{mn^i}_{X_q} [3 - (\alpha^i_{mn})^2 + 3\, \alpha^i_{mn}] \qquad (3.4.5)$$

where

$$\alpha^i_{mn} = \beta_o R^i_{mn} \;,\; R^i_{mn} = |\vec{r}_{m_1} - \vec{r}_{n_i}|$$

$$\text{Cos}\, \theta^{mn^i}_{X_p} = \frac{X^m_p - X^{n^i}_p}{R^i_{mn}} \;,\; \text{Cos}\, \theta^{mn^i}_{X_q} = \frac{X^m_q - X^{n^i}_q}{R^i_{mn}}$$

$i = 1,2,3,4$ (The quadrant number)

and

$$\vec{r}_m = (X^m_1, X^m_2, X^m_3), \; \vec{r}_{n_i} = (X^{n^i}_1, X^{n^i}_2, X^{n^i}_3)$$

3.4.2 A Matrix

From (3.3.7) the three components of the incident electric field at the center of the m^{th} body subvolume located in the first quadrant are given as

$$E^m_X = \sum_{n=1}^{N'} A^{mn}_X \eta_n$$

$$E^m_Y = \sum_{n=1}^{N'} A^{mn}_y \eta_n \qquad m = 1,2,\ldots,N$$

$$E^m_Z = \sum_{n=1}^{N'} A^{mn}_Z \eta_n$$

By comparing the above equations with (2.5.5), (2.5.6), and (2.5.7) the following expressions for the elements of the matrix A can be obtained

$$A_X^{mn} = (C_n^1 + C_n^2 + C_n^3 + C_n^4)\ (X_1^m - X_1^n) \tag{3.4.6}$$

$$A_Y^{mn} = (C_n^1 + C_n^4)\ (X_2^m - X_2^n) + (C_n^2 + C_n^3)\ (X_2^m + X_2^n) \tag{3.4.7}$$

$$A_Z^{mn} = (C_n^1 + C_n^2)\ (X_3^m - X_3^n) + (C_n^3 + C_n^4)\ (X_3^m + X_3^n) \tag{3.4.8}$$

where

$$C_n^k = \frac{\Delta S_e^n}{4\pi\epsilon_o}\ \frac{1+j\beta_o R_{mn}^k}{(R_{mn}^k)^3}\ e^{-j\beta_o R_{mn}^k}\ ,\ k = 1,2,3,4$$

and

$$R_{mn}^k = |\vec{r}_m - \vec{r}_n^{\,k}|$$

$$\vec{r}_m = (X_1^m,\ X_2^m,\ X_3^m),\ \vec{r}_n^{\,k} = (X_1^{n^k},\ X_2^{n^k},\ X_3^{n^k})$$

again k represents the quadrant number.

3.4.3 G^S Matrix

In Chapter II the expressions for the elements of the matrix G^S were developed and the results are as follows.

For $m \neq k$ (off-diagonal elements),

$$G_{m_k}^S = \frac{\Delta S_e}{\epsilon_o}\ [G^1(\vec{r}_m^{\,S},\ \vec{r}_k^{\,S}) + G^2(\vec{r}_m^{\,S},\ \vec{r}_k^{\,S}) + G^3(\vec{r}_m^{\,S},\ \vec{r}_k^{\,S}) + G^4(\vec{r}_m^{\,S},\ \vec{r}_k^{\,S})] \tag{3.4.9}$$

where

$$G^i(\vec{r}_m^S, \vec{r}_k^S) = \frac{e^{-j\beta_o|\vec{r}_m^S - \vec{r}_k^{S^i}|}}{4\pi|\vec{r}_m^S - \vec{r}_k^{S^i}|}$$

$m = 1,2,\ldots,N'$

$i = 1,2,3,4$

$\vec{r}_m^S = (X_m^S, Y_m^S, Z_m^S)$ is the cartesian coordinates of the m^{th} subarea on the electrode.

$\vec{r}_k^{S^i} = (X_k^{S^i}, Y_k^{S^i}, Z_k^{S^i})$ is the cartesian coordinates of the k^{th} subarea in the i^{th} quadrant. It should be noted that all surface cells are assumed to have the same area ΔS_e, and

$$X_k^{S^i} = \begin{cases} 0 & \text{if } k \le N_1 \\ D & \text{if } N_1 < k \le N_1+N_2 \end{cases}, \quad X_m^S = \begin{cases} 0 & \text{if } m \le N_1 \\ D & \text{if } N_1 < m < N_1+N_2 \end{cases}$$

where D is the distance between the electrodes.

For $m = k$ (diagonal elements) we have,

$$G_{mm}^S = \frac{1}{2j\beta_o\epsilon_o}\left(e^{-j\beta_o\sqrt{\frac{\Delta S_e}{\pi}}} - 1\right) + \frac{\Delta S_e}{\epsilon_o}\left[G^2(\vec{r}_m^S,\vec{r}_m^S) + G^3(\vec{r}_m^S,\vec{r}_m^S) + G^4(\vec{r}_m^S,\vec{r}_m^S)\right] \tag{3.4.10}$$

3.4.4 C Matrix

From (3.3.5.a) we have

$$C_{m\ell} = \frac{j\tau_\ell}{\epsilon_o\omega}\sum_{i=1}^{4} G_{m\ell}^i \Delta S_b^\ell \qquad \begin{array}{l} \ell = 1,2,\ldots,N_B \\ m = 1,2,\ldots,N' \end{array}$$

where

$$G^i_{m\ell} \doteq G^i(\vec{r}^{\,S}_m, \vec{r}^{\,b}_\ell)$$

It is straightforward to show that

$$C_{m\ell} = j \frac{\Delta S_b}{\epsilon_o \omega} \tau_\ell [G'(\vec{r}^{\,S}_m, \vec{r}^{\,b}_\ell) + G^2(\vec{r}^{\,S}_m, \vec{r}^{\,b}_\ell) + G^3(\vec{r}^{\,S}_m, \vec{r}^{\,b}_\ell) + G^4(\vec{r}^{\,S}_m, \vec{r}^{\,b}{}_\ell)] \qquad (3.4.11)$$

where $$G^i(\vec{r}^{\,S}_m, \vec{r}^{\,b}_\ell) = \frac{e^{-j\beta_o |\vec{r}^{\,S}_m - \vec{r}^{\,b^i}_\ell|}}{4\pi |\vec{r}^{\,S}_m - \vec{r}^{\,b^i}|} \quad , \; i = k,2,3,4$$

and $\vec{r}^{\,S}_m = (\vec{X}^S_m, \vec{Y}^S_m, \vec{Z}^S_m)$ is the cartesian coordinates for the center of the m^{th} subarea on the electrodes with

$$X^S_m = \begin{cases} 0 & \text{for } m \leq N_1 \\ D & \text{for } N_1 < m \leq N_1+N_2 \end{cases}$$

$\vec{r}^{\,b^i}_\ell = (X^{S^i}_\ell, Y^{S^i}_\ell, Z^{S^i}_\ell)$ is the coordinates for the center of the ℓ^{th} subarea on the body surface located in the quadrant

$$X^{S^i}_\ell = \begin{cases} g & \text{for } \ell \leq \frac{N_B}{2} \\ D\text{-}g & \text{for } \frac{N_B}{2} < \ell \leq N_B \end{cases}$$

where g is the seperation between the body and the electrodes.

When the voltage between the electrodes is left floating, by the same argument given in Chapter II for the free space case, (3.3.9) can be modified into the following form:

$$\begin{array}{cc} & \begin{array}{ccccc} & 3N & & N' & 1 \end{array} \\ \begin{array}{c} \\ 3N \\ \\ N' \\ 1 \end{array} & \left[\begin{array}{ccc|c|c} G_{XX} & G_{XY} & G_{XZ} & A_X & 0 \\ G_{YX} & G_{YY} & G_{YZ} & A_Y & 0 \\ G_{ZX} & G_{ZY} & G_{ZZ} & A_Z & 0 \\ \hline C' & 0 & 0 & G^S & -1 \\ \hline 0 & 0 & 0 & \Delta S_e & 0 \end{array}\right] \end{array} \left[\begin{array}{c} E_X \\ E_Y \\ E_Z \\ \hline \eta_1 \\ \vdots \\ \eta_{N'} \\ \hline V_{S_1} \end{array}\right] = -V \left[\begin{array}{c} 0 \\ 0 \\ 0 \\ \hline 0 \\ 1 \\ \hline 0 \end{array}\right] \begin{array}{c} \\ 3N \\ \\ N_1 \\ N_2 \\ 1 \end{array} \qquad N_1+N_2=N' \qquad (3.4.12)$$

where V_{S_1} is the potential of the electrode S_1 and V is the applied voltage.

3.5 Numerical Results for SAR's and Electric Fields

Equations (3.3.9) and (3.4.12) can be solved easily by the computer for the total electric field inside a conducting body and the density of induced charge on the electrodes. In this section the numerical results for various geometries shown in Figure 3.1 will be presented. The dimension of the body is chosen to be 6X6X3 cm, and a potential of 2 volts at 15 MH_z is applied between the electrodes. The gap between the electrode and the body in each case is assumed to be 2.5 mm.

Figure 3.4 shows the distributions of the electric charge density along the edge (Y-axis) on the upper electrode for the free space case and the case when a conducting body is introduced between the electrodes. The electrodes have the same dimension (4X4 cm), and a potential difference of 2 volts at 15 MH_z is applied between the electrodes. From Figure 3.4.a it is seen that in the presence of a

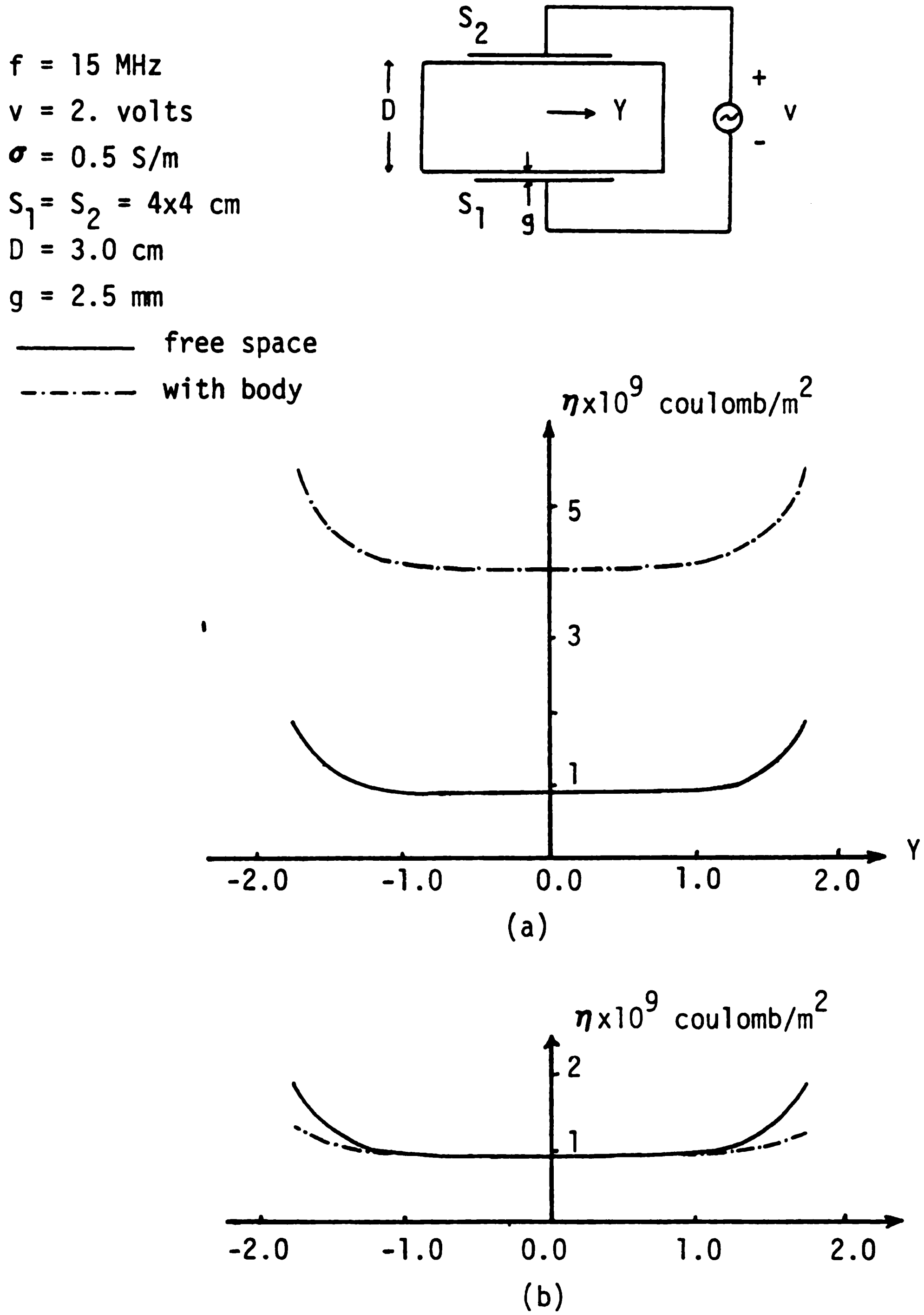

Figure 3.4. The distributions of the electric charge along the Y axis on the electrod for the free space case and the case with a body between the electrodes. In figure (b) the charge distributions are normalized by their maximum values to show the relative variation.

conducting body the induced charge on the electrodes increases greatly as compared to that of the free space case. In Figure 3.4.b, the charge distributions for the cases are hormalized by their maximum values. It is noted that for the case when a conducting body is placed between the electrodes, the distribution of the charge on the electrodes is more uniform than that of the free space case.

In Figure 3.5 the electrodes of equal dimension (4X4 cm) with floating potentials are used to heat the body. One quarter of the body is divided into three layers and each layer contains 9 cubic cells of 1 cm^3 volume. The specific absorption rate of energy (SAR), and the components of the total electric field at the center of each cell are shown. It is noted that the electric field, as is expected, is mainly in the X-direction and is uniformly distributed in the body between the electrodes. The magnitude of the electric field drops drastically in the region of body outside the electrodes. This phenomenon is important in practical applications where it is required to focus the EM energy in a desired region of a biological body for the purpose of local heating.

Figure 3.6 shows the distributions of SAR's, and electric fields in various body cells when the lower of the two identical electrodes (4X4 cm) is grounded. It is seen that unlike the floating potential case the shown quantities are not equal in the first and the third layers. Instead, the SAR's are maximum near the upper electrode and decrease along the X-axis towards the lower electrode.

In Figure 3.7 the distributions of SAR's and electric fields in various cells are shown for the case when the electrodes of different dimensions are placed across the body. The upper electrode is 2 x 2 cm

Electrode-body gap = 2.5 mm

$\epsilon_r = 80$

$\sigma = 0.5$ S/m

f = 15 MHz

V = 2. volts

$S_1 = S_2 = 4x4$ cm

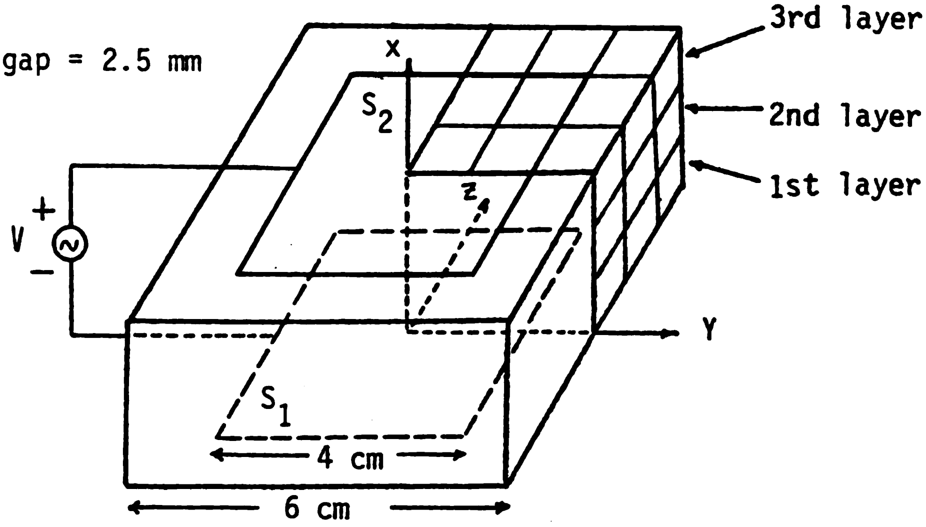

1st layer

4.4	3.5	0.6
122.2	121.4	3.5
121.7	122.2	4.4

2nd layer

4.6	3.8	6.7
120.0	119.0	3.8
121.0	120.0	4.6

3rd layer

4.4	3.8	6.7
122.2	121.4	3.5
121.7	122.2	4.4

Absorbed power density (μWatt/Kgm)

13.0 0.0 0.8	11.0 0.1 0.9	4.0 0.2 0.2
69.0 0.1 0.4	69.0 0.5 0.5	11.0 0.9 0.1
69.0 0.1 0.1	69.0 0.4 0.1	13.0 0.8 0.0

13.0 0.0 0.0	12.0 0.0 0.0	5.0 0.0 0.0
69.0 0.0 0.0	69.0 0.0 0.0	12.0 0.0 0.0
69.0 0.0 0.0	69.0 0.0 0.0	13.0 0.0 0.0

13.0 0.0 0.8	11.0 0.1 0.9	4.0 0.2 0.2	E_x E_y E_z
69.0 0.1 0.4	69.0 0.5 0.5	11.0 0.9 0.1	
69.0 0.1 0.1	69.0 0.4 0.1	13.0 0.8 0.0	

components of the induced electric field (E_x , E_y , E_z)(10mv/m)

Figure.3.5. Distributions of SAR and induced electric field in one quarter of a body maintained by a capacitor plate applicator with electrodes of-the same size.

Electrode-body gap = 2.5 mm

$\epsilon_r = 80$

$\sigma = 0.5$ S/m

f = 15 MHz

V = 2. volts

$S_1 = S_2 = 4\text{x}4$ cm

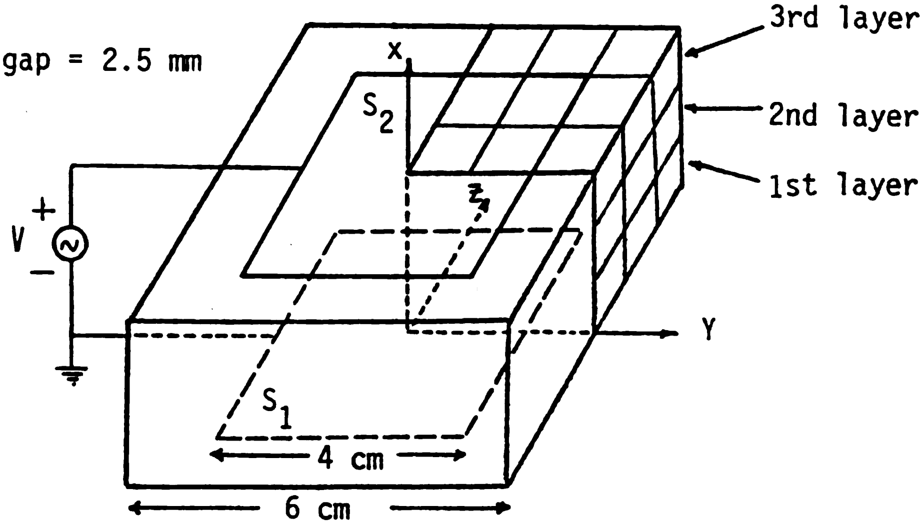

1st layer

5.4	5.5	3.9
98.0	95.0	5.5
101.0	98.0	5.4

2nd layer

5.2	4.8	1.9
121.4	120.8	4.8
121.1	121.4	5.2

3rd layer

5.5	5.4	2.2
150.2	154.6	5.4
144.1	150.2	5.5

Absorbed power density (μWatt/Kgm)

1st layer

13.0 1.0 5.0	12.0 5.0 6.0	7.0 7.0 7.0
62.0 1.0 4.0	61.0 5.0 5.0	12.0 6.0 5.0
63.0 1.0 1.0	62.0 4.0 1.0	13.0 5.0 1.0

2nd layer

13.0 1.0 4.0	12.0 4.0 5.0	5.0 5.0 5.0
69.0 1.0 4.0	69.0 5.0 5.0	12.0 5.0 4.0
69.0 1.0 1.0	69.0 4.0 1.0	13.0 4.0 1.0

3rd layer

12.0 1.0 7.0	11.0 5.0 8.0	1.0 6.0 6.0	E_x E_y E_z
77.0 2.0 5.0	78.0 6.0 6.0	11.0 8.0 1.0	
75.0 1.0 1.0	77.0 5.0 1.0	12.0 7.0 1.0	

components of the induced electric field (E_x , E_y , E_z)(10mv/m)

Figure 3.6. Distributions of SAR and induced electric field in one quarter of a body maintained by a capacitor-plate applicator with electrodes of the same size and one electrode grounded.

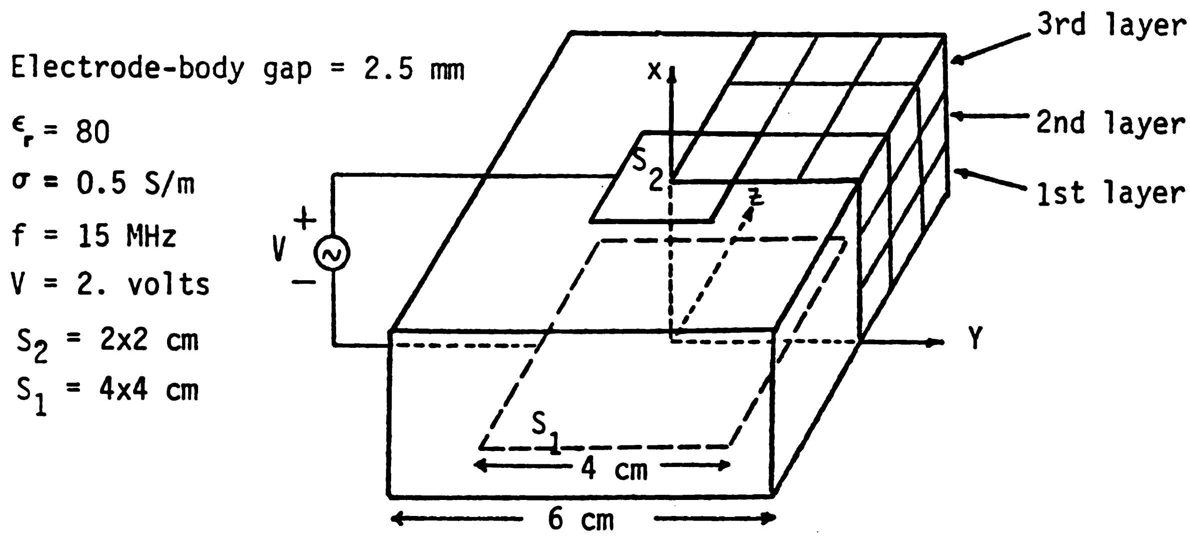

1st layer

0.6	0.4	0.0
16.0	9.8	0.4
68.3	16.0	0.6

2nd layer

0.4	0.2	0.0
12.4	5.2	0.2
116.9	12.4	0.4

3rd layer

0.28	0.16	0.0
9.96	2.16	0.16
186.6	9.96	0.28

Absorbed power density (μWatt/Kgm)

4.0 0.8 1.0	3.0 0.9 1.0	1.0 0.2 0.2
24.0 0.6 5.0	19.0 0.0 0.0	3.0 1.0 0.9
51.0 3.0 3.0	24.0 5.0 0.6	4.0 1.0 0.8

3.0 0.8 2.0	3.0 0.9 0.7	1.0 0.2 0.2
21.0 0.6 5.0	14.0 0.1 0.1	3.0 0.7 0.9
67.0 4.0 4.0	21.0 5.0 0.6	3.0 2.0 0.8

1.0 1.0 2.0	2.0 1.0 1.0	1.0 0.1 0.1	E_x E_y E_z
17.0 0.9 8.0	9.0 0.5 0.5	2.0 1.0 1.0	
85.0 4.0 4.0	17.0 8.0 0.9	1.0 2.0 1.0	

components of the induced electric field (E_x , E_y , E_z)(10mv/m)

Figure 3.7. Distributions of SAR and induced electric field in one quarter of a body maintained by a capacitor-plate applicator with electrodes of different sizes.

and the lower one is 4 X 4 cm and the potentials of the electrodes are left floating. The interesting observation is that like in the free space case, the intensity of the electric field is maximum near the smaller electrode and decreases rather rapidly along the X-axis towards the lower larger electrode. As a result the absorbed power is maximum near the smaller electrode. Similar phenomenon occurs when the lower larger electrode is grounded (Figure 3.8). In this case the concentration of the power density near the smaller electrode becomes even more significant compared to the floating potential case.

In Figure 3.9 a heterogeneous body with an embedded tumor is placed between two electrodes of equal dimension (4 X 4 cm). The conductivity of the tumor is assumed to be 0.35 S/m, and that of the surrounding cells is 0.5 S/m. It is seen that the absorbed power in the tumor is greater than that of the neighboring cells. On the other hand, if the conductivity of the tumor is higher than that of the surrounding cells, less power will be absorbed by the tumor. The numerical results for this case are shown in Figure 3.10 where the conductivity of the tumor is assumed to be 0.65 S/m.

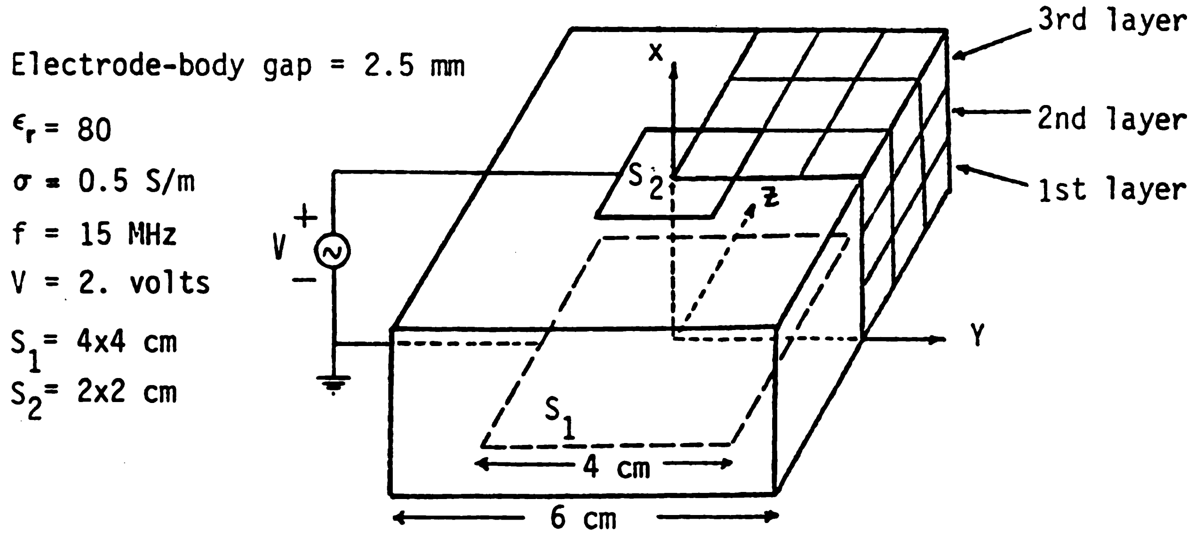

1st layer

0.9	0.4	0.4
10.4	4.4	0.4
60.1	10.4	0.9

2nd layer

0.6	0.3	0.2
9.2	2.6	0.3
116.8	9.2	0.6

3rd layer

0.6	0.2	0.2
10.0	1.5	0.2
201.6	10.0	0.6

Absorbed power density (μWatt/Kgm)

4.0	3.0	2.0	2.0	2.0	1.0	0.9	0.9	0.1	E_x
1.0	2.0	2.0	1.0	2.0	2.0	1.0	3.0	2.0	E_y
4.0	1.0	2.0	3.0	0.8	2.0	4.0	1.0	2.0	E_z
18.0	13.0	3.0	17.0	10.0	2.0	16.0	6.0	0.9	
1.0	1.0	1.0	1.0	1.0	0.8	1.0	2.0	1.0	
7.0	1.0	2.0	7.0	1.0	2.0	10.0	2.0	3.0	
48.0	18.0	4.0	68.0	17.0	2.0	89.0	16.0	0.9	
4.0	7.0	4.0	4.0	7.0	3.0	5.0	10.0	4.0	
4.0	1.0	1.0	4.0	1.0	1.0	5.0	1.0	1.0	

components of the induced electric field (E_x , E_y , E_z)(10mv/m)

Figure 3.8. Distributions of SAR and induced electric field in one quarter of a body maintained by a capacitor-plate applicator with electrodes of different sizes and one electrode grounded.

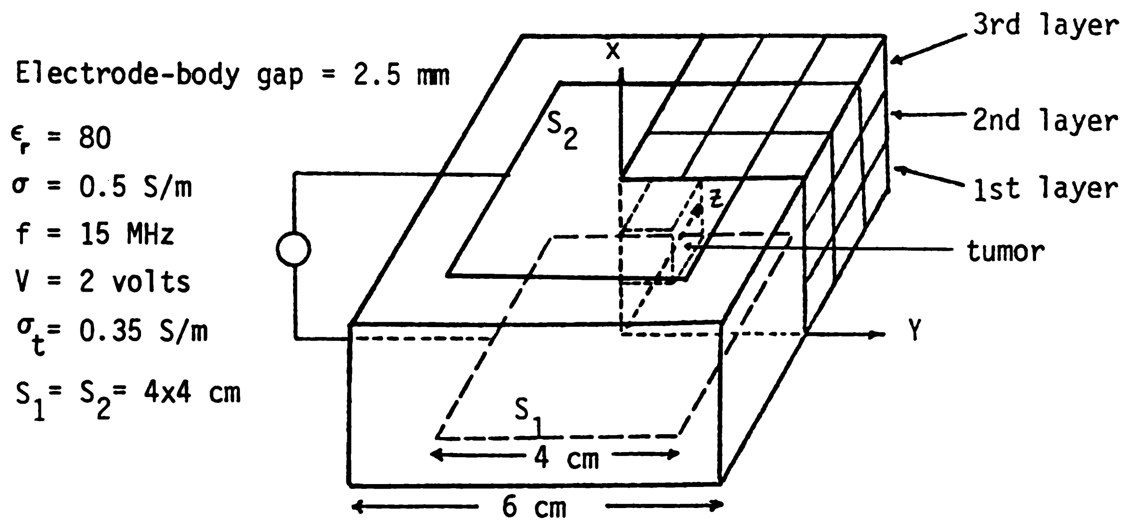

1st layer

4.4	3.5	0.6
122.2	121.4	3.5
121.4	122.2	4.4

2nd layer

4.6	3.8	0.7
120.8	119.5	3.8
169.1	120.8	4.6

3rd layer

4.4	3.5	0.6
122.2	121.4	3.5
121.4	122.2	4.4

Absorbed power density (Watt/Kgm)

13.0 0.0 0.8	11.0 0.1 0.9	4.0 0.2 0.2
69.0 0.1 0.4	69.0 0.5 0.5	11.0 0.9 0.1
69.0 0.1 0.1	69.0 0.4 0.1	13.0 0.8 0.0

13.0 0.0 0.0	12.0 0.0 0.0	5.0 0.0 0.0
69.0 0.0 0.0	65.0 0.0 0.0	12.0 0.0 0.0
98.0 0.0 0.0	69.0 0.0 0.0	13.0 0.0 0.0

13.0 0.0 0.8	11.0 0.1 0.9	4.0 0.2 0.2	E_x E_y E_z
69.0 0.1 0.4	69.0 0.5 0.5	11.0 0.9 0.1	
69.0 0.1 0.1	69.0 0.4 0.1	13.0 0.8 0.0	

components of the induced electric field (E_x , E_y , E_z)(10mv/m)

Figure 3.9. Distributions of SAR and induced electric field in one quarter of a heterogeneous body, alower conductivity region at the center . maintained by a capacitor-plate applicator with electrodes of the same size.

Electrode-body gap = 2.5 mm

$\epsilon_r = 80$

$\sigma = 0.5$ S/m

f = 15 MHz

V = 2. volts

$\sigma_t = 0.65$ S/m

$S_1 = S_2 = 4x4$ cm

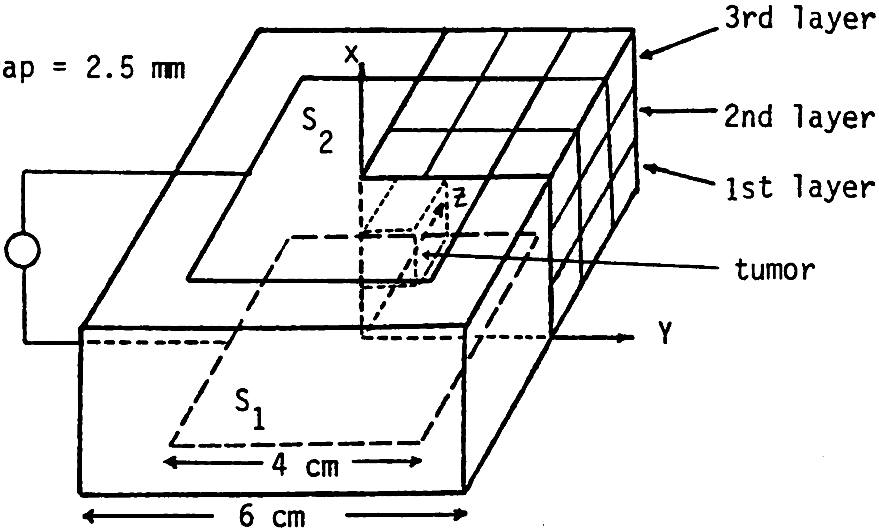

1st layer

4.4	3.5	0.6
122.2	121.4	3.5
121.8	122.2	4.4

2nd layer

4.6	3.8	0.7
120.8	119.4	3.8
93.8	120.8	4.6

3rd layer

4.4	3.5	0.6
122.2	121.4	3.5
121.8	122.2	4.4

Absorbed power density (μ Watt/Kgm)

13.0 0.0 0.8	11.0 0.1 0.9	4.0 0.2 0.2
69.0 0.1 0.4	69.0 0.5 0.5	11.0 0.9 0.1
69.0 0.1 0.1	69.0 0.4 0.1	13.0 0.8 0.0

13.0 0.0 0.0	12.0 0.0 0.0	5.0 0.0 0.0
69.0 0.0 0.0	69.0 0.0 0.0	12.0 0.0 0.0
53.0 0.0 0.0	69.0 0.0 0.0	13.0 0.0 0.0

13.0 0.0 0.8	11.0 0.1 0.9	4.0 0.2 0.2	E_x E_y E_z
69.0 0.1 0.4	69.0 0.5 0.5	12.0 0.9 0.1	
69.0 0.1 0.1	69.0 0.4 0.1	13.0 0.8 0.0	

components of the induced electric field (E_x , E_y , E_z)(10mv/m)

Figure 3.10. Distributions of SAR and induced electric field in one quarter of a heterogeneous body, a higher conductivity region at the center, maintained by a capacitor-plate applicator with electrodes of the same size.

3.6 Synthesis of the Potential Distribution for Selective Heating

Theoretically it is possible to sythesize the voltage distribution on the electrodes in such a way that the induced electric field vanishes everywhere inside the body except in a specific cell. In this section we attempt to find the scheme for such a synthesis.

A system of linear equations for the induced electric field inside the body and the induced charge density on the electrodes was developed in section 3.4. This is rewritten here for convenience:

$$\left[\begin{array}{ccc:c} & G & & A \\ \hdashline C' & 0 & 0 & G^S \end{array}\right] \left[\begin{array}{c} E_X \\ \hdashline E_Y \\ \hdashline E_Z \\ \hdashline \eta_1 \\ \vdots \\ \eta_{N'} \end{array}\right] = \left[\begin{array}{c} 0 \\ \vdots \\ 0 \\ \hdashline V_1 \\ V_2 \\ \vdots \\ V_{N'} \end{array}\right] \qquad (3.6.1)$$

The elements of the matrices G, G^S, A, C' were all defined earlier in this chapter.

The equation (3.6.1) can be decomposed into the following two systems.

$$\left[\; G \;\right] \begin{bmatrix} E_X \\ E_Y \\ E_Z \end{bmatrix} + \left[\; A \;\right] \begin{bmatrix} \eta_1 \\ \vdots \\ \eta_{N'} \end{bmatrix} = 0 \qquad (3.6.1.a)$$

Where [G] is a 3NX3N matrix, and [A] is 3NXN' and

$$\begin{array}{cc} & \begin{array}{cc} \overbrace{\qquad\qquad\qquad}^{3N} & \overbrace{\qquad\quad}^{N'} \end{array} \\ N' & \left[\begin{array}{c:c:c:c} C' & 0 & 0 & G^S \end{array}\right] \end{array} \begin{array}{c} \left[\begin{array}{c} E_X \\ \hdashline E_Y \\ \hdashline E_Z \\ \hdashline \eta_1 \\ \cdot \\ \cdot \\ \eta_{N'} \end{array}\right] \end{array} \begin{array}{l} \left.\begin{array}{c} \\ \\ \\ \end{array}\right\} 3N \\ \left.\begin{array}{c} \\ \\ \\ \end{array}\right\} N' \end{array} = \begin{array}{cc} \left[\begin{array}{c} V_1 \\ V_2 \\ \cdot \\ V_{N'} \end{array}\right] & N' \end{array} \tag{3.6.1.b}$$

We demand that the induced electric field $\vec{E}(\vec{r}_m) = \hat{x}1$ V/m in the m^{th} body cell and zero elsewhere. Thus, (3.6.1.a) reduces to

$$\begin{array}{cc} & N' \\ 3N & \left[\begin{array}{c} \\ \\ A \\ \\ \\ \end{array}\right] \end{array} \left[\begin{array}{c} \eta_1 \\ \cdot \\ \cdot \\ \eta_{N'} \end{array}\right] = \left[\begin{array}{c} G(m,1) \\ G(m,2) \\ \cdot \\ \cdot \\ \cdot \\ G(m,3N) \end{array}\right] \tag{3.6.2}$$

In order that the equation (3.6.2) can be solved for η uniquely, the number of equations must be equal to the number of unknowns. In other words, the matrix [A] must be a square matrix. This is possible only when

$$3N = N'$$

or the number of surface subareas is three times the number of body cells. Satisfying this condition, we find from (3.6.2)

$$3N \begin{bmatrix} \eta_1 \\ \cdot \\ \cdot \\ \cdot \\ \eta_{N'} \end{bmatrix} = \begin{bmatrix} & & \\ & A & \\ & & \end{bmatrix}^{-1}_{3N} \begin{bmatrix} G(m,1) \\ G(m,2) \\ \cdot \\ \cdot \\ G(M,3N) \end{bmatrix} \tag{3.6.3}$$

once η's are determined from (3.6.3), the potential at any subarea on the electrodes can be calculated from (3.6.1.b).

3.7 Numberical Results for Synthesized Voltage Distributions

Based on the discussion in the preceding section, the distributions of potentials on the electrodes required to produce a localized induced electric field inside the body is calculated for three cases, and the results are presented here.

Figure 3.11 shows the geometry of a body with dimension (6X6X9 cm) placed in between two electrodes of equal dimension (4.8X4.8 cm). One eighth of the body is divided into three layers with four cells (1 cm^3) in each layer. One quarter of the upper electrode is divided into 6 rows each containing 6 subarea cells. The desired patterns for the induced electric field in different layers of the body are shown in the figure as well; where $\vec{E} = 1\hat{x}$ in the cell located at the center of the body and zero elsewhere. The distribution of the potential on one quarter of the upper electrode which is required to produce the desired pattern of the induced electric field is shown in Figure 3.12. This figure indicates that the required voltages of

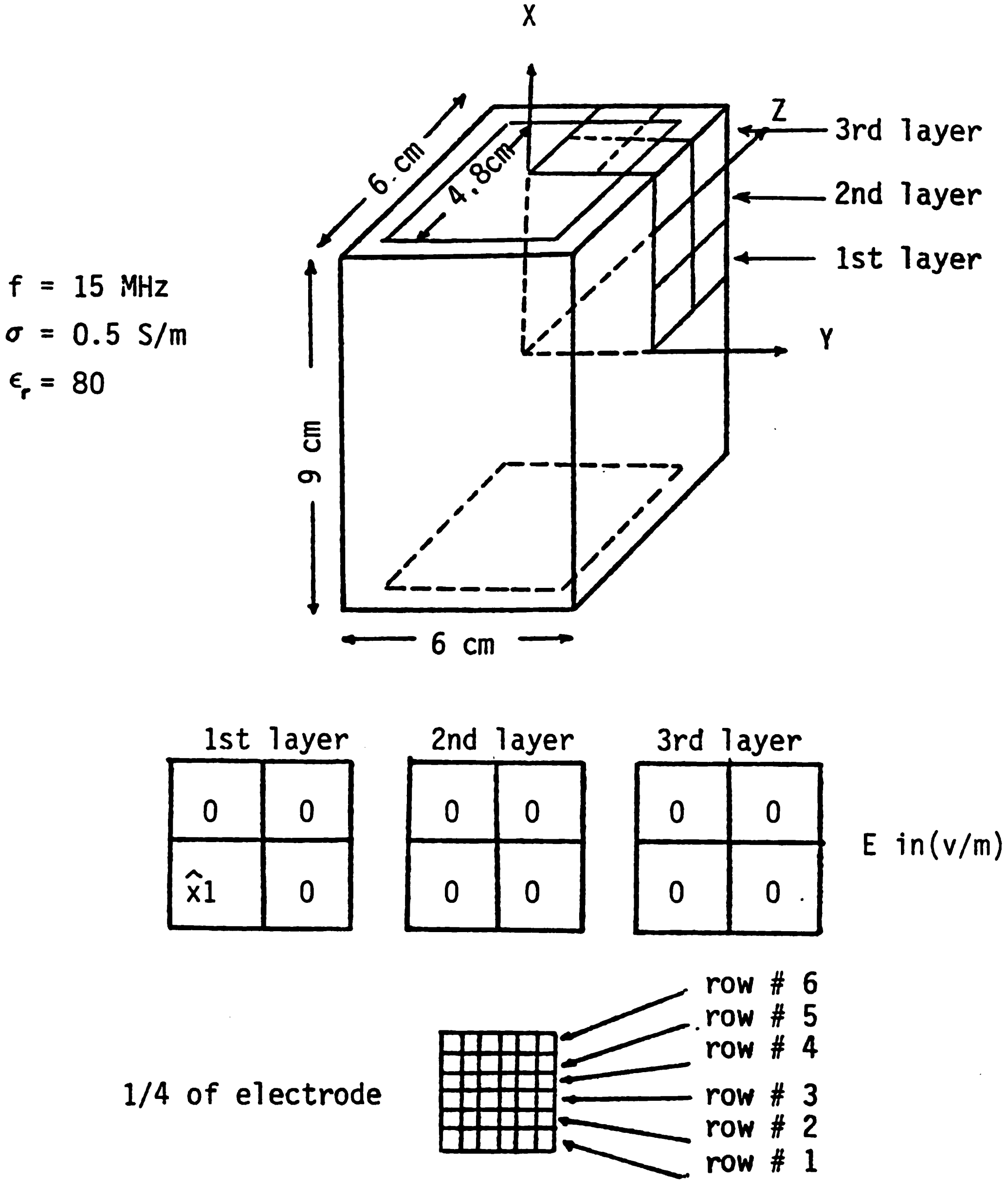

Figure 3.11.Geometry of body and a capacitor- plate applicator with subsectioned electrodes for localized heating at the center of the body. The distribution of required voltages is shown in the next figure.

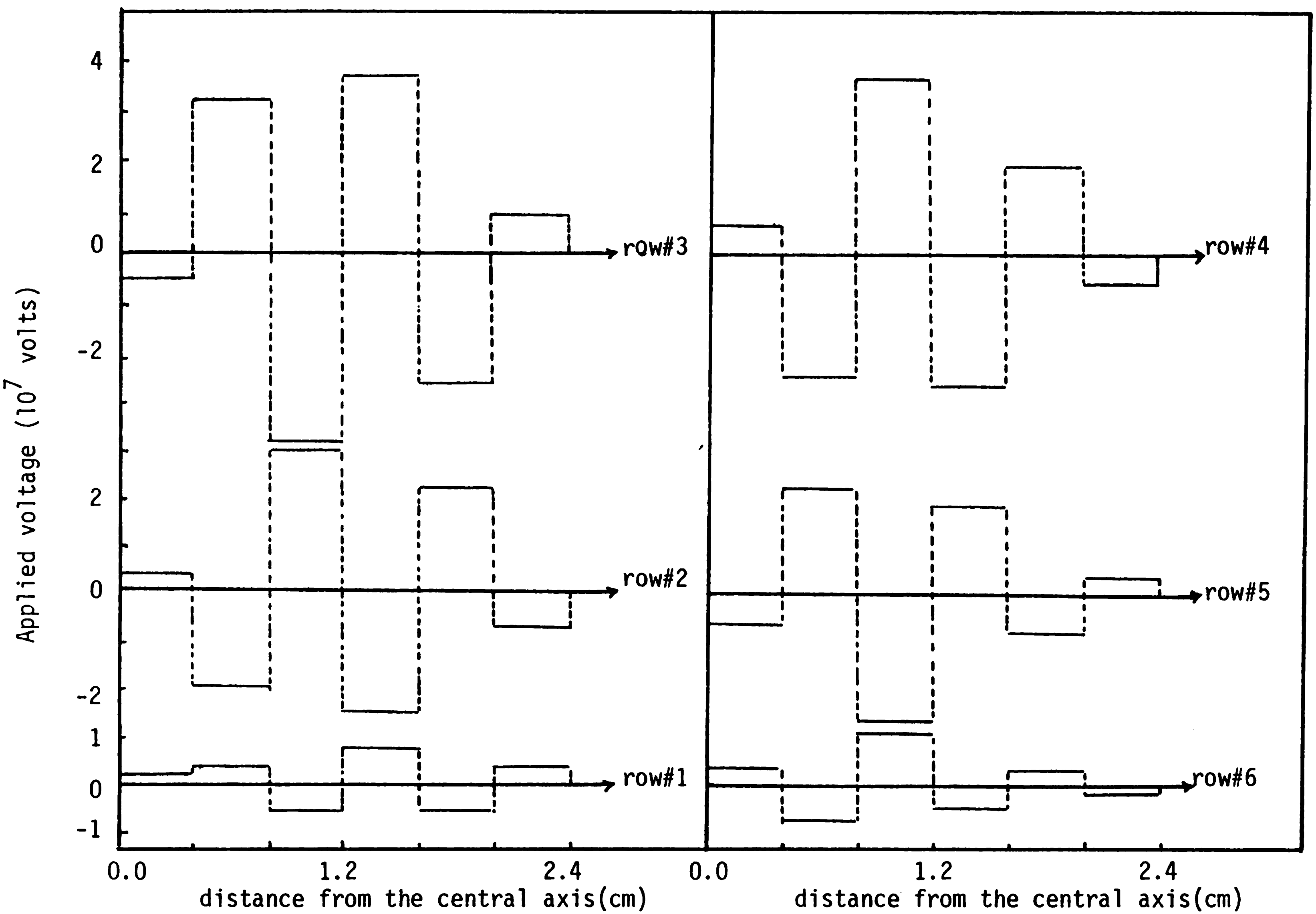

Figure 3.12. Distributions of the required voltages on the electrodes to obtain a localized heating at the center of the body.

neighboring sub-electrodes alternate their signs, and the amplitudes of the required voltages are very high. It is also found that this distribution of the required voltages is extremely unstable in that a small error in the required voltages will lead to a quite different pattern of induced electric field than that specified in Figure 3.11.

Figure 3.13 shows the case where a localized electric field of $1\hat{x}$ V/m is induced in the cell located at the centers of the body surfaces which face the electrodes. The required potential distribution on different rows of sub-electrodes is shown in Figures 3.14(a) and 3.14(b). Again, a voltage distribution of alternating signs between neighboring sub-electrodes is required. However, the magnitude of the required voltages is considerably smaller than the case of Figure 3.12. Finally, Figure 3.15 shows the case when the induced electric field is to be concentrated in the central column of the body along the X axis. The amplitude and the phase distributions of the required potential are shown in Figures 3.16 and 3.17. The required potential distribution for this case is considerably smaller in magnitude than the two previous cases where a localized electric field is to be induced in an isolated cell.

The theoretical results obtained in this section may not have easy practical applications because the required voltage distribution is of very high magnitude and with a rapid phase variation. However, with the advent of computer technology, the implementation of such a voltage distributions may not be a very difficult task.

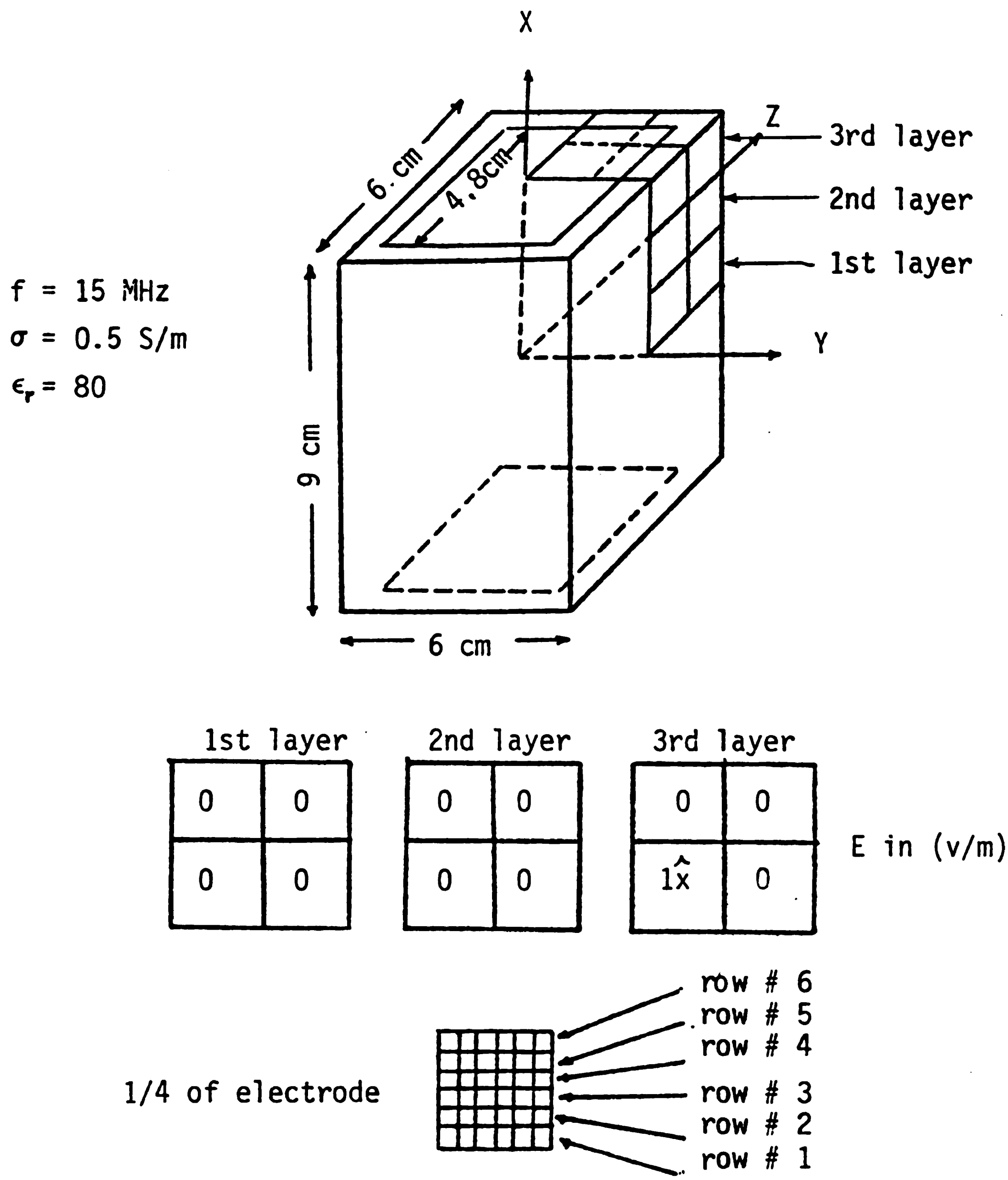

Figure 3.13. Geometry of a body and a capacitor-plate applicator with subsectioned electrodes for localized heating at the - center of the body surface. The distribution of the required voltages on the electrodes is shown in next figures.

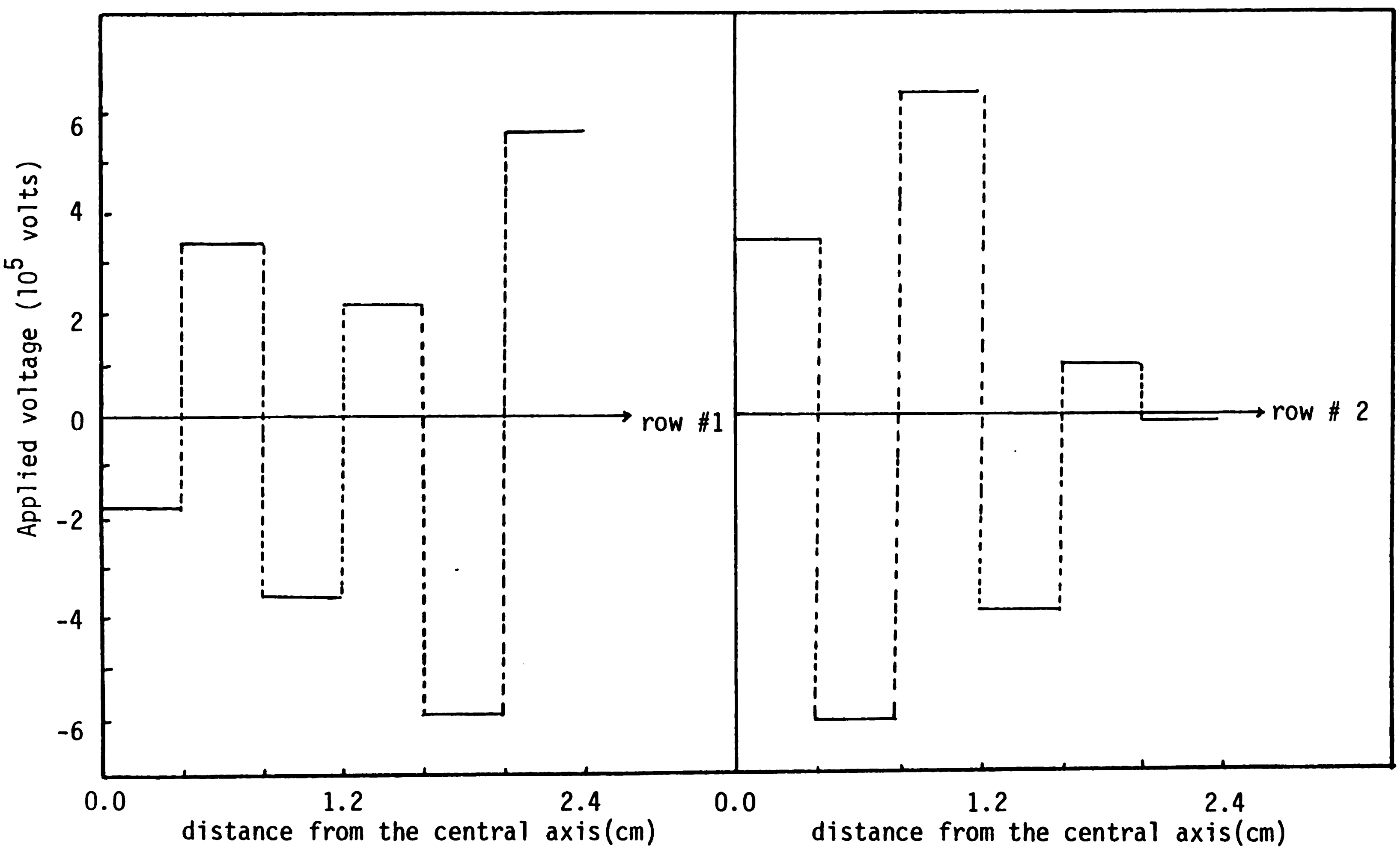

Figure 3.14.a Distributions of the required voltages on the electrodes to obtain a localized heating at the center of the body surface.

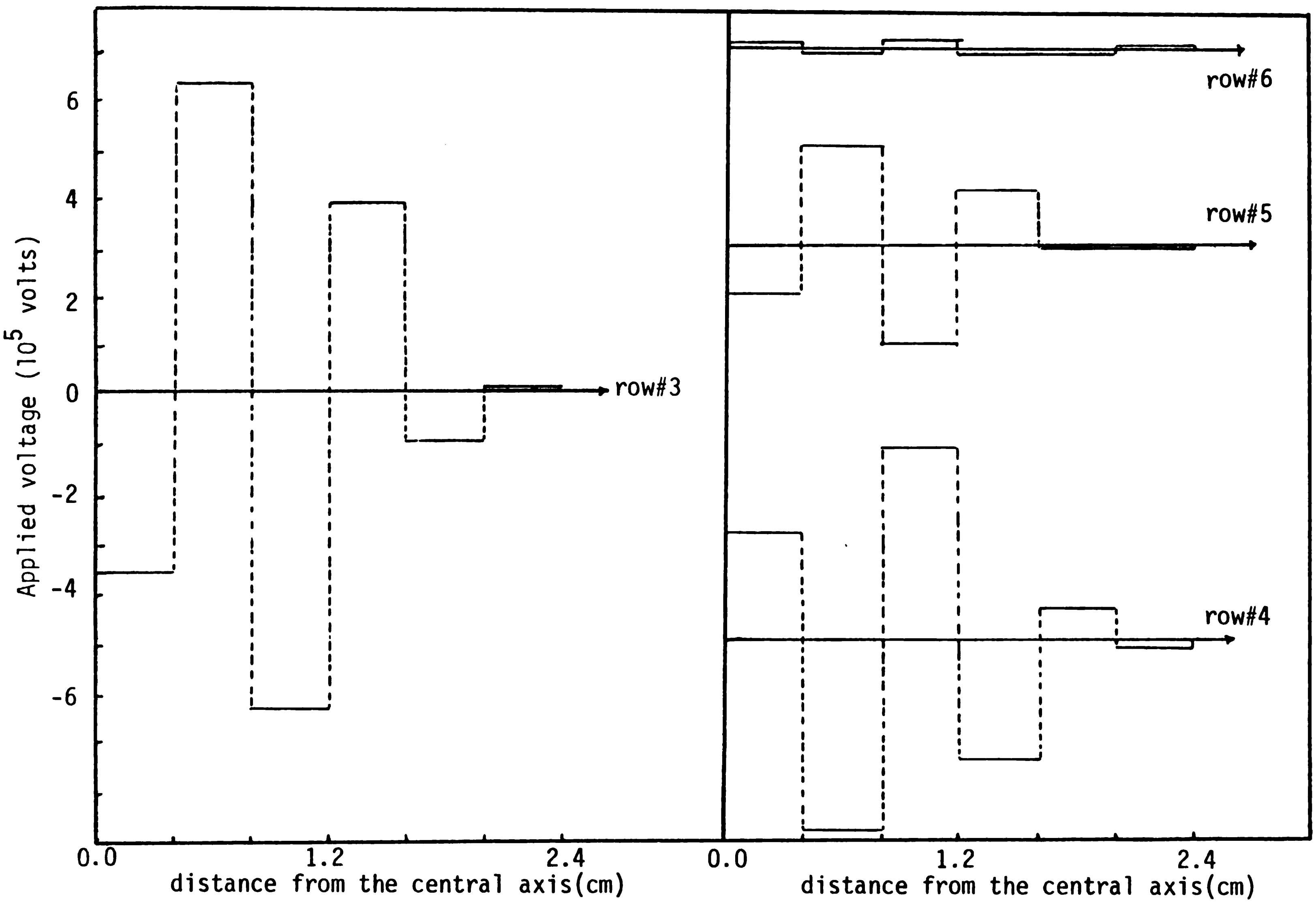

Figure 3.14.b. Distributions of the required voltages on the electrodes to obtain a localized heating at the center of the body.

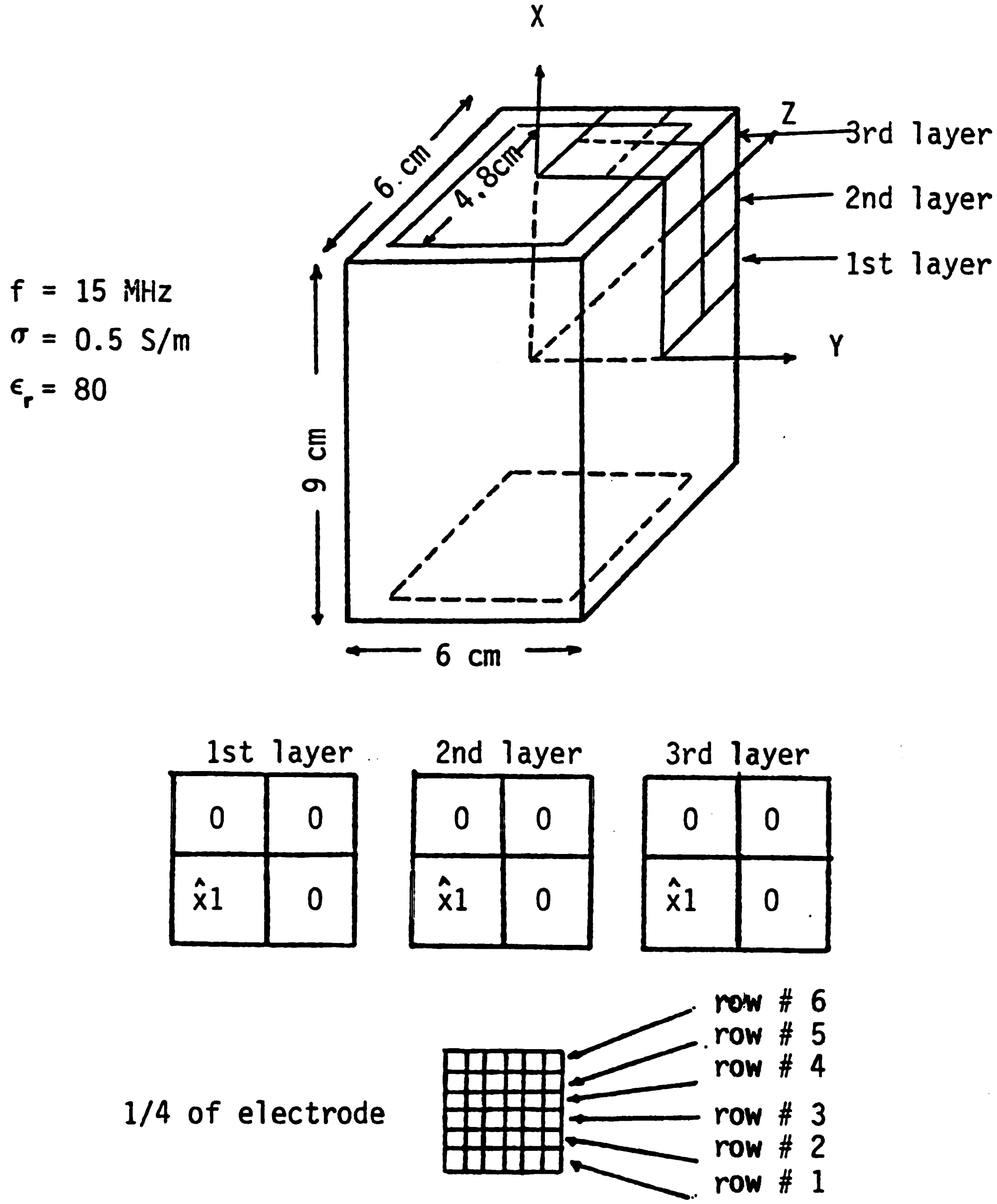

Figure 3.15. Geometry of a body and capacitor-plate applicator with subsectioned electrodes for localized heating at the - central column of the body. The distribution of required voltages on the electrode is shown in next figures.

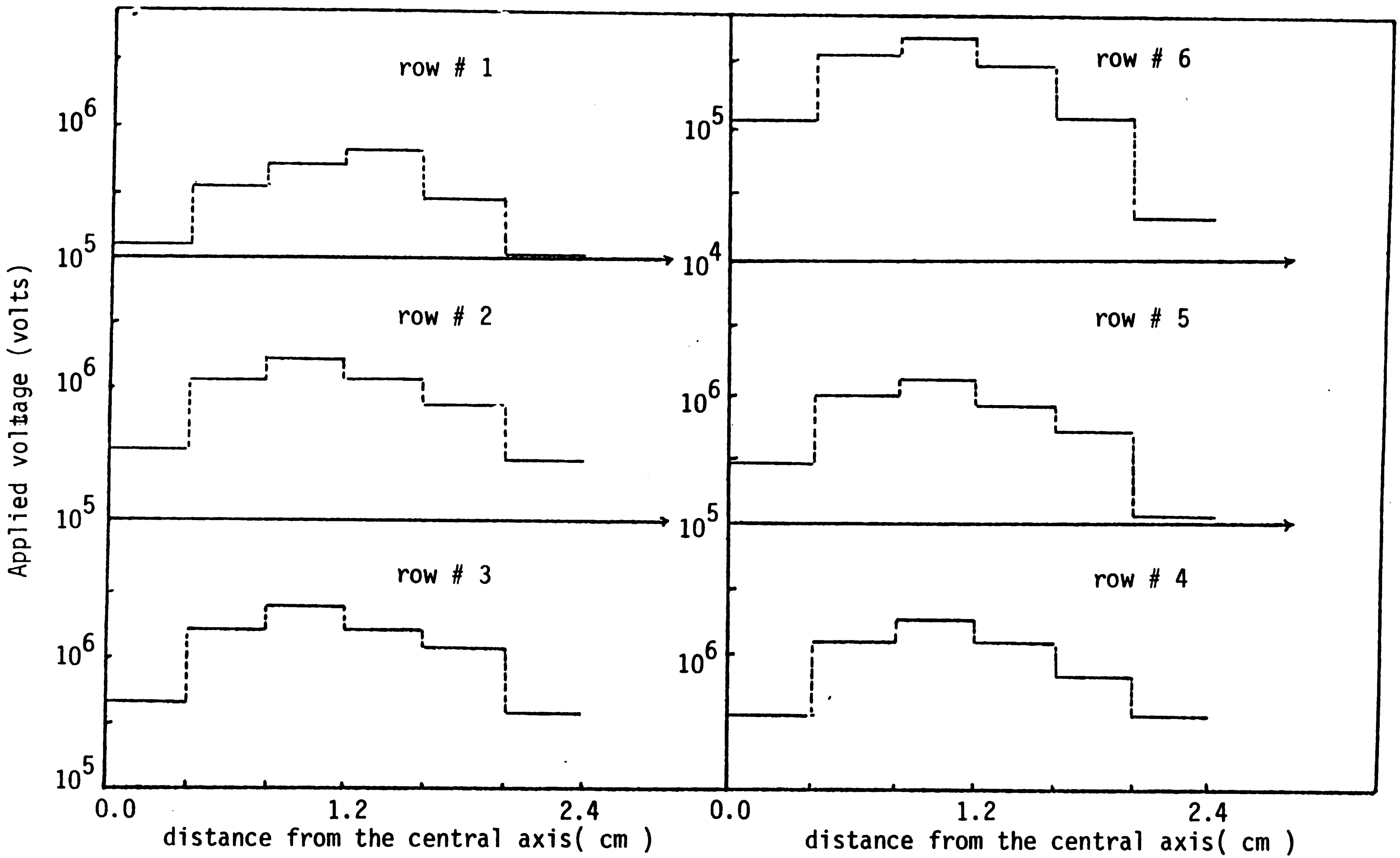

Figure 3.16. Distributions of the amplitude of the required voltage on the electrode to obtain a localized heating at the central column of the body.

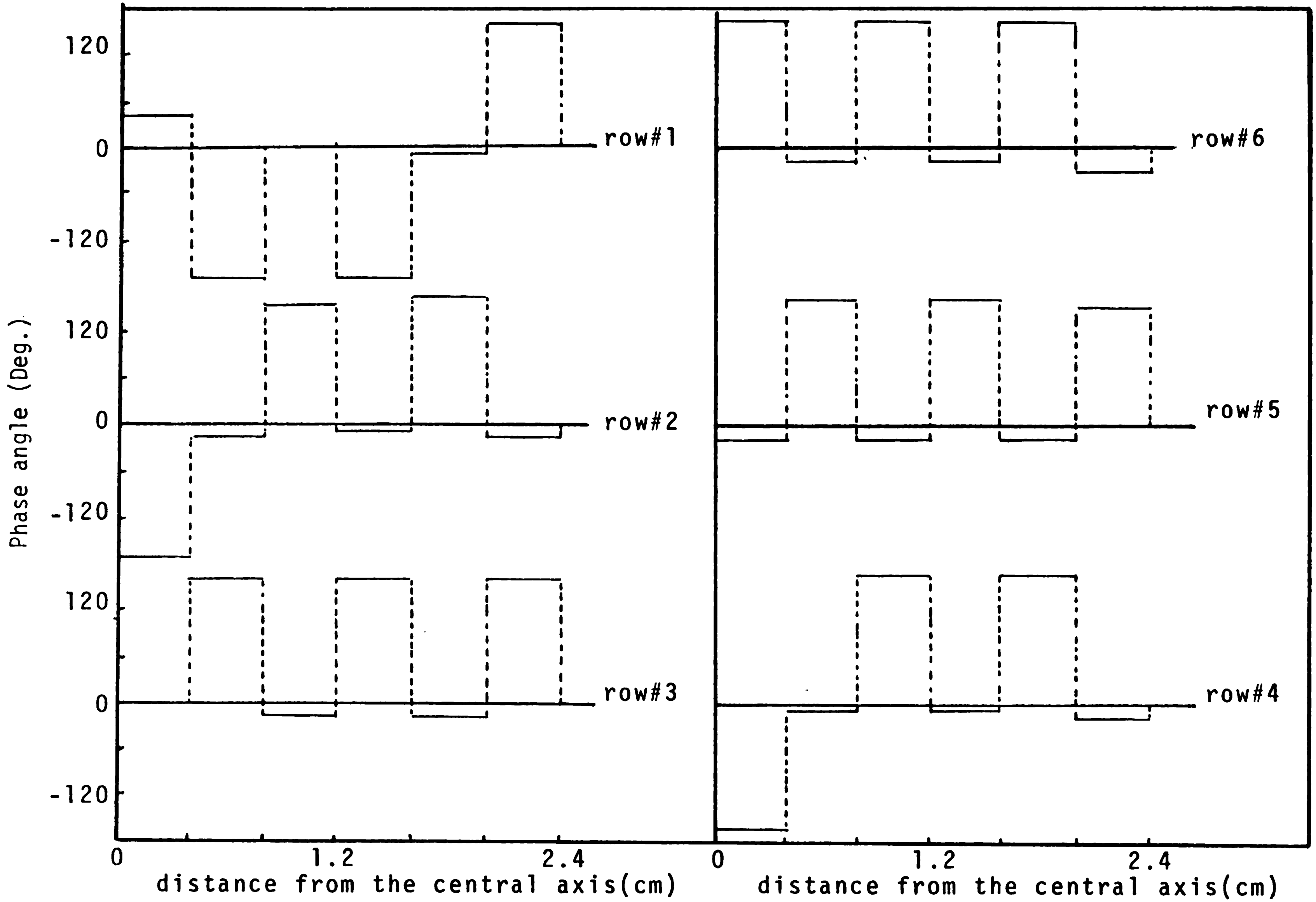

Figure 3.17 Distributions of the phase angle of the required voltage on the electrodes to obtain a localized heating at the central column of the body.

3.8 Comparison of Numerical Results and Experimental Results

To confirm the theoretical results presented in section 3.6 a series of expreiments was conducted to measure the induced electric field inside a simulated biological body, a volume of saline solution, with an implantable electric field probe. Since the experimental set up will be described in Chapter V, only the experimental results will be used here to compare with the numerical results.

Figure 3.18 depicts a body of (8X8X4 cm) dimensions with a conductivity of 0.5 S/m placed between two electrodes of equal dimension (4X4 cm). The spacing between the electrode and the body is 2.5 mm. A potential difference of 2. volts at 20 MHz is applied between the electrodes. The distributions of the theoretical (solid lines) and experimental (discrete points) values of the X-component of the induced electric field inside the body along the Y-axis are shown in Figure 3.18. On the same figure, the corresponding distributions of the X-component of the electric field in free space along the Y-axis are also included. It is seen that there is a good agreement between theory and experiment.

In Figure 3.19 the electrodes of equal dimension (6X6 cm) are placed across a body of dimensions (8X8X8 cm), and a conductivity of 0.5 S/m. The applied voltage and frequency are the same as that in Figure 3.18. The distributions of the theoretical and experimental values of the X-component of the electric fields inside the body along the X-axis are shown. The corresponding results for the free space

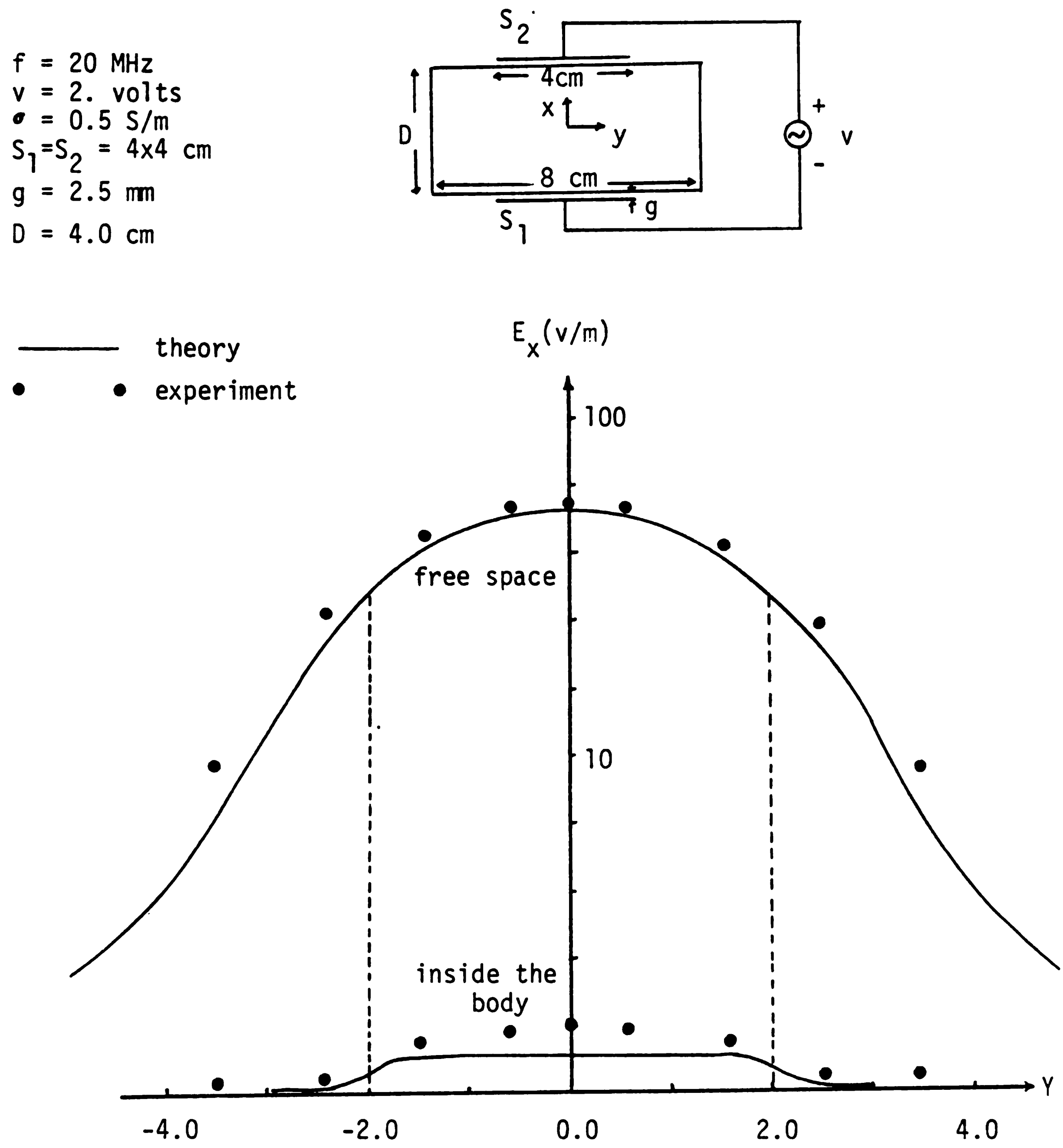

Figure 3.18. Distributions of the theoretical and experimental values of the X-component of electric field along Y axis maintained in the body between two electrodes of equal dimension.

f = 20 MHz

v = 2. volts

σ = 0.5 S/m

$S_1 = S_2$ = 6x6 cm

g = 2.5 mm

——— theory

• • experiment

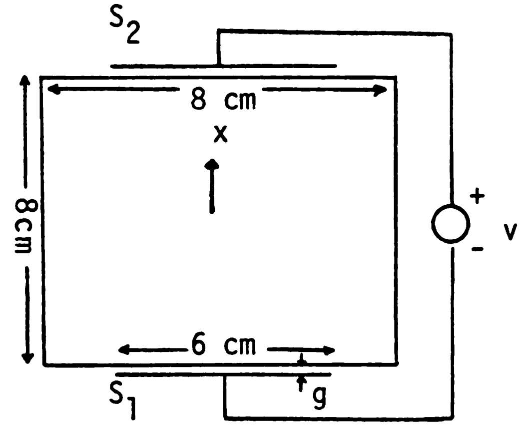

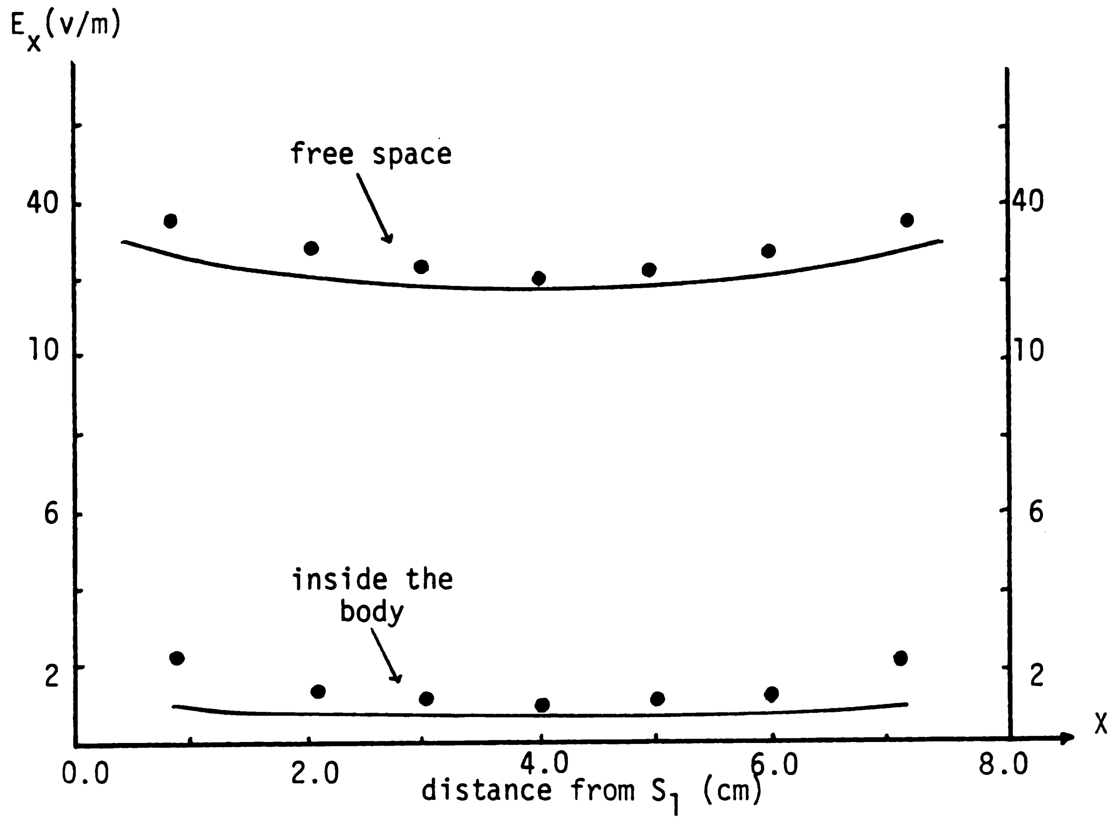

Figure 3.19. Distributions of the theoretical and experimental values of the X-component of electric field along the X axis maintained in the body between two electrodes of equal dimension.

case are also included in the same figures. The distributions of the same quantities for the case when the electrodes are of different dimensions are shown in Figure 3.20. In both cases, Figures 3.19 and 3.20, a good agreement between theory and experiment is observed.

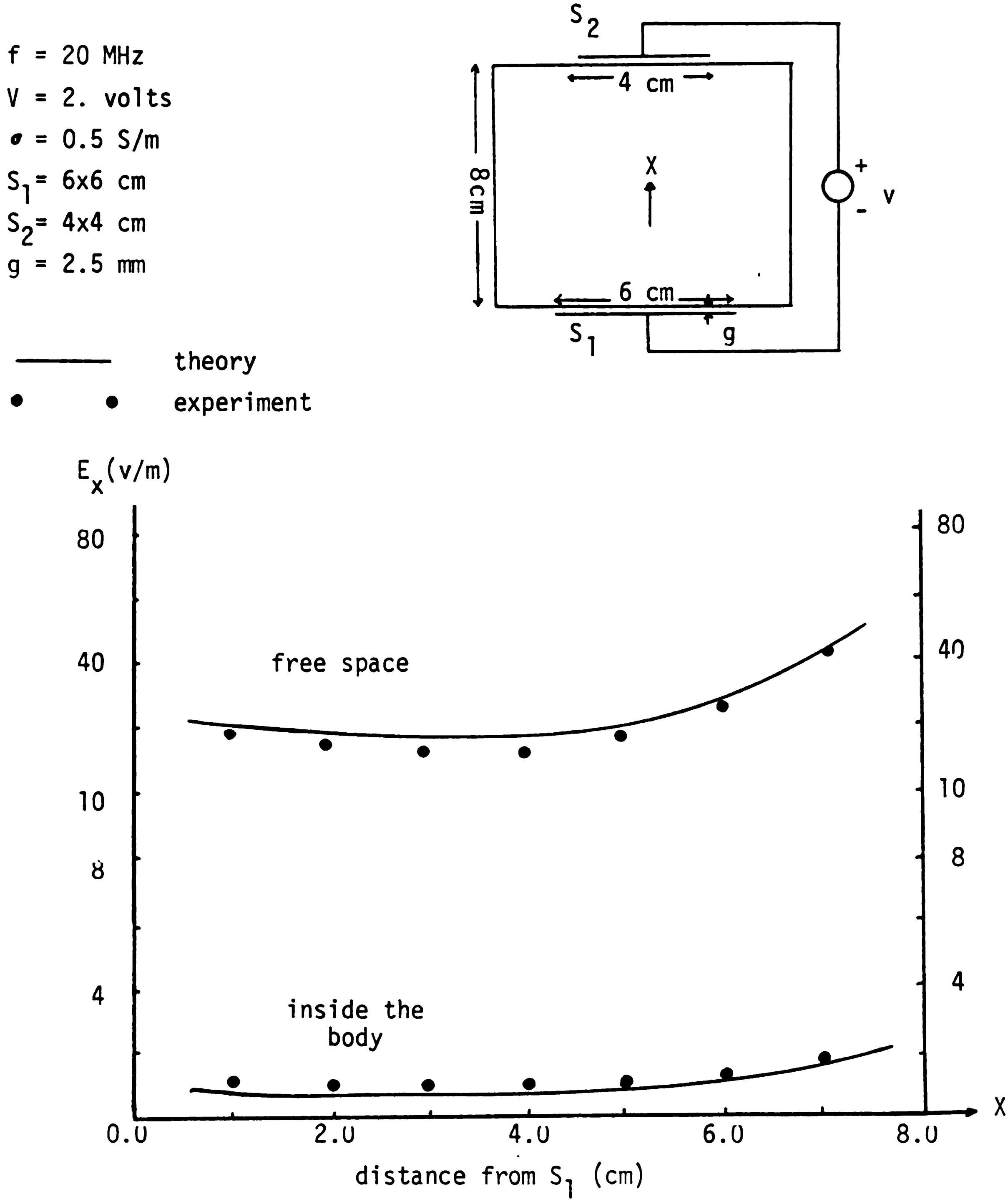

Figure 3.20. Distributions of the theoretical and experimental values of the X-component of electeric field along the X axis maintained in the body between two electrodes of different dimensions.

CHAPTER IV

LOCAL HEATING WITH HF MAGNETIC FIELD

Electromagnetic local heating of a biological body can be accomplished with the application of an HF magnetic field. In fact the utilization of an HF magnetic field provides an important advantage over the use of an HF electric field for not overheating the region under the skin. In this chapter, a pancake, or a current disk, which produces an HF magnetic field for the purpose of FM local heating is studied.

4.1. Introduction

The capacitor plate applicator used for local heating of a biological body was discussed in detail in the preceding chapter. This scheme suffers a major drawback of overheating the fat region under the skin. This difficulty can be explained by considering a biological body consisted of three different layers as shown in Figure 4.1. The layers 1 and 2 represent the skin and the fat layers, and the layer 3 represnets the muscle.

From Maxwell's equations we have

$$\nabla \cdot (\sigma + j\omega \epsilon)\vec{E}(\vec{r}) = 0 \tag{4.1.1}$$

where $\vec{E}(\vec{r})$ is the total electric field inside the body. Integrating (4.1.1) over the volume V enclosed by the surface S as shown in Figure 4.1, and applying the divergence theorem gives.

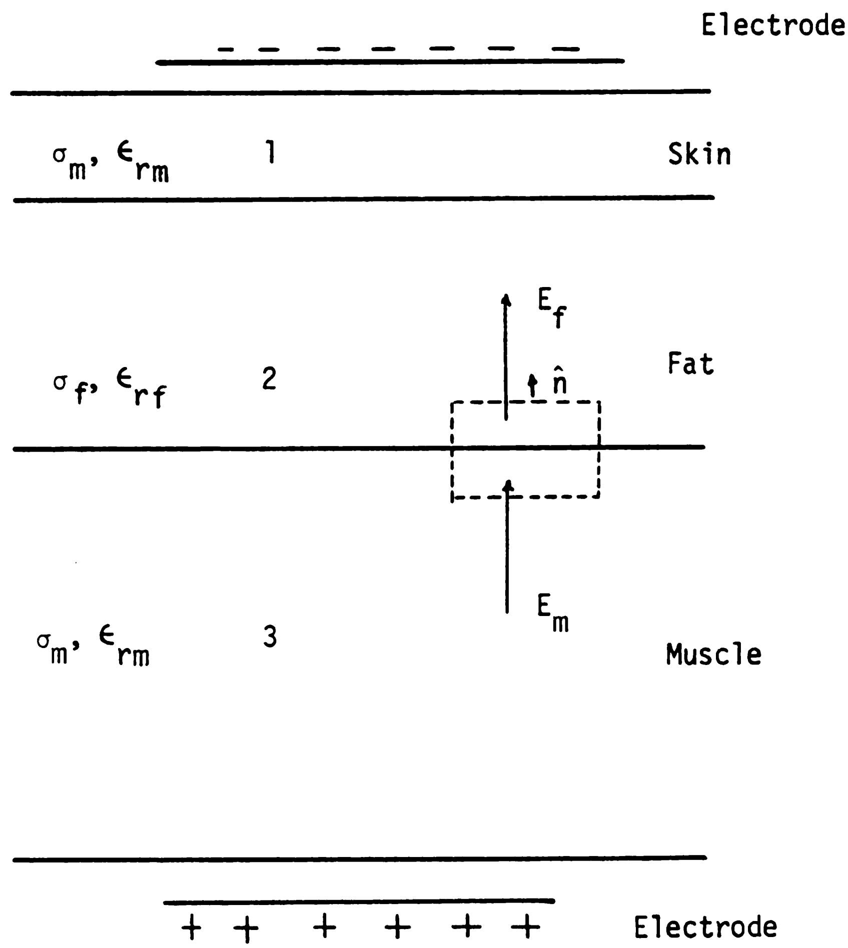

Figure 4.1. A biological body consisted of skin, fat and muscle layers placed between a pair of electrodes for the purpose of local heating.

$$E_m(\sigma_m + j\omega\, \epsilon_o \epsilon_{rm}) = E_f(\sigma_f + j\omega\, \epsilon_o \epsilon_{rf}) \tag{4.1.2}$$

where the subscripts m and f stand for the muscle and the fat layers. Thus, the ratio of the absorbed power density in the muscle layer to that in the fat layer is given by

$$\frac{P_m}{P_f} = \frac{\sigma_m |\vec{E}_m|^2}{\sigma_f |\vec{E}_f|^2} = \frac{\sigma_m |\sigma_f + j\omega\, \epsilon_o \epsilon_{rf}|^2}{\sigma_f |\sigma_m + j\omega\, \epsilon_o \epsilon_{rm}|^2} \tag{4.1.2}$$

For example, at 27.12 MH_z we have [17]

$$\sigma_m = 0.61 \text{ S/m}, \ \epsilon_{rm} = 113$$

$$\sigma_f = 0.11 \sim 0.43 \text{ S/m}, \ \epsilon_{r_f} = 20$$

therefore (4.1.2) gives

$$1.5 \leq \frac{P_f}{P_m} \leq 5.6$$

which implies that the density of the power absorbed in the fat layer is between 1.5 to 5.6 times higher than that absorbed in the muscle layer. Therefore, for the cases when the tumor is located inside the muscle layer, a sever burn may occur in the fat layer before adequate heat can be produced at the tumor.

4.2. Theoretical analysis

The geometry of the problem is shown in Figure 4.2. A circular disk of radius b carrying a circulatory current is placed on the surface of a body with conductivity $\sigma(\vec{r})$, permittivity $\epsilon(\vec{r})$, and permeability μ_o. The density of the current on the disk is represented by $\hat{\varphi}\, K_\varphi(\rho')$. It is assumed that the geometry of the body and disk is

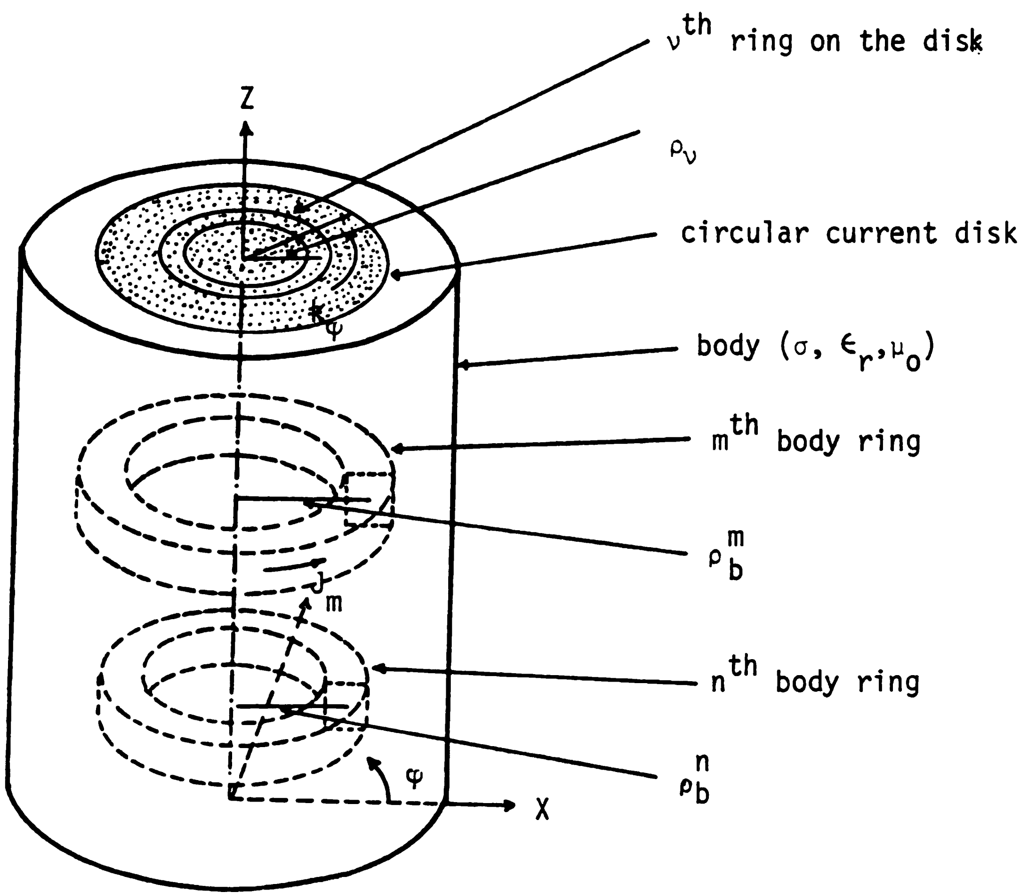

Figure 4.2. Geometry of a circular disk carrying a ciculatory current placed on a body for local heating.

rotationally symmetric, this implies that all quantities are independent of the azimuthal angle φ.

4.2.1 Impressed electric field

The vector potential at any point $\vec{r}$ inside the body maintained by the current is the absence of the body is

$$\vec{A}(\vec{r}) = \frac{\mu_o}{4\pi} \int_{S_d} \hat{\varphi}' \, K_\varphi(\vec{r}') \, \frac{e^{-j\beta_o R(\vec{r},\vec{r}')}}{R(\vec{r},\vec{r}')} \, ds' \tag{4.2.1}$$

where $\vec{r}$ and $\vec{r}'$ are the position vectors for the field and source points, respectively, and S_d represents the surface of the disk. In the cylindrical coordinate system, $R(\vec{r},\vec{r}')$ can be expressed as follows.

$$R(\vec{r},\vec{r}') = [\rho'^2 + \rho^2 - 2\rho\rho' \cos\varphi + (z-L)^2]^{\frac{1}{2}} \tag{4.2.2}$$

where ρ and ρ' are the radial distances of the field and source points from the Z axis and L is the height of the body. Due to the symmetry the field point is chosen at $\varphi = 0$. The unit vector $\hat{\varphi}'$ can be written in terms of the unit vectors $\hat{x}$ and $\hat{y}$ as

$$\hat{\varphi}' = -\hat{x} \sin\varphi' + \hat{y} \cos\varphi' \tag{4.2.3}$$

with (4.2.3), (4.2.1) becomes

$$\vec{A}(\rho,z) = \frac{\mu_o}{4\pi} [-\hat{x} \int_0^b K_\varphi(\rho')\rho' d\rho' \int_0^{2\pi} \sin\varphi' \, \frac{e^{-j\beta_o R(\vec{r},\vec{r}')}}{R(\vec{r},\vec{r}')} \, d\varphi'$$
$$+ \hat{y} \int_0^b K_\varphi(\rho')\rho' d\rho' \int_0^{2} \cos\varphi' \, \frac{e^{-j\beta_o R(\vec{r},\vec{r}')}}{R(\vec{r},\vec{r}')} \, d\varphi'] \tag{4.2.4}$$

The first term on the right hand side of (4.2.4) integrates to zero, since the integrand of the inner integral is an odd function of φ'. Thus, the impressed electric field $\vec{E}^i$ at any point is

$$\vec{E}^i(\rho,z) = -j\omega\vec{A}(\rho,z) = -\hat{\varphi}\frac{j\omega\mu_o}{2\pi}\int_0^b K_\varphi(\rho')\rho'd\rho' \int_0^\pi \cos\varphi' \frac{e^{-j\beta_o R(\vec{r},\vec{r}')}}{R(\vec{r},\vec{r}')}d\varphi' \tag{4.2.5}$$

4.2.2 Scattered electric field

As it is shown by (4.2.5), the impressed electric field is of the circulatory type which induces an eddy current inside the body. The induced current becomes a source for a secondary or the scattered electric field $\vec{E}^s$. To find $\vec{E}^s$ at any point inside the body the volume of the body is divided into N rings, and the eddy current density inside the n^{th} ring is represented by $\vec{J}_n$. The vector potential at the center of the m^{th} ring due to $\vec{J}_n$ is

$$\vec{A}_{mn} = \frac{\mu_o}{4\pi}\int_{n^{th}\text{ring}} \vec{J}_n \frac{e^{-j\beta_o R_{mn}}}{R_{mn}} dv \tag{4.2.6}$$

where

$$R_{mn} = [(\rho_b^m)^2 + (\rho_b^n)^2 - 2\rho_b^m\rho_b^n \cos\varphi' + (Z_b^m - Z_b^n)^2]^{\frac{1}{2}}$$

$\beta_o = 2\pi f\sqrt{\mu_o\epsilon_o}$, f is the operating frequency, and ρ_b^m and ρ_b^n are the radial distances of the m^{th} and n^{th} rings from the Z axis, respectively.

If the cross sections of the rings are small enough, the density of the current J_n can be assumed to be constant over the cross section and (4.2.6) reduces to

$$\vec{A}_{mn} = \hat{\varphi}\,\frac{\mu_o}{4\pi}\,J_n S_n \rho_b^n H_{mn} \tag{4.2.7}$$

where

$$H_{mn} = \int_0^{\pi} \cos\varphi' \;\frac{e^{-j\beta_o R_{mn}}}{R_{mn}}\; d\varphi'$$

and S_n is the cross section area of the n^{th} ring.

The total vector potential at the center of the m^{th} ring is

$$\vec{A}_m = \sum_{n=1}^{N} \vec{A}_{mn} = \hat{\varphi} \sum_{n=1}^{N} \frac{\mu_o}{2\pi}\,J_n S_n \rho_b^n H_{mn} \tag{4.2.8}$$

The vector potential at the center of a ring due to the current in the same ring should be evaluated more carefully, since for this case the integrand in (4.2.6) becomes infinite. It has been shown that $\vec{A}_{mm}$ can be expressed as [18]

$$\vec{A}_{mm} = \hat{\varphi}\,\frac{\mu_o}{2\pi}\,J_m S_m \rho_b^m H_{mm} \tag{4.2.9}$$

where

$$H_{mm} = \frac{2\pi}{S_m}\,[R_{mm}(\alpha) - R_{mm}(0)] \int_0^{\pi} \cos\varphi'\; e^{-j\beta_o R_{mm}(0)}\, d\varphi'$$

with $\alpha = \frac{2a}{\sqrt{\pi}}$, and a is the length of the side of the square cross section of the ring, and

$$R_{mm}(c) = \rho_b^m [2(1-\cos\varphi) + \frac{c^2}{(\rho_b^m)^2}]^{\frac{1}{2}}$$

The induced current $\vec{J}_n$ is related to the total electric field $\vec{E}_n$ by the following relation;

$$\vec{J}_n = \tau_n \vec{E}_n$$

where $\tau_n = (\sigma_n + j\omega(\epsilon_{rm} - \epsilon_o))$ is the complex conductivity. Thus, the scattered electric field $\vec{E}_m^s$ at the center of the m^{th} ring may be written as

$$\vec{E}_m^s = -j\omega\vec{A}_m = -\hat{\varphi}\,\frac{j\omega\mu_o}{2}\sum_{n=1}^{N} S_n\rho_b^n H_{mn}\tau_n E_n \tag{4.2.10}$$

The total electric field at any point inside the body is the sum of the impressed and scattered electric fields at that point.

$$\vec{E}_m = \vec{E}_m^i + \vec{E}_m^s \tag{4.2.11}$$

substituting (4.2.10) into (4.2.11) gives

$$E_m + \sum_{n=1}^{N} jf\mu_o S_n\rho_b^n H_{mn}\tau_n E_n = E_m^i \tag{4.2.12}$$

$$m = 1,2,\ldots,N$$

Equation (4.2.12) can be transformed into the following matrix representation

$$\begin{array}{cc} & N \\ N & \begin{bmatrix} \\ \quad M \quad \\ \\ \end{bmatrix} \end{array} \begin{bmatrix} E_1 \\ E_2 \\ \cdot \\ \cdot \\ E_n \end{bmatrix} = \begin{bmatrix} E_1^i \\ E_2^i \\ \cdot \\ \cdot \\ E_N^i \end{bmatrix} \tag{4.2.13}$$

where

$$M_{nn} = 1 + jf\mu_o S_n\rho_b^n H_{nn}\tau_n$$

and

$$M_{mn} = jf\mu_o S_n\rho_b^n H_{mn}\tau_n$$

The value for the impressed electric field E^i maintained by the current disk at the center of the m^{th} body ring can be obtained from (4.25) as.

$$E_m^i = E^i(\rho_b^m, z_b^m)$$

$$= \frac{j\omega\mu_o}{2\pi} \int_0^b K_\varphi(\rho')\rho' d\rho' \int_0^\pi \cos\varphi' \frac{e^{-j\beta_o[(\rho_b^m)^2+\rho'^2-2\rho_b^m\rho' \cos\varphi' + (Z_b^m-L)^2]^{1/2}}}{[(\rho_b^m)^2+\rho'^2-2\rho_b^m\rho' \cos\varphi' + (Z_b^m-L)^2]^{1/2}} d\varphi' \tag{4.2.14}$$

To evaluate the integral in (4.2.14), the area of the disk is divided into N' concentric surface rings, over the area of each ring the density of the surface current is assumed to be constant. The impressed electric field at the center of the m^{th} body ring due to the current flowing on the ν^{th} surface ring can be written as

$$\vec{E}_{m\nu}^i = \hat{\varphi} \frac{j\omega\mu_o}{2\pi} K_\nu P_\nu \Delta\rho_\nu A_{m\nu} \tag{4.2.15}$$

where

$$A_{m\nu} = \int_0^\pi \cos\varphi' \frac{e^{-j\beta_o[(\rho_b^m)^2 + \rho_\nu^2-2\rho_b^m\rho_\nu \cos\varphi' + (Z_b^m-L)^2]^{1/2}}}{[(\rho_b^m)^2 + \rho_\nu^2-2\rho_b^m\rho_\nu \cos\varphi' + (Z_b^m-L)^2]^{1/2}} d\varphi' \tag{4.2.16}$$

and K_ν is the density of the current on the ν^{th} ring of the disk. ρ_ν and $\Delta\rho_\nu$ are the radial distance and the width of the ν^{th} surface ring, respectively.

The total impressed electric field at the center of the m^{th} body ring is

$$\vec{E}_m^i = \sum_{\nu=1}^{N'} \vec{E}_{m\nu}^i = \hat{\varphi} \frac{j\omega\mu_o}{2\pi} \sum_{\nu=1}^{N'} K_\nu \rho_\nu \Delta\rho_\nu A_{m\nu} \tag{4.2.17}$$

$$m = 1,2,\ldots,N'$$

Equation (4.1.17) can be written into the following matrix form.

$$N \begin{bmatrix} E_1^i \\ \cdot \\ \cdot \\ \cdot \\ E_N^i \end{bmatrix} = \begin{bmatrix} \\ \\ P \\ \\ \\ \end{bmatrix} \begin{bmatrix} K_1 \\ \cdot \\ \cdot \\ \cdot \\ K_{N'} \end{bmatrix} \qquad (4.2.18)$$

where

$$P_{m\nu} = \frac{j\omega\mu_o}{2\pi} K_\nu \rho_\nu \Delta\rho_\nu A_{m\nu}$$

If the surface current K on the current disk is given, the impressed electric field $\vec{E}^i$ is determined by (4.2.18). once $\vec{E}^i$ is determined the induced electric field $\vec{E}$ can be obtained from (4.2.13).

4.3. Numerical results

The total induced electric field induced in a body for several different cases is calculated numerically and the results are persented in this section. Unless otherwise specified, in each case the operating frequency is fixed at 100 MHz and the conductivity and relative permittivity of the body are assumed to be 0.5 S/m, and 80, respectively.

In Figure 4.3 a disk of radius 2.cm carrying a uniform circulatory current with a density of 200 $\frac{\text{Amp}}{\text{m}}$ is placed on the surface of a cylindrical body of 5 cm radius and 4. cm height. The body is divided into 4 layers and each layer is divided into 5 rings. The distributions for the amplitude and phase of the total electric field induced inside each layer of the body are shown. The quasi-static approximations for the phase and for the amplitude of the total electric field in the first layer of the body are also included in the figure. It is seen that the intensity of the electric field is zero at the center of the body as expected. The total electric field obtained form the present numerical method is close to the quasi-static solution, however, when the frequency increases the discr pancy between the numerical solution and the quasi-static solution becomes more significant. It is also noted that the intensity of the electric field is high in the region of the body close to the disk and drops significantly in both vertical and radial directions as we move away from the disk.

In Figure 4.4 the distributions of the amplitude of the electric field in different layers of a body are shown at 100, and 30 MHz. The radius of the current disk is 3. cm and the body has a radius of 5 cm. The current density on the disk is 200 Amp/m. At 100 MHz the intensity of the field is considerably higher than that at 30 MHz. Comparing

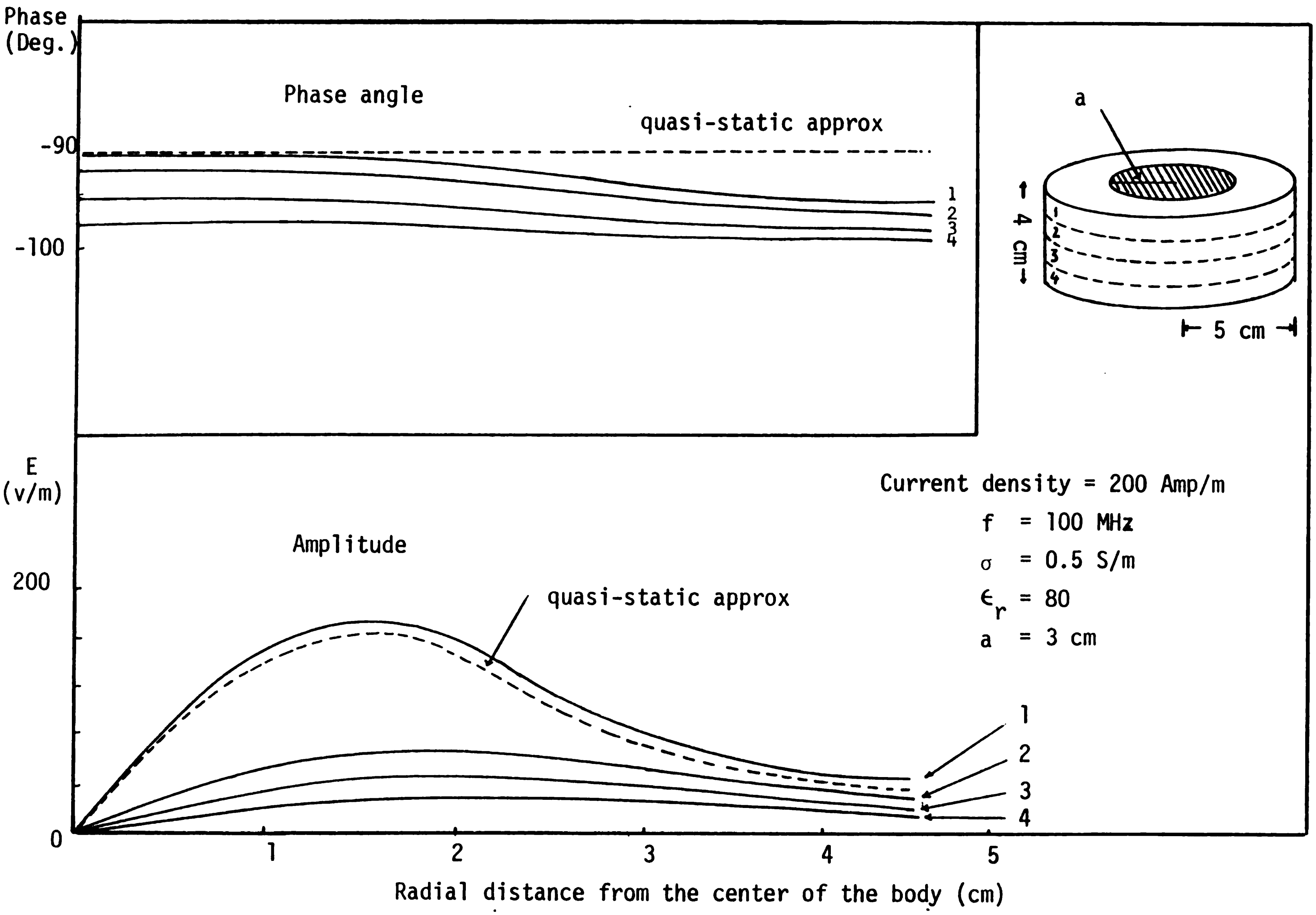

Figure 4.3. Distributions of amplitude and phase of the electric field in different layers of a body induced by a disk of uniform current.

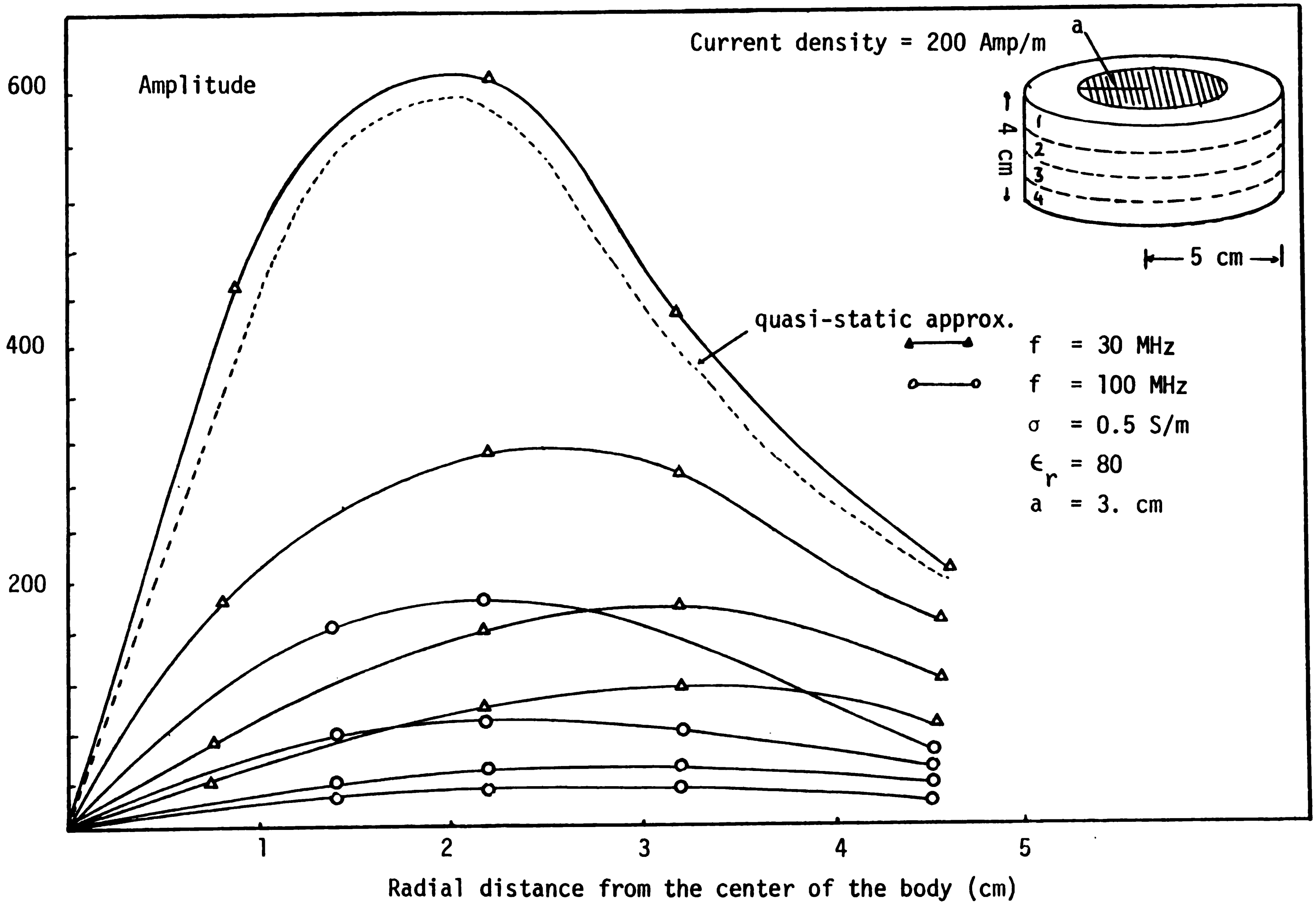

Figure 4.4. Distributions of the amplitude of the electric field in different layers of a body induced by a disk of uniform current at 30 MHz and 100 MHz.

Figures 4.3, and 4.4 we notice that for the same frequency and body dimension, the amplitude of the induced electric field inside the body increases considerably as the radius of the current disk increases.

In Figure 4.5 a current disk of radius 5 cm is located on the surface of a body of 12 cm radius and 15. cm height. The body is divided into 10 layers each containing 4 rings. The distributions of the amplitude of the induced electric field in different layers are shown in the same figure. The distributions of the phase angle of the induced electric field in each layer is depicted in Figure 4.6.

Figure 4.7 shows the distributions of the amplitude of the total electric field inside a body induced by three different kinds of current distributions (1) a single current loop, (2) a uniform current distribution, and (3) a triangular type of current distribution (zero at the edge of the disk and increases linearly towards the center). The radius of the body is 5 cm and its height is 4 cm. The distributions of the relative amplitude of the electric field in the first two layers of the body are depicted for each case. It is observed that for a single current loop of radius 2.5 cm the maximum electric field occurs at a radial distance equal to the radius of the current loop and the electric field decreases rather rapidly on either side. When the current is distributed uniformly over the surface of the disk the point of the maximum electric field moves closer to the center of the body and the distribution of the elecric field becomes more uniform. If the current on the disk has a triangular form of distribution the peak of the electric field distribution moves even closer to the center of the body as compared with the previous cases.

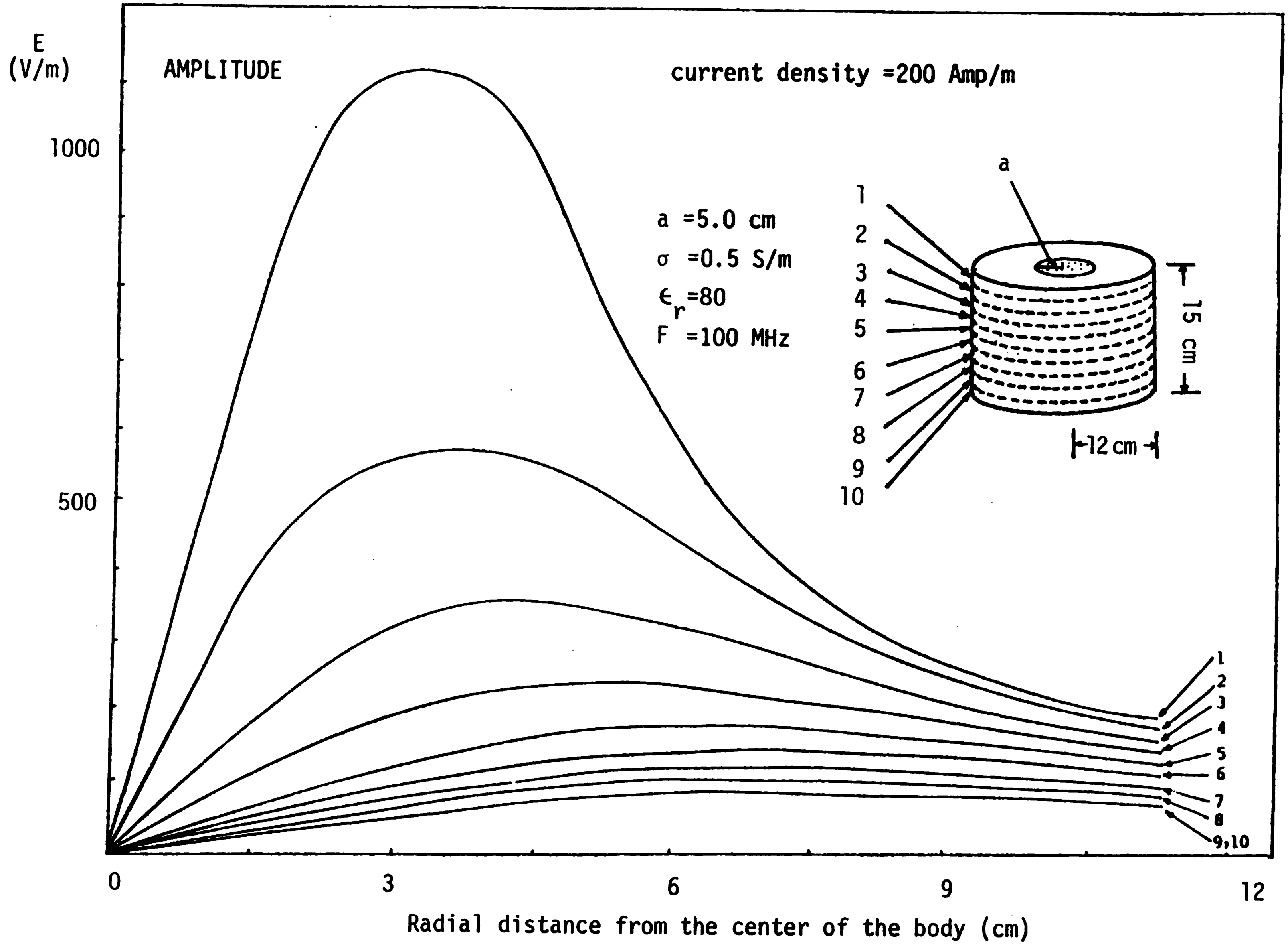

Figure 4.5. Distributions of the amplitude of electric field in different layers of a body induced by a disk of uniform current.

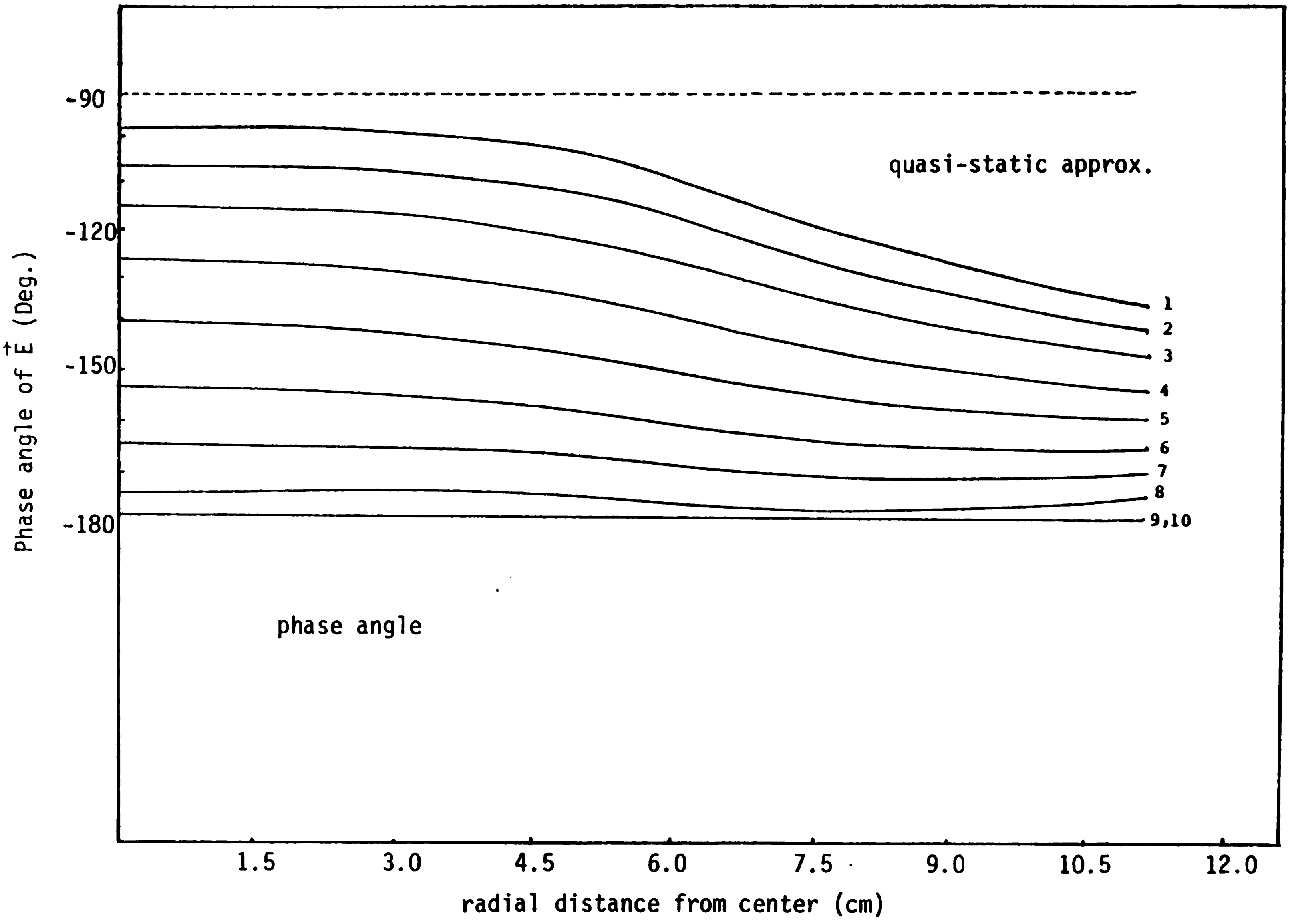

Figure 4.6. Distributions of the phase angle of the electric field in different layers of a body induced by a disk of uniform current.

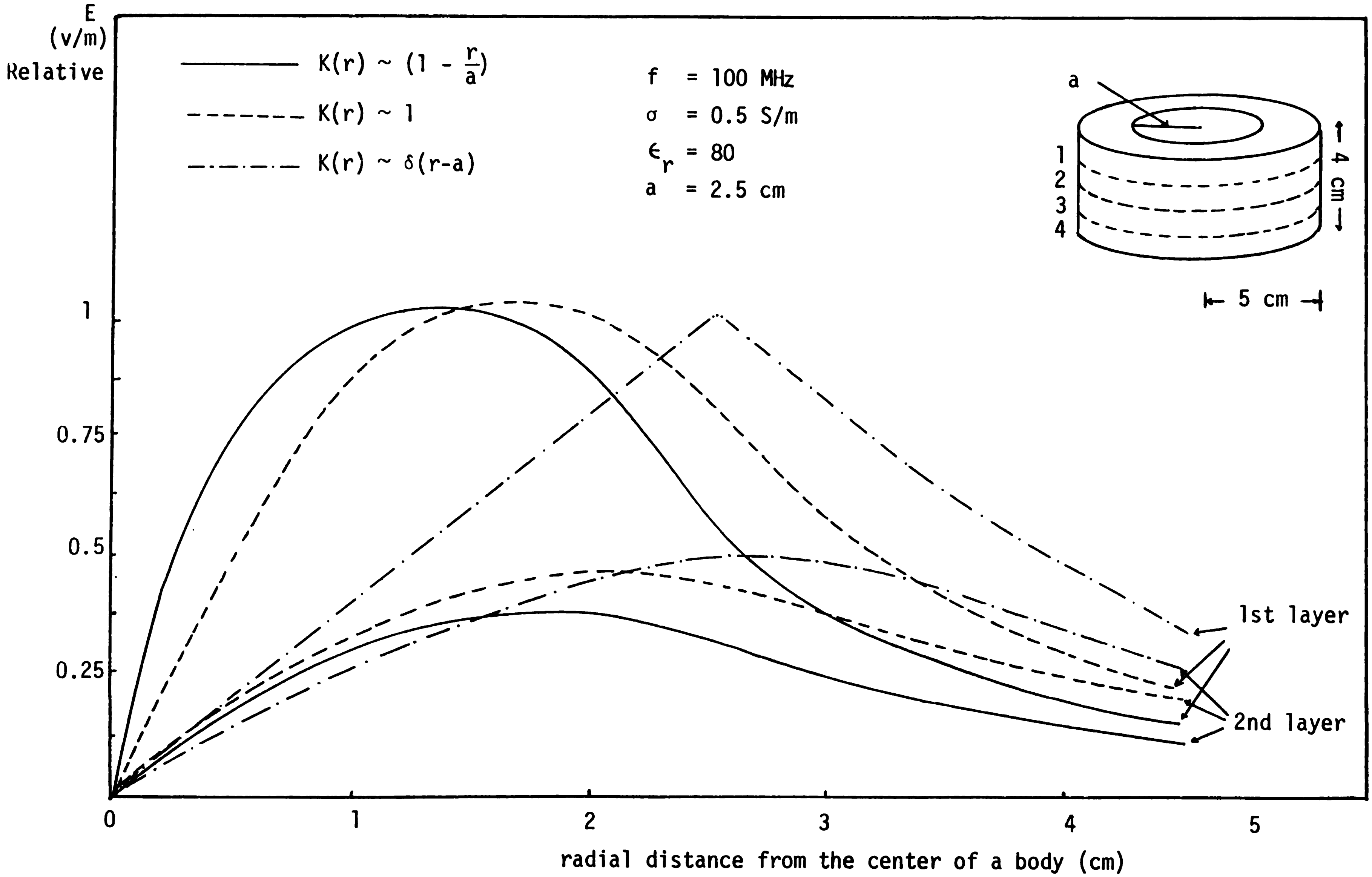

Figure 4.7. Distributions of the electric field in the first two layers of a body induced by three kinds of loop currents: a single loop current, a uniform surface current and a triangular surface current.

4.4. Synthesis of the current distributions for selective heating

In this section we attempt to develope a theoretical scheme for synthesizing the distribution of the current on a disk in order to obtain a desired heating pattern inside a biological body.

Suppose that it is desired to have an indicued electric field of 1 v/m at the center of the m^{th} ring and zero electric field in the rest of the body. From (4.2.13) and (4.2.18) we obtain

$$\begin{array}{cc} & N' \\ N & \begin{bmatrix} \\ \\ & P & \\ \\ \\ \end{bmatrix} \end{array} \begin{bmatrix} K_1 \\ \cdot \\ \cdot \\ K_{N'} \end{bmatrix} = \begin{bmatrix} M(m,1) \\ M(M,2) \\ \cdot \\ \cdot \\ \cdot \\ \cdot \\ M(m,N) \end{bmatrix} \tag{4.4.1}$$

It is required that the matrix P be a square matrix if K's are to be determined uniquely, that is,

$$N = N' \tag{4.4.2}$$

which means that the number of the rings in the body must be equal to the number of the surface rings on the current disk.

Some numerical example are given here to illustrate this scheme. In the first example a current disk of 3 cm radius is placed on the surface of a body of 10 cm radius and 5 cm height. The body is divided into a total of 25 rings. It is desired to produce an electric field with an amplitude of 10 V/m in a ring of radius 0.5 cm which is located at the center of the body, and zero in the remaining part of the body.

The distributions for the phase angle and the amplitude of the current required to produce the desired pattern for the electric field are shown in Figure 4.8. It is noted that the amplitude of the required current density is extremely high at the center of the disk and it decreases rapidly towards the edge of the disk. The phase angle for the required current density undergoes rapid fluctuations from one surface ring to another.

In the second example we consider a body of 15 cm radius and 4.5 cm height, and the radius of the current disk is chosen to be the same as that of the body. The objective is to produce an induced electric field of amplitude 10 V/m which is uniformly distributed over the volume of a ring in the first layer having an outer radius of 4.5 cm. The distributions of the phase angle and the amplitude of the required current density to produce the prescribed pattern are shown in Figure 4.9. It is noted that the amplitude of the current is very much smaller as compared to that obtained in the previous example.

It is found that like the case of voltage synthesis in a capacitor plate applicator, the theoretical results are unstable and a small error in the phase or the amplitude of the required current may produce a distribution of electric field which is quite different from the desired one.

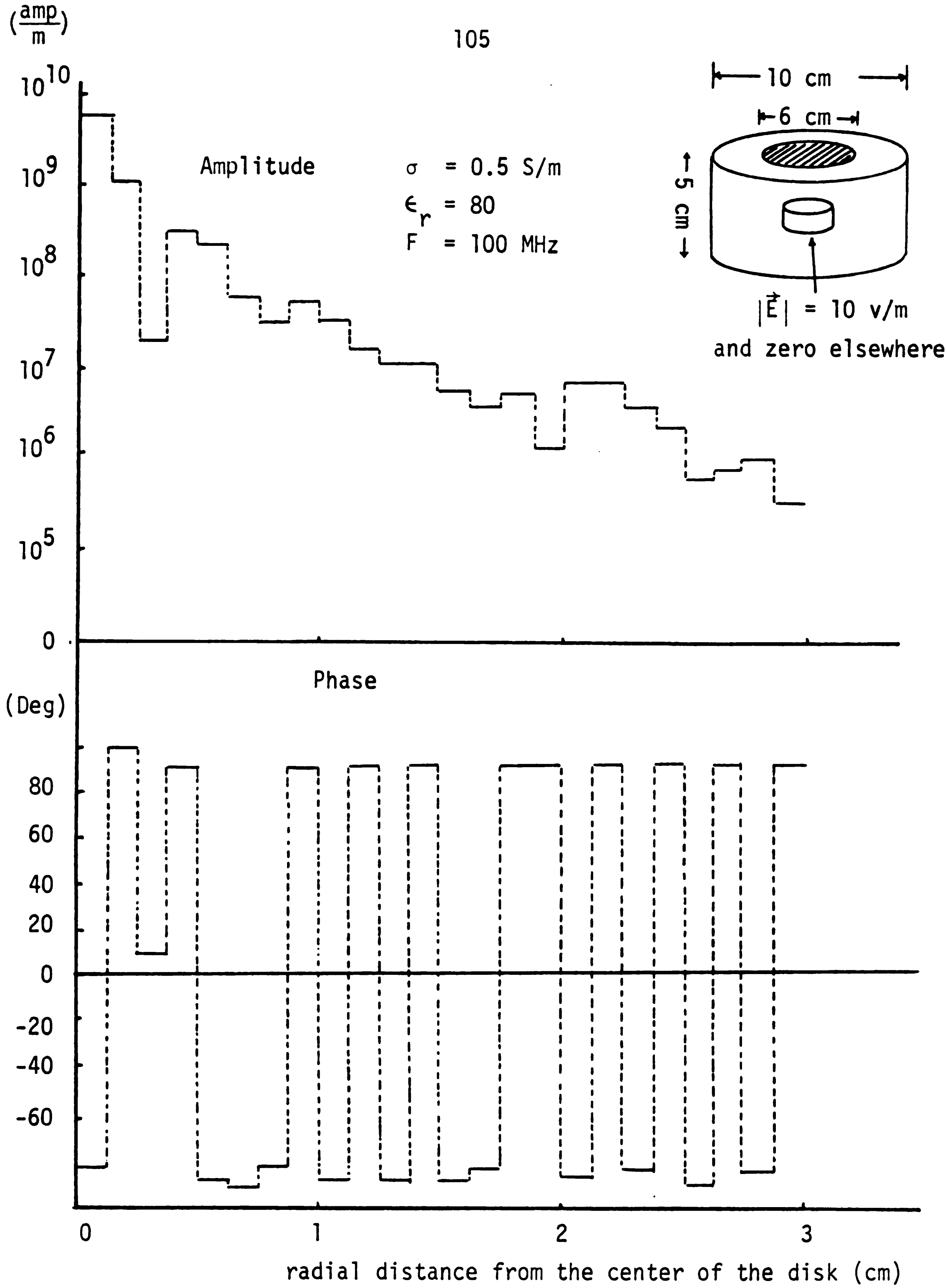

Figure 4.8. Distributions of phase and amplitude of the required current density on a disk to maintain a localized heating at the center of a body.

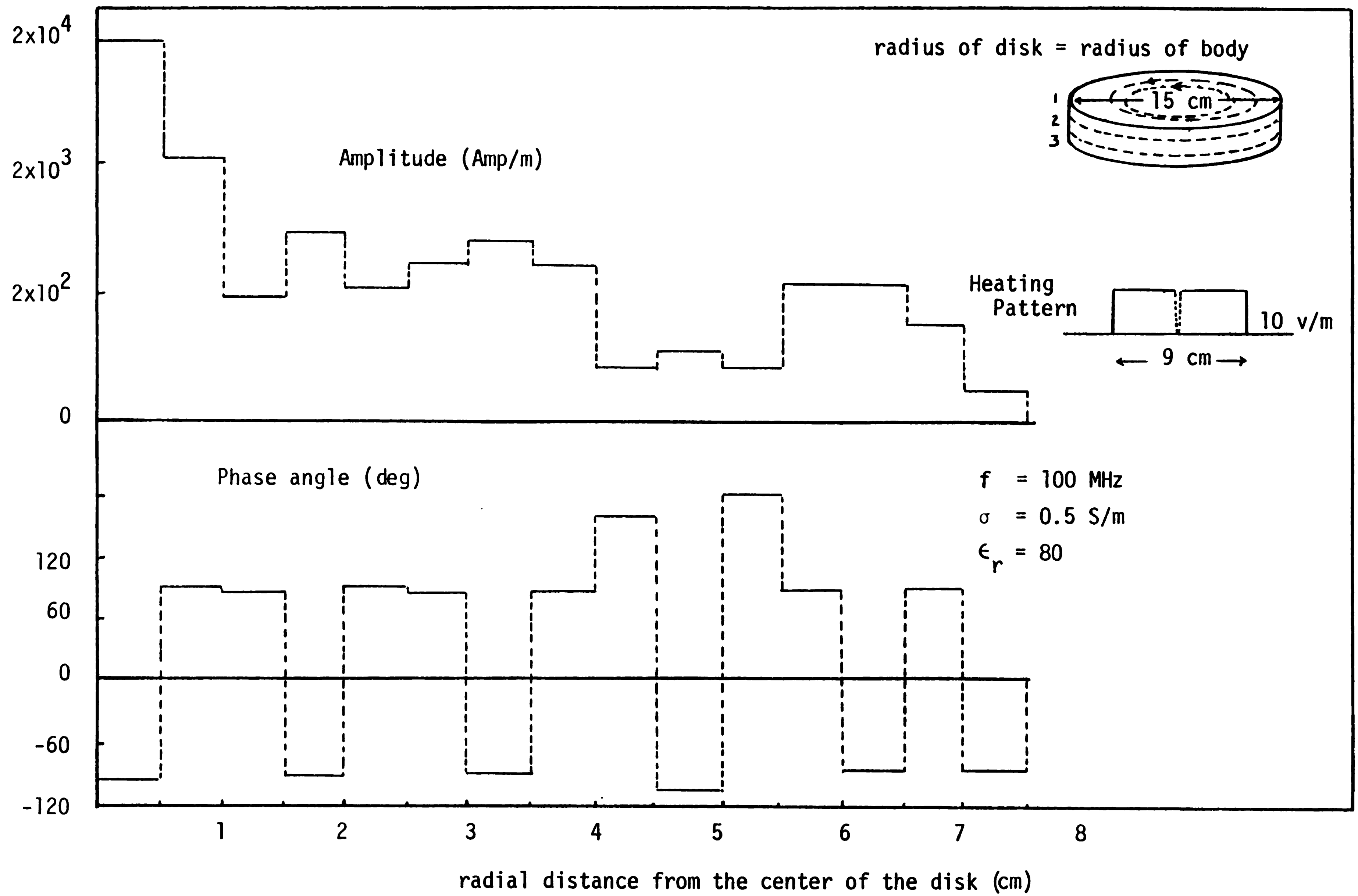

Figure 4.9. Distributions of the phase and amplitude of the required current on a disk to maintain a uniform heating in the first layer of the body.

4.5 Comparison of theoretical results with experimental results

The electric field induced inside a simulated biological body (saline solution) by three kinds of current distributions was measured by an implantable electric field probe. The measured values along with the theoretical results in relative amplitude are shown for each case in Figures 4.10 to 4.12. It is noted that due to the finite length of the prob in each case the measured values deviate from the theoretical values near the center, but for the region away from the origin the agreement between experiment and theory is considered to be good. The details of the experimental set up and the simulations for different current distributions will be explained in Chapter V.

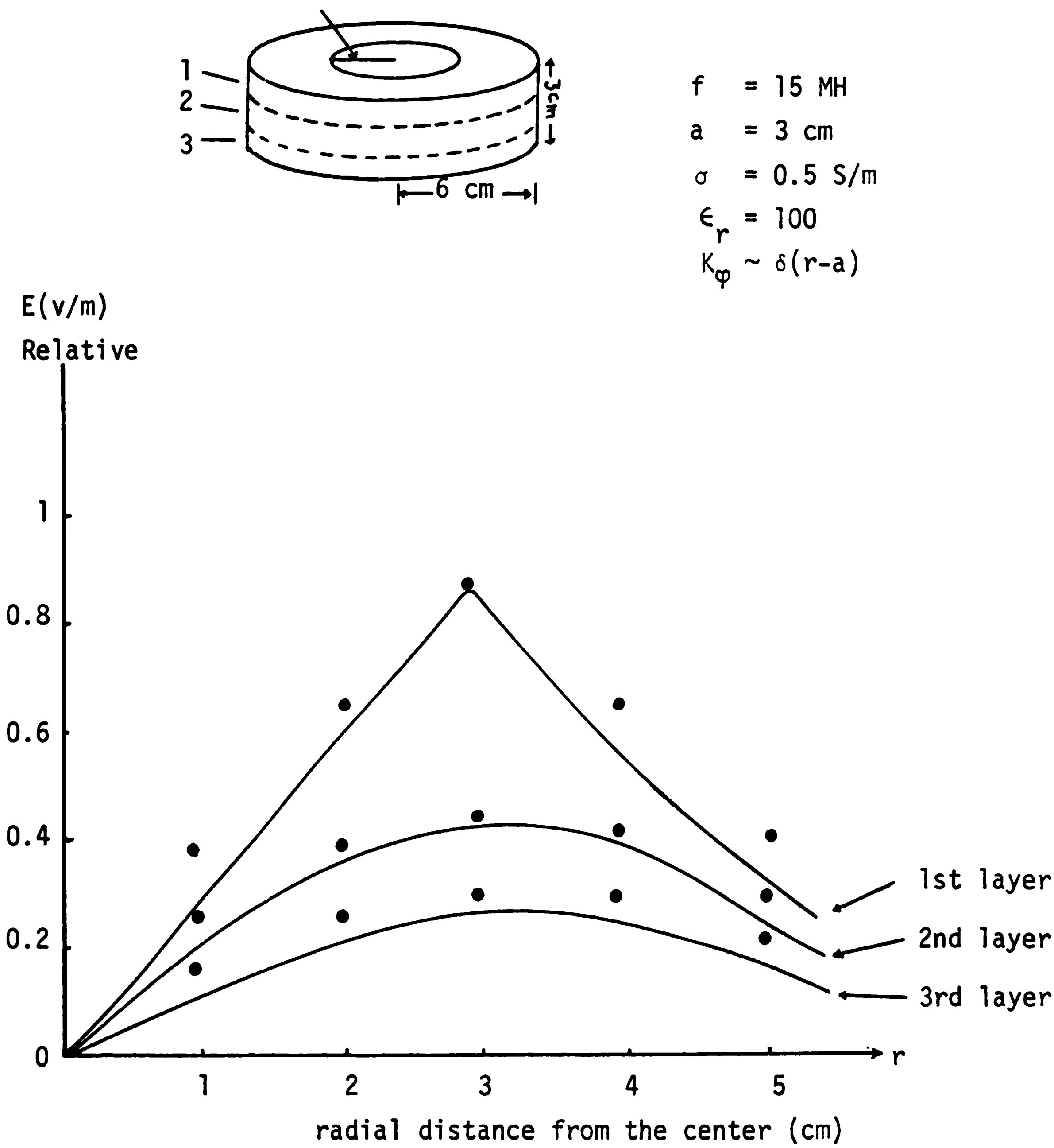

Figure 4.10. Distributions of the theoretical (solid lines) and experimental values (discrete points) for the electric field in different layers of a body induced by a single current loop.

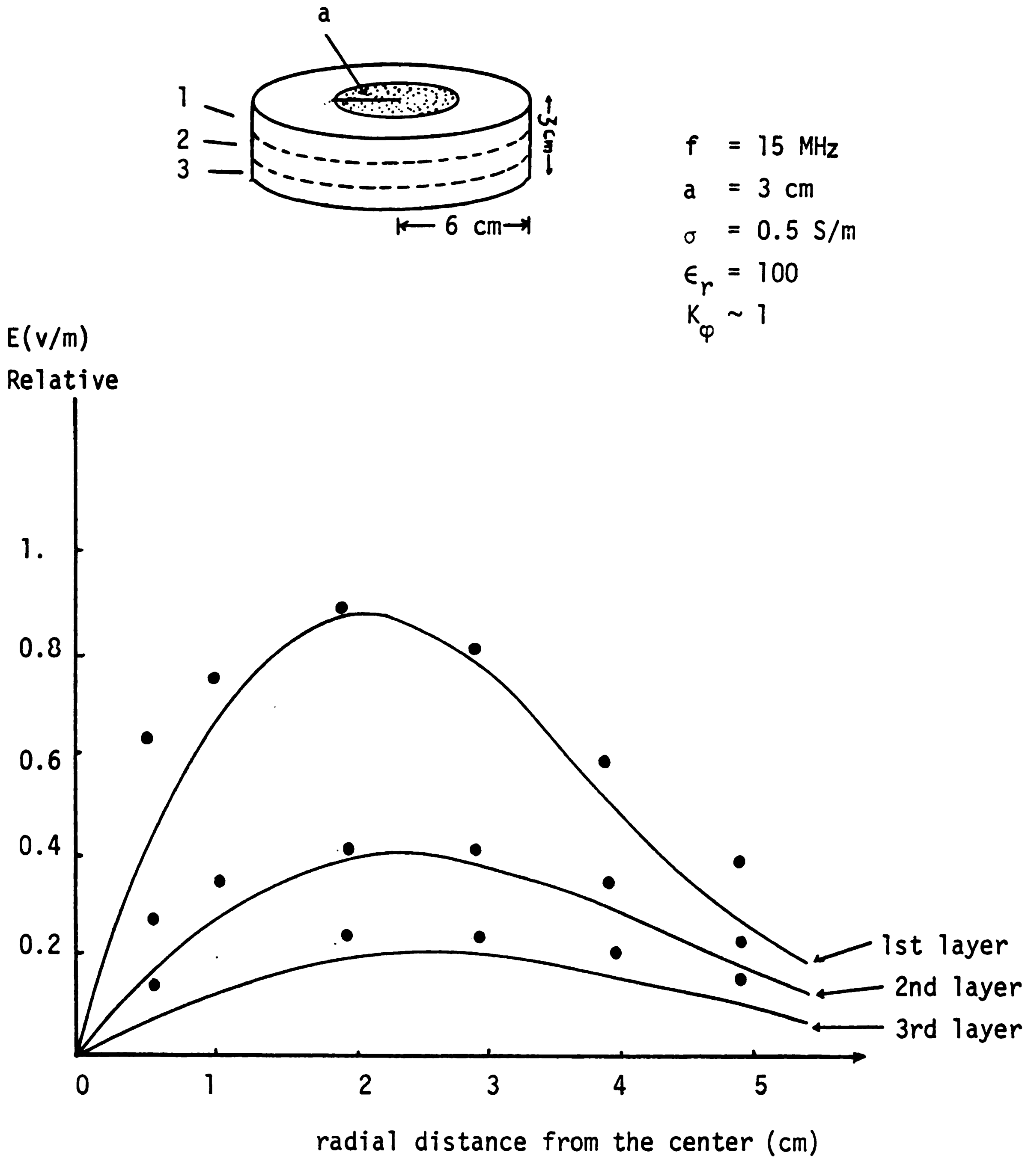

Figure 4.11. Distributions of the theoretical (solid lines) and experimental values (discrete points) for the electric field in different layers of a body induced by a disk of uniform current.

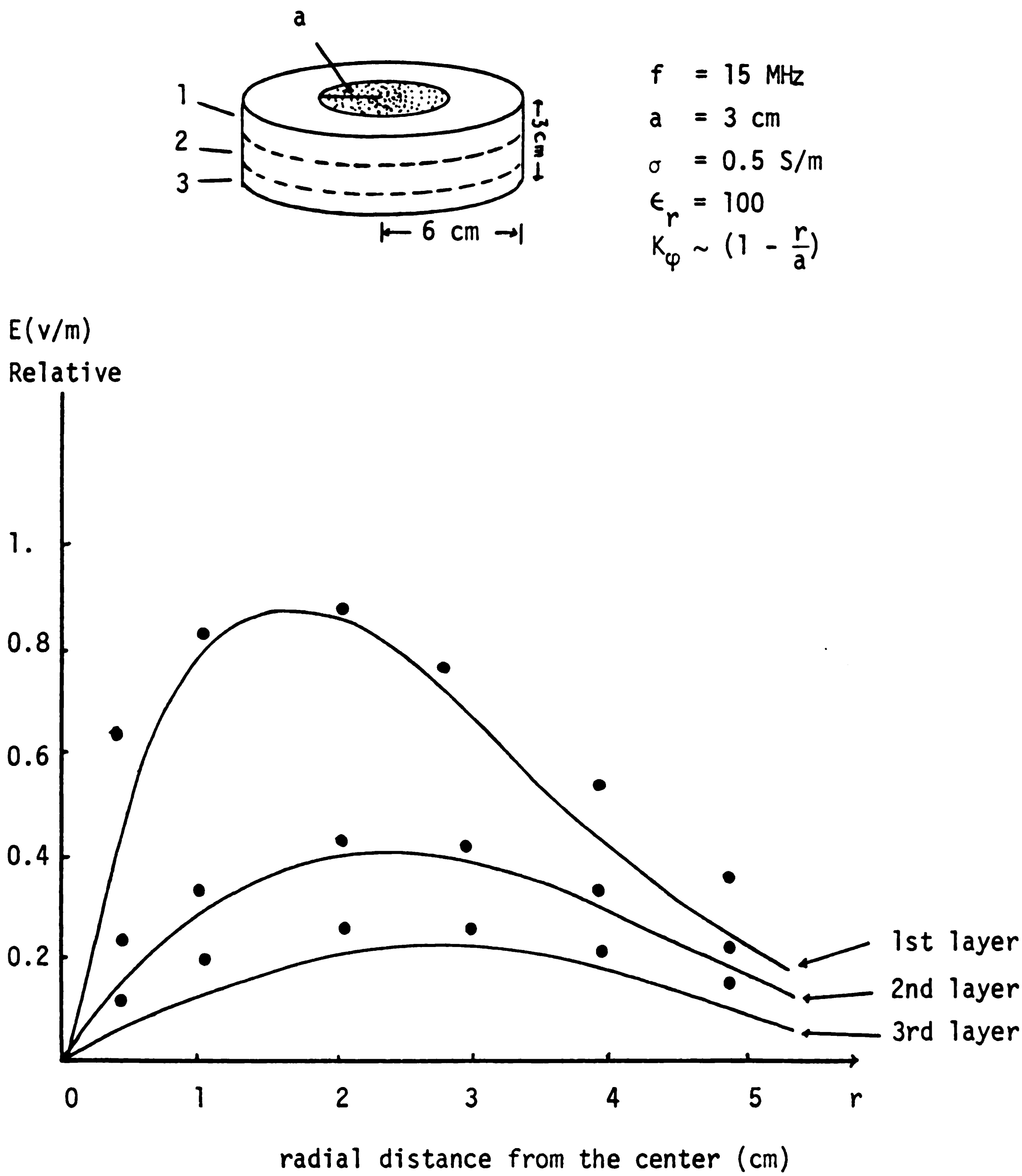

Figure 4.12. Distributions of the theoretical (solid lines) and experimental values (discrete points) for the electric field in different layers of a body induced by a triangular type of current distribution.

CHAPTER V

EXPERIMENTAL SETUP

In order to verify the theoretical results obtained in the preceding chapters, a series of experiments was conducted where the induced electric field inside a body maintained by a capacitor plate applicator or a current disk was measured. In this chapter the descriptions of the setups for such measurements are given.

5.1 Construction of an Implantable Probe

The procedure involving the construction of an inexpensive implantable probe has been given by K.M. Chen, et al. [19]. This probe has been tested successfully and proven efficient in measuring the induced electric field inside a phantom model of a biological body. A brief description of the probe is presented in this section.

In Figure 5.1 the schematic diagram of the probe is shown. This probe consists of a conventional short electric dipole loaded with a zero bias microwave diode (Microwave Associates, MA 40234). The probe output is connected to the measuring device (d.c. voltmeter or SWRM) with a pair of very thin resistive parallel wires. The resistive wires are loaded with two series of resistors in the sections adjacent to the diode. This scheme reduces the induced current in the lead wires, and consequently, minimizes the noise in the measurment. The probe and the lead wires are encased in a plexiglass stick with the help of epoxy glue.

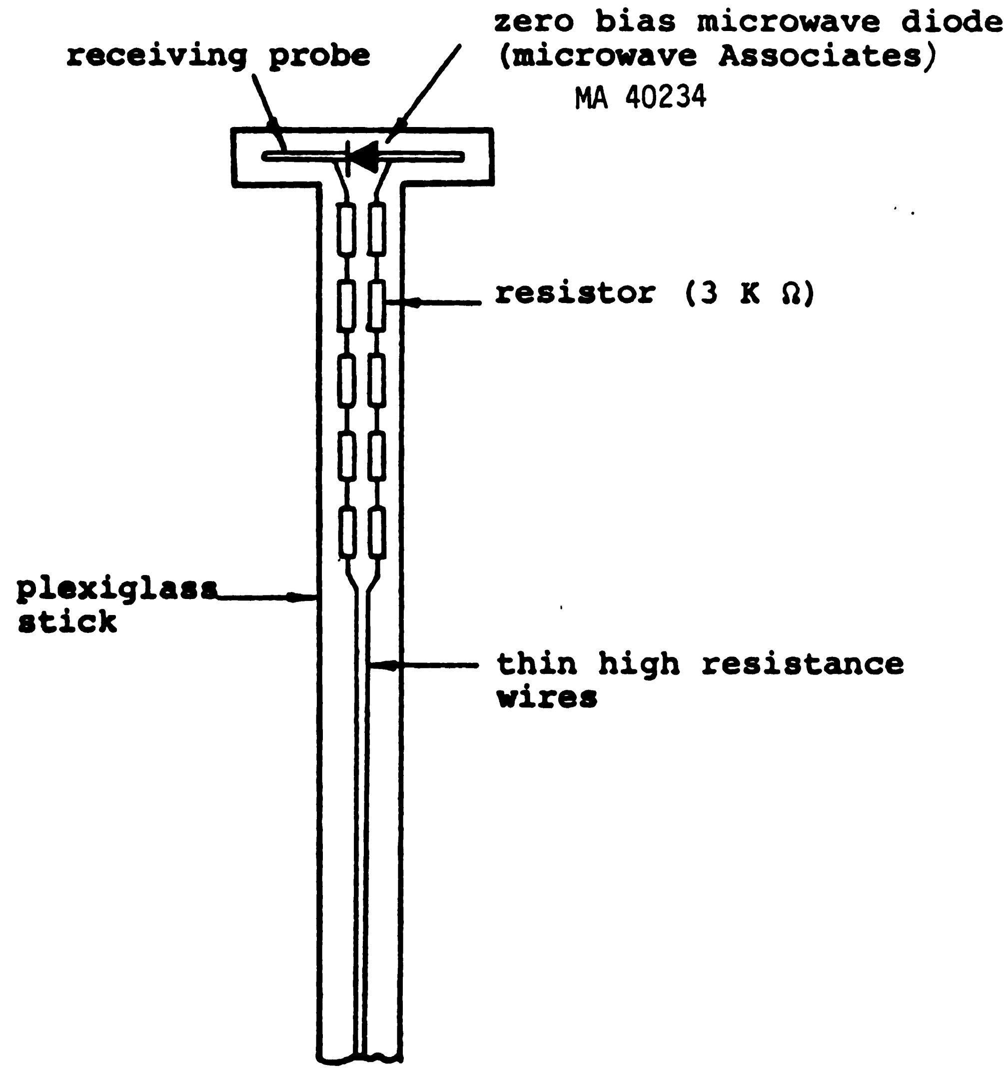

Figure 5.1. **A non-interferring, electric field probe for measuring the induced electric field in a biological body.**

The electric field in any direction at a given point can be measured by orientating the probe parallel to that direction.

5.2. Construction of a balun.

A difficulty encountered in the measurment of the electric field is associated with the direct connection of a coaxial line to a balanced two-wire line. The problem can be explained by considering the situation depicted in Figure 5.2.

In Figure 5.2 a coaxial transmission line is directly connected to a two-wire line. Like in most practical applications the outer conductor of the coaxial line is assumed to be grounded. Since the wires 1 and 2 of the two-wire are line at different potentials with respect to ground, the capacitances with respect to ground of the wires are different and as a result the currents i_1 and i_2 in the wires are different. This implies that a current $i_d = i_1 - i_2$ flows on the outer surface of the coaxial line.

The current on the two wire line in Figure 5.2a may be decomposed into symmetric and antisymmetric modes as shown in Figure 5.2b. For the symmetric mode, equal currents flow in opposite directions on the two wires, while for antisymmetric mode, two currents of equal magnitude flow in the same direction. The anitsymmetric component of the line current does not energize the applicator but it produces a strong electric field around the applicator and will lead to an ambiguous probe measurment.

One way to eliminate the antisymmetric component of the current is by making the impedance seen by i_d in Figure 5.2d very high and thus,

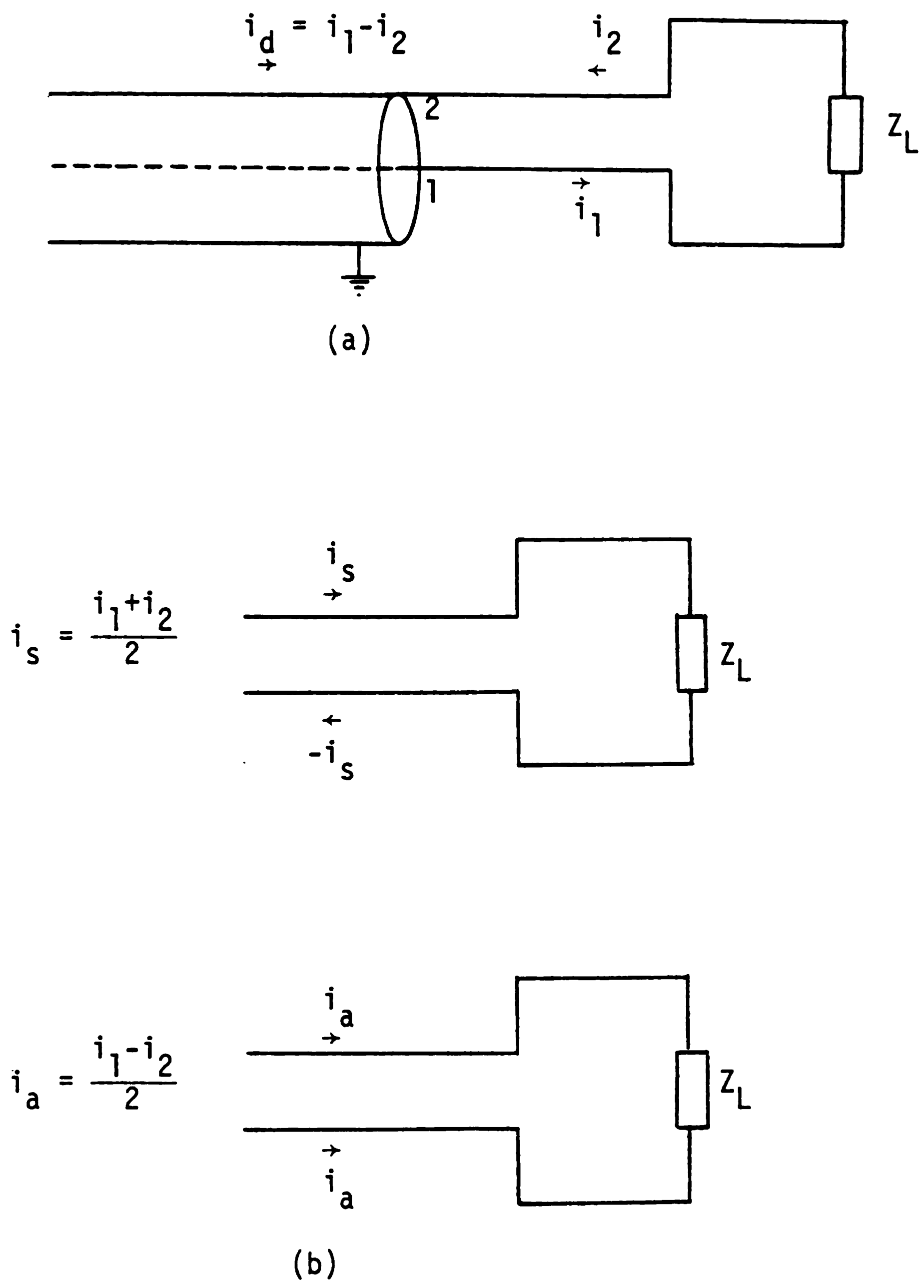

Figure 5.2. (a) direct connection of a coaxial line to a two wire line.
(b) decomposition of the current on the two-wire line into symmetric and antisymmetric modes.

prevent the current from flowing on the outer surface of the coaxial line. This can be accomplished by using a balance to unbalance convertor or a balun for short. One such balun is shown in Figure 5.3 where a coaxial line is forked into a pair, one of which is a dummy. The center conductor of the coaxial line is connected to the shield of the dummy coaxial line and the shields are joined to the paralle-wire line. The coaxial line and the dummy are wound on a ferrite toroid to prevent a short circuit at the input terminal of the paralled-wire and at the same time to suppress the current flowing on the outer surface of the coaxial line. The detailed theory and the structure for different kinds of baluns are reported in many sources [20,21]

5.3. Experimental setup for the measurement of the electric field in a conducting medium maintained by a capacitor-plate applicator and probe-electrode interaction.

The setup for the measurment of the electric field inside a body maintained by a capacitor-plate applicator is shown in Figure 5.4. An HF voltage, form an HF signal generator processed through an amplifier is applied to a pair of capacitor plate placed across a box of plexiglass filled with saline solution. A variable inductor is used for the tunning purpose.

The equivalent circuit for an isolated probe is shown in Figure 5.5a where Z_{in} is the input impedance of the short electric dipole and Z_L is the impedance of the diode, V is the equivalent driving voltage induced by the impressed electric field, and V_0 is the output

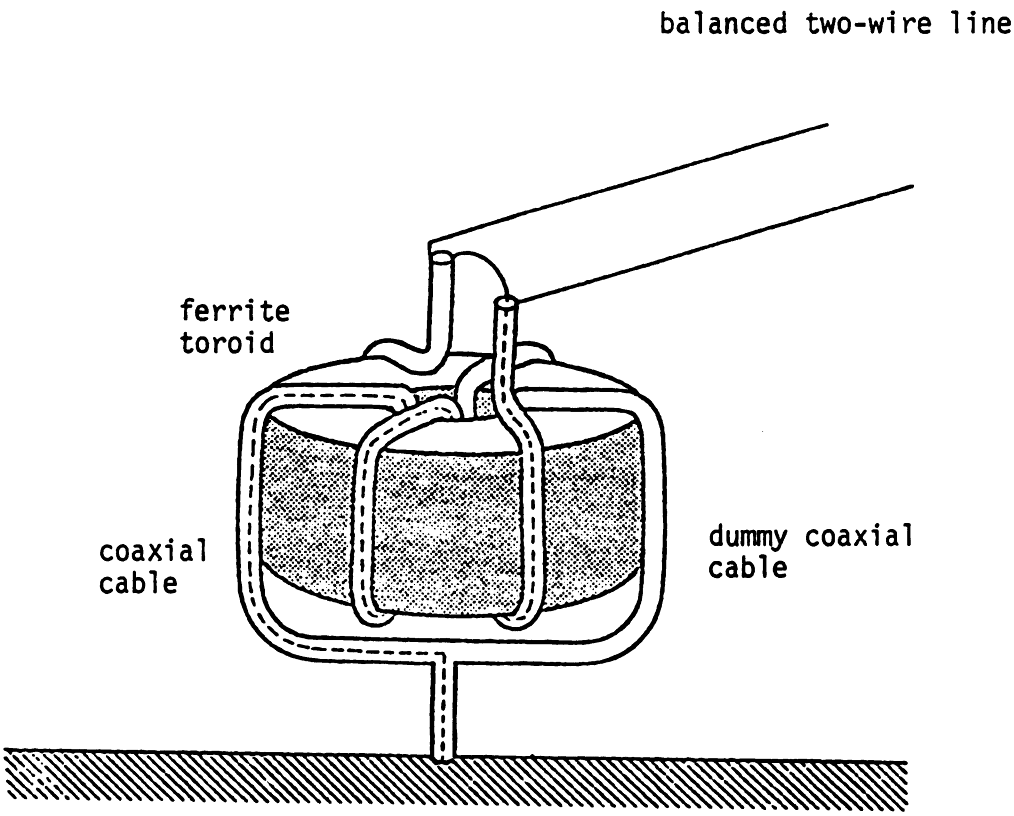

Figure 5.3. A balun for converting a coaxial line to a balanced two-wire line.

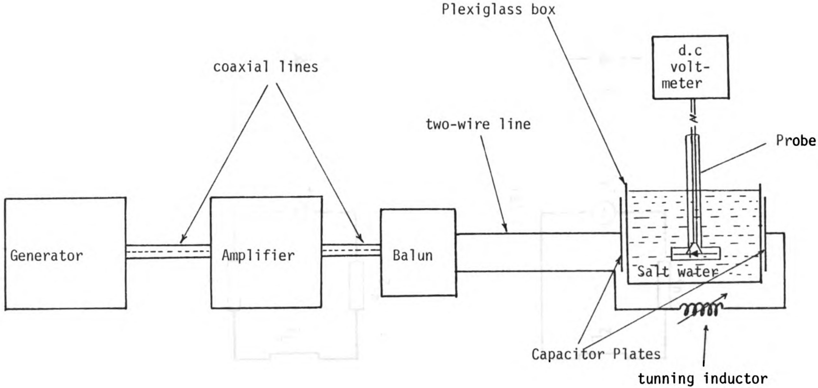

Figure 5.4. Experimental setup for the measurment of the electric field in a conducting medium maintained by a pair of capacitor-plate electrodes.

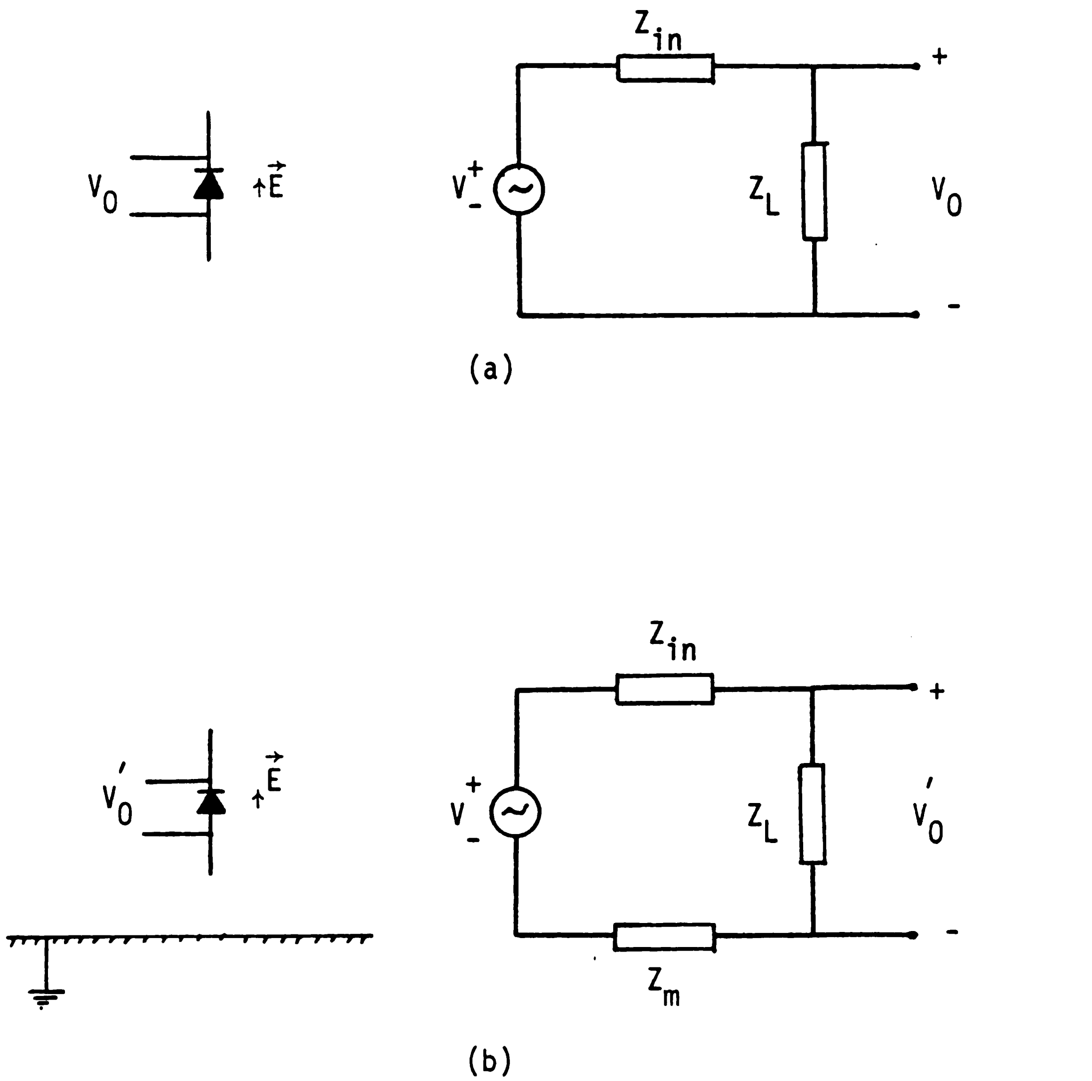

Figure 5.5. Equivalent curcuits for a probe. (a) an isolated probe (b) a probe located close to a grounded plane.

voltage of the probe. When the probe is located close to the surface of the conducting electrode, the image effect due to the electrode should be considered. The image effect of the electrode can be taken account for by introducing an additional impedance Z_m in the equivalent circuit (Figure 5.5b). Therefore, in measuring the electric field between two electrodes the effect of conducting electrodes on the performance of the probe should be investigated and corrections should be made in the measured values of the electric field if necessary.

It is possible to obtain a rough estimate for Z_m. To do this we assume that the electrode is of infinite extent and held at zero potential. We also neglect the effect of the lead wires. With these assumptions, the conducting plane in Figure 5.5b can be replaced by an image dipole as shown in Figure 5.6. The mutual impedance between the dipole (1) and its image (2) can be obtained from the follwoing expression [22]:

$$Z_m = -\frac{1}{I_1(-d)I_2(d)} \int_{h-d}^{-h-d} E_{2Z}(z)I_1(z)dz \tag{5.3.1}$$

where d is the distance from the center of the dipole to the conducting plane and h is half of the dipole length. $I_1(-d)$ and $I_2(d)$ are the magnitudes of the currents at the centers of the dipole and its image, respectively. E_{2Z} represents the z component of the electric field at the surface of the dipole maintained by the current on the image dipole (2), and finally $I_1(z)$ is the current distribution on the dipole. Since $h << \lambda$ the currents $I_1(z)$ and $I_2(z)$ on the dipole and its image can be approximated with triangular distributions of

$$I_1(z) = I_o(1- \frac{|z+d|}{h}) \tag{5.3.1}$$

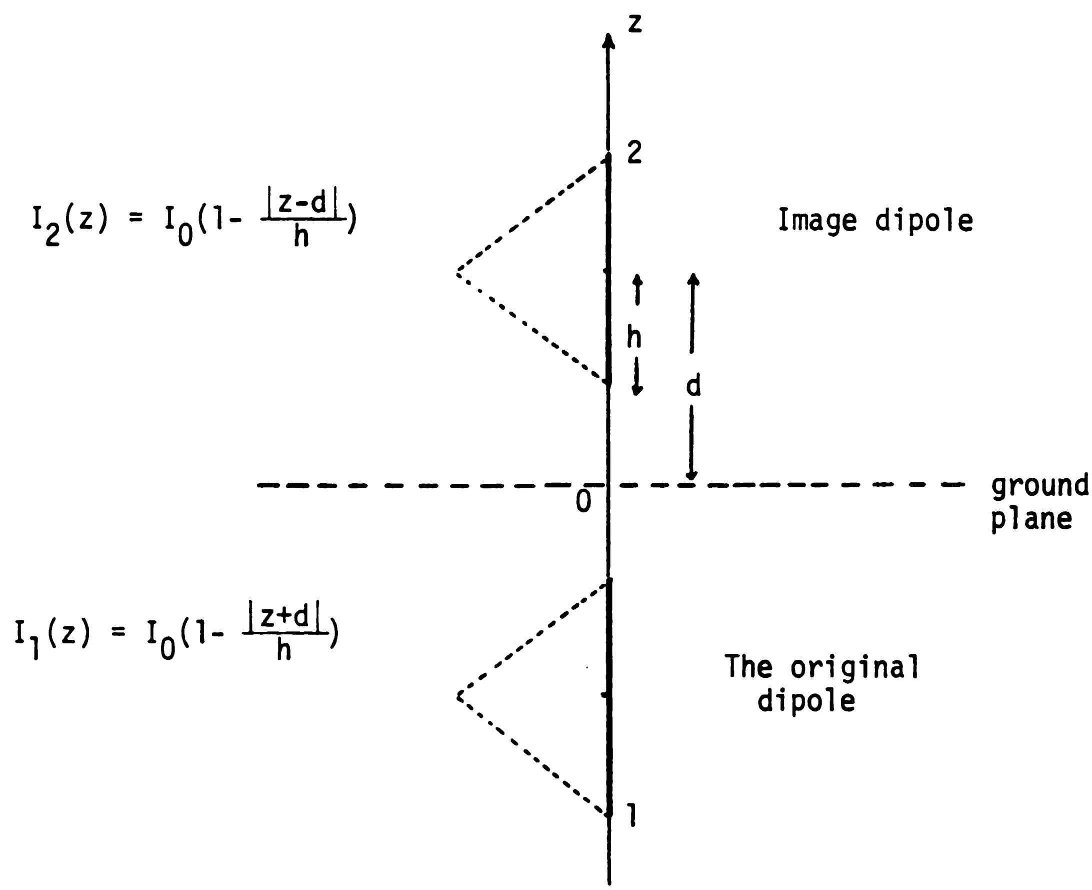

Figure 5.6. Distribution of the currents on a short electric dipole and its image caused by the ground plane.

$$I_2(z) = I_o(1- \frac{|z-d|}{h}) \tag{5.3.2}$$

where

$$I_1(-d) = I_2(d) = I_o$$

The Z component of the electric field at the surface of the dipole due to the current flowing on the image dipole can be obtained from the following relation,

$$E_{2Z}(z) = - \frac{j\omega}{\beta_o^2} \frac{\partial^2}{\partial z^2} [A_{2Z}(z)] - j\omega\ A_{2Z}(z)] \tag{5.3.3}$$

where

$$A_{2Z}(z) = \frac{\mu_o I_o}{4\pi} \int_{d-h}^{d+h} (1 - \frac{|z'-d|}{h}) \frac{1}{z'-z} dz' \tag{5.3.4}$$

with the assumption that $e^{-j\beta_o|z'-z)} \simeq 1$.

Equation (5.3.4), after evaluating the integral, gives

$$A_{2Z}(z) = \frac{\mu_o I_o}{4\pi} [(1 - \frac{d}{h} + \frac{z}{h}) \ln \frac{d-z}{d-z-h} + (1 + \frac{d}{h} - \frac{z}{h}) \ln \frac{d+h-z}{d-z}] \tag{5.3.5}$$

with (5.3.5), (5.3.3) becomes

$$E_{2Z}(z) = - \frac{j\omega\mu_o I_o}{2\pi} [\frac{h}{B_o^2} \frac{1}{(d-z)(d+h-z)(d-h-z)} + \frac{1}{2} A_{2Z}] \tag{5.3.6}$$

Then from (5.3.1) we obtain

$$Z_m = \int_{h-d}^{-h-d} E_{2Z}(z)(1 - \frac{|z+d|}{h})dz \tag{5.3.7}$$

It is traight forward but very tedious to evaluate the integral in (5.3.7). However, it can be done numerically with computer. For

$h = 0.5$ cm, $d = 0.7$ cm and $f = 15\ MH_z$ we obtain

$$Z_m \simeq j\ 2800\ \Omega$$

The input impedance of a short dipole receiving antenna is well known [23] and is given by

$$Z_{in} \simeq -j\ \frac{\zeta_o[\ell n\,(\frac{h}{a})\ -1]}{\beta_o\ h\pi}$$

where $\zeta_o = 120\pi$. For $h = 0.5$ cm, $\frac{h}{a} \simeq 10$ and $f = 15\ MH_z$,
$Z_{in} \simeq -\ j\ 100 \times 10^3 \Omega$.
Thus, it is obvious that $Z_m << Z_{in}$. Consequenlty, the effect of the ground plane on the performance of the probe can be neglected.

5.4. Experimental setup for the measurment of the electric field in a conducting medium maintained by a current disk.

The experimental setup for this case is shown in Figure 5.7. The capacitor C is connected in series with the current disk to create a resonance in the circut. This allows the maximum current to flow in the current disk. Two 25Ω resistors in the circuit are used to prevent short circuit in the output terminals of the amplifier.

In Figure 5.8 the experimental models for three kinds of current distributions are shown. In Figure 5.8.a, a single current loop consists of several turns of enameled copper wire. The total length of the wire is chosen to be shorter than a wavelength to ensure a constant current distribution along the loop. In Figure 5.8.b, a single piece of enameled copper wire is wound into a number of circular loops

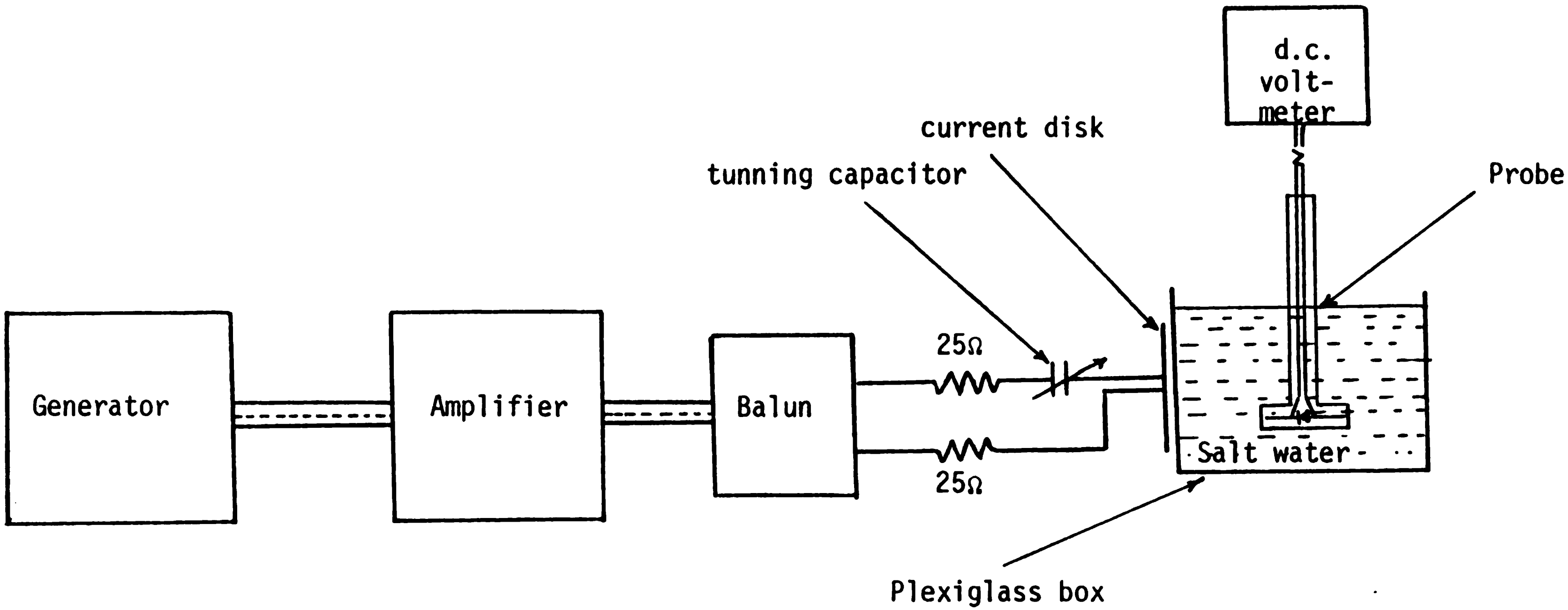

Figure 5.7. Experimental setup for the measurment of the electric field in a conducting medium maintained by a current disk.

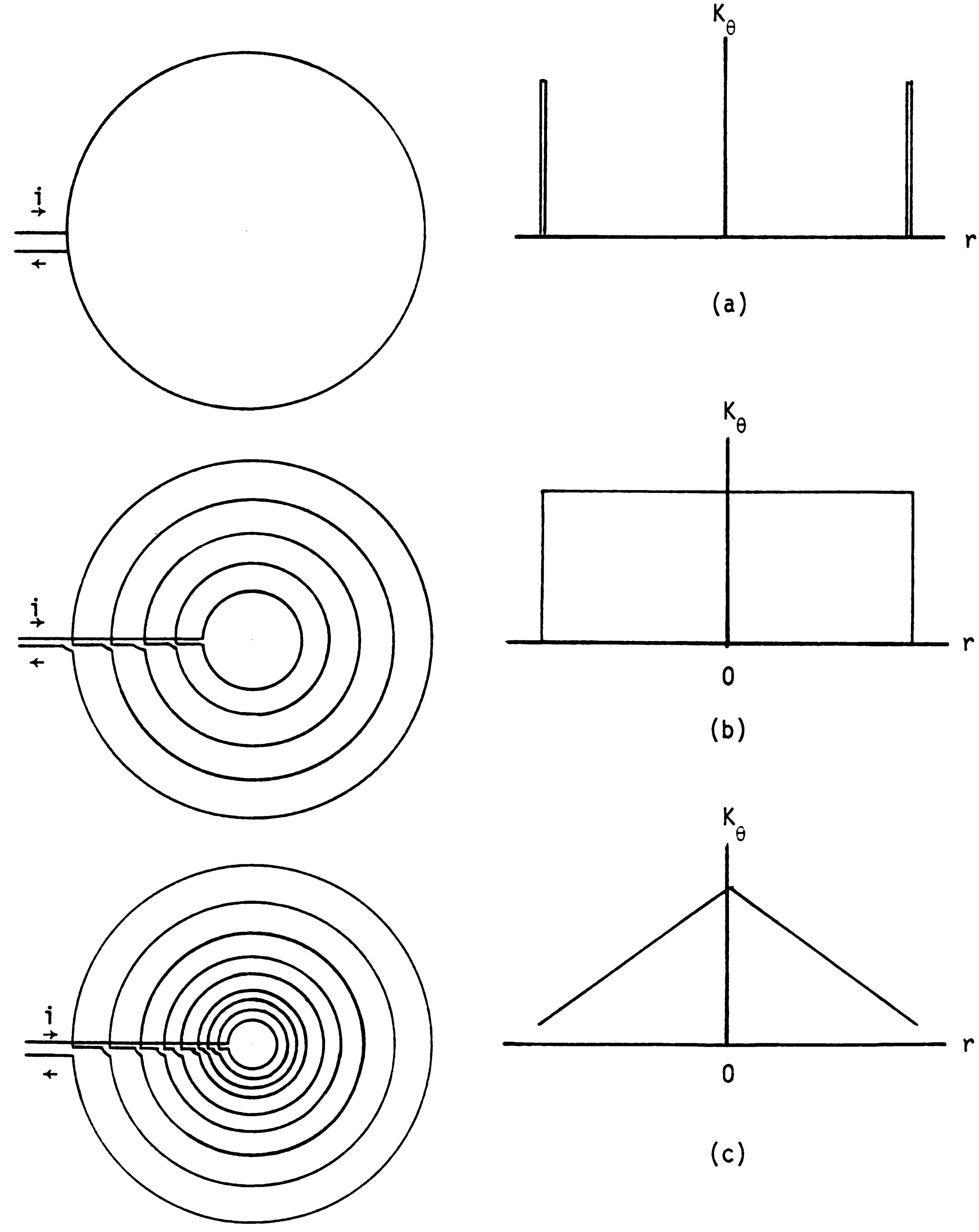

Figure 5.8. Experimental models for three kinds of current distributions: (a) single current loop (b) uniform current distribution (c) triangular current distribution.

with equal spacing to approximate a uniform current distribution. Finally the experimental model for a triangular current distribution is shown in Figure 5.8.c where the spacing between two adjacent loops is varied accordingly.

CHAPTER VI

A USER'S GUIDE TO COMPUTER PROGRAM USED TO CALCULATE THE ELECTRIC FIELD INSIDE A BIOLOGICAL BODY INDUCED BY A PAIR OF CAPACITOR PLATE APPLICATOR

Part I of this chapter briefly explains the computer program used to determine the electric field inside a biological body induced by a pair of capacitor-plate applicator placed across that body. This program enables one to evaluate the density of electric charge on the electrodes as well.

The geometry of the problem is shown in Figure 6.1. One quarter of the body is divided into a number of cubic cells. Similarly, one quarter of each electrode is partitioned into subareas. The matrix representation for a set of linear algebraic equations in terms of the unknowns induced electric field at the center of each body cell, and the charge densities on different subareas of electrodes was presented in Chapter III and is rewritten here

$$\left[\begin{array}{c:c} G & A \\ \hdashline C' & G^s \end{array}\right] \left[\begin{array}{c} E \\ \hdashline \eta \end{array}\right] = V \left[\begin{array}{c} 0 \\ \hdashline 0 \\ \hdashline 1 \end{array}\right] \qquad (6.1)$$

Given the necessary data the program solves equation (6.1) for E and η, for both floating and grounded potential cuses.

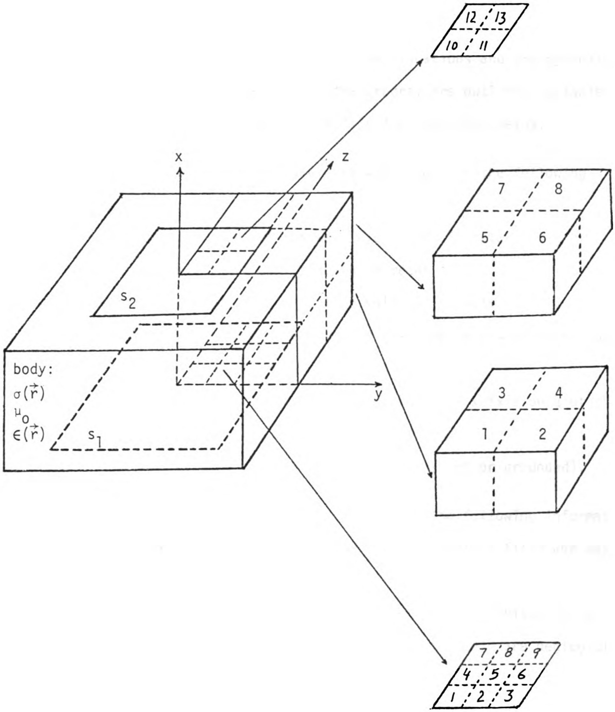

Figure 6.1. Geometry of a body located between two energized electrodes for the purpose of local heating. The numbering order of ¼ of the body and electrodes are shown.

6.1 Description of input data files.

The symbolic name for the program is "FIELD" and the sequential structure of the data files, the format specifications and the symbolic names of the input variables used in the program are outlined in Table 6.1, and the information on each data file are explained below.

First data file - contains only one card which defines the following variables.

"D" - The thickness of the body between electrodes in meter.

"DL" - Defines the electrode-body spacing in meter.

"V" - Shows the amplitude of the applied voltage in volts.

"SLP,SUP" - Specify ½ of the dimensions of the lower and upper electrodes, respectively in meter.

"NSL,NSU" - Define the number of partitions along the x-axis on ¼ of the lower and upper electrodes, respectively.

"V mode" - Shows the mode of applied voltage (floating or grounded).

Second data file - with only one card containing the following informations

"Comp" - Specifies the components of the induced electric field and may have one of the following forms.

"X-only" For x-component of the induced electric field. This code is used when the other components of electric field are neglegible.

"X,Y,Z." - Used when it is desired to compute all three components of induced electric field.

"Q(j), j = 1,4"-Is the symbolic name for quadrants.

"FMEG"-Reads the frequency of applied voltage in MHz.

Table 6.1. The symbolic names for the input variables and format specifications used in program "FIELD".

File No.	Card No.	Columns	Variable Name	Format
1	1	1-10	D	F10.4
		11-20	DL	F10.4
		21-30	V	F10.4
		31-40	SLP	F10.4
		41-50	SUP	F10.4
		51-53	NSL	I3
		54-56	NSU	I3
		59-61	V mode	A3
2	1	1-6	COMP	A6
		11-13	Q_1 to Q_4	4A1
		18-27	FMEG	F10.0
3	1	1-2	NX	I2
		6-7	NY	I2
		11-12	NZ	I2
4	1-N	1-10	AMX	F10.3
		11-20	AMY	F10.3
		21-30	AMZ	F10.3
		31-40	RELPI	F10.3
		41-50	SIGI	F10.3
		51-60	DXCM	F10.3
		61-70	DYCM	F10.3
		71-80	DZCM	F10.3

Third data file - contains one card which specifies the number of cells in X,Y,Z directions (NX, NY, NZ).

Fourth data file - contains as many cards as there are number of cells in ¼ of biological body, and on each card the following informations are punched.

"AMX", "AMY", "AMZ" which correspond to the maximum boundaries of a cell in the X,Y and Z directions in centimeter with reference to the origin.

"RLEPI" and "SIGI" are the codes for relative dielectric constant and conductivity (mho/m) of each cell.

"DXCM", "DYCM", "DZCM" are the dimension of the cell in X,Y and Z, in centimeter.

This concludes the description of input data files. An example is worked out in the next section to supplement this user's guide.

6.2 Numerical example In this example the electrodes are considered to be of different sizes with lower electrode grounded. The lower electrode 3x3 cm and the upper electrode is 2.0x2.0 cm. A voltage of 2. volts at 15 MHz is applied between electrodes. The numbering order of electrodes subareas is presented in Figure 6.1. Based on the given informations, the input data files have the following form.

File No.	Informations on the file.							
1	0.02	0.0025	2.0	0.015	0.01	003002	GRD*	
2	X,Y,Z. 1234		15.0					
3	02 02 02							
4.1	1.0	1.0	1.0	80.0	0.5	1.0	1.0	1.0
4.2	1.0	2.0	1.0	80.0	0.5	1.0	1.0	1.0
4.3	1.0	1.0	2.0	80.0	0.5	1.0	1.0	1.0
4.4	1.0	2.0	2.0	80.0	0.5	1.0	1.0	1.0
4.5	2.0	1.0	1.0	80.0	0.5	1.0	1.0	1.0
4.6	2.0	2.0	1.0	80.0	0.5	1.0	1.0	1.0
4.7	2.0	1.0	2.0	80.0	0.5	1.0	1.0	1.0
4.8	2.0	2.0	2.0	80.0	0.5	1.0	1.0	1.0

*GRD is the code for grounded potential case, for floating potential case "FLT" should be used instead.

It is noted that NX * NY * NZ is the number of cells in ¼ of the body.

The numerical results and program listing are presented in the following pages.

```
      PROGRAM FIELD(INPUT,OUTPUT)
C*****************************************************************************
C      THIS PROGRAM CALCULATES THE ELECTRIC FIELD INSIDE A BIOLOGICAL
C      BODY INDUCED BY A PAIR OF ELECTRODES PLACED ACROSS THE BODY.
C*****************************************************************************
      COMPLEX G,GMAT,DET,SS,U,CHARGE
      REAL MU
      COMMON VOL(120,7),XO,YO,ZO,K4,NERR
      COMMON/FIELD/SIZE(3),K1,K2,PI,EPS,MU,WVN,OMEG
      COMMON/BLKGMT/NDIV,GRID,PART,START1,START2,START3,
     1 ADD1,ADD2,ADD3,DENOM,REX1
      COMMON G(120,121)
      DIMENSION ZP(80),Y(80)
      READ 700,D,DL,V,SLP,SUP,NSL,NSU,VMODE
      IFLAG=0
      IF(VMODE.EQ.3HFLT) IFLAG=1
      PI=3.1415926536            $          EPS=8.854E-12
      MU=1.257E-6                $          NERR=0
      NLP=NSL*NSL                $          NUP=NSU*NSU
      DCM=D*100.                 $          DLCM=DL*100.
      SLPCM=SLP*200.             $          SUPCM=SUP*200.
      PRINT 701,DCM,DLCM,V,SLPCM,SUPCM,NUP,NLP
      DSP=(SLP*SLP)/NLP          $          R=SQRT(DSP/PI)
      NT=NLP+NUP                 $          NT1=NT+IFLAG
      CALL SUM1(ZP,Y,NSL,NSL,SLP,SLP,0)
      CALL SUM1(ZP,Y,NSU,NSU,SUP,SUP,NLP)
      NDIV=2                     $     GRID = FLOAT(NDIV)
      PART = GRID ** 3           $     DENOM = 4.* PI* PART
      GFACT = 0.5 * (( 1.0/ GRID ) - 1.0 )
      READ 100,COMP,Q1,Q2,Q3,Q4,FMEG
      IF(COMP.EQ.6HX,Y,Z.)  KRON=3
      IF(COMP.EQ.6HX-ONLY)   KRON=1
      READ 101, NX, NY, NZ
      OMEG = 2.0 *PI* FMEG * 1.0E6  $     WVN = OMEG*SQRT(MU*EPS)
      N=NX*NY*NZ
      MA=KRON*N+NT1
      MAP1=MA+1
      DO 300 I=1,MA,1
      DO 300 J=1,MAP1,1
  300 G(I,J)=CMPLX(0.0,0.0)
      REX1 = OMEG * MU * WVN         $     PRINT 151
      PRINT 171
C*****************************************************************************
C
C      THIS PART CALCULATES THE ELEMENTS OF GS MATRIX.
C
C*****************************************************************************
      DO 200 I=1,NT1
      K=KRON*N+I
      DO 200 J=1,NT
      L=KRON*N+J
      IF(IFLAG.EQ.0) GO TO 222
      IF(I.EQ.NT1) GO TO 70
  222 ZF=ZP(I)                   $          YF=Y(I)
      ZS=ZP(J)                   $          YS=Y(J)
      NN=J/(NLP+1)
      IF(I.EQ.J) GO TO 40
      IF(I.GT.NLP) GO TO 50
      R1=SQRT((ZF-ZS)**2+(YF-YS)**2+NN*(D+2.*DL)**2)
      R2=SQRT((ZF-ZS)**2+(YF+YS)**2+NN*(D+2.*DL)**2)
      R3=SQRT((ZF+ZS)**2+(YF+YS)**2+NN*(D+2.*DL)**2)
      R4=SQRT((ZF+ZS)**2+(YF-YS)**2+NN*(D+2.*DL)**2)
      GO TO 60
   50 R1=SQRT((ZF-ZS)**2+(YF-YS)**2+(1-NN)*(D+2.*DL)**2)
      R2=SQRT((ZF-ZS)**2+(YF+YS)**2+(1-NN)*(D+2.*DL)**2)
      R3=SQRT((ZF+ZS)**2+(YF+YS)**2+(1-NN)*(D+2.*DL)**2)
      R4=SQRT((ZF+ZS)**2+(YF-YS)**2+(1-NN)*(D+2.*DL)**2)
   60 G(K,L)=DSP*(SS(R1)+SS(R2)+SS(R3)+SS(R4))
      GO TO 200
   40 S1=2.*PI*R
      R2=SQRT((ZF-ZS)**2+(YF+YS)**2)
      R3=SQRT((ZF+ZS)**2+(YF+YS)**2)
      R4=SQRT((ZF+ZS)**2+(YF-YS)**2)
      G(K,L)=S1+DSP*(SS(R2)+SS(R3)+SS(R4))
      GO TO 200
   70 G(K,L)=DSP
  200 CONTINUE
```

```
          DO 301 M=1,NT
          K=KRON*N+M
          IF(IFLAG.EQ.0) GO TO 333
          G(K,MAP1)=(M/(NLP+1))*V       $          G(K,MA)=-1.0
          GO TO 301
  333     G(K,MAP1)=(M/(NLP+1))*V
  301     CONTINUE
          DO 303 M = 1,N
          READ 104, AMX,AMY,AMZ,RLEP1,SIG1,DXCM,DYCM,DZCM
          AMX=AMX-00.0
          AMY=AMY+00.0
          VOL(M,1) = (AMX - (0.5 * DXCM))/ 100.0
          VOL(M,2) = (AMY - (0.5 * DYCM))/ 100.0
          VOL(M,3) = (AMZ - (0.5 * DZCM))/ 100.0
          DELTAX = DXCM / 100.0             $     DELTAY = DYCM / 100.0
          DELTAZ = DZCM / 100.0             $ VOL(M,4)=DELTAX*DELTAY*DELTAZ
          VOL(M,5)=RLEP1           $           VOL(M,6)=SIG1
          VOL(M,7) = DELTAX            $       Z = VOL(M,3)
  303     PRINT 172,M,AMX,AMY,AMZ,DXCM,DYCM,DZCM
          PRINT 153                    $     DO 304 J=1,N
  304     PRINT 172,J,(VOL(J,L),L=1,6)
          NSB=NZ*NY
C***************************************************************************
C
C         THIS PART CALCULATES THE ELEMENTS OF C MATRIX.
C
C***************************************************************************
          DO 400 I=1,NT
          K=KRON*N+I                   $             K1=2*NSB
          DO 400 J=1,KI
          L=J
          IF(J.GT.NSB)     L=J+N-2*NSB
          DSB=VOL(L,7)*VOL(L,7)
          ZF=ZP(I)                     $              YF=Y(I)
          ZS=VOL(L,3)                  $             YS=VOL(L,2)
          NQ=2*(J/(NSB+1))-1
          IF(I.GT.NLP) GO TO 71
          RB1=SQRT((ZF-ZS)**2+(YF-YS)**2+(DL+(J/(NSB+1))*D)**2)
          RB2=SQRT((ZF-ZS)**2+(YF+YS)**2+(DL+(J/(NSB+1))*D)**2)
          RB3=SQRT((ZF+ZS)**2+(YF+YS)**2+(DL+(J/(NSB+1))*D)**2)
          RB4=SQRT((ZF+ZS)**2+(YF-YS)**2+(DL+(J/(NSB+1))*D)**2)
          GO TO 80
   71     RB1=SQRT((ZF-ZS)**2+(YF-YS)**2+(DL+(1-J/(NSB+1))*D)**2)
          RB2=SQRT((ZF-ZS)**2+(YF+YS)**2+(DL+(1-J/(NSB+1))*D)**2)
          RB3=SQRT((ZF+ZS)**2+(YF+YS)**2+(DL+(1-J/(NSB+1))*D)**2)
          RB4=SQRT((ZF+ZS)**2+(YF-YS)**2+(DL+(1-J/(NSB+1))*D)**2)
   80     G(K,L)=DSB*(EPS*(VOL(L,5)-1.0)+VOL(L,6)/CMPLX(0.0,OMEG))*
     1    NQ*(SS(RB1)+SS(RB2)+SS(RB3)+SS(RB4))/(4.*PI*EPS)
  400     CONTINUE
C***************************************************************************
C
C         THIS PART CALCULATES THE ELEMENTS OF A MATRIX.
C
C***************************************************************************
          DO 500 I=1,N
          K=I                          $            X1=I+N
          K2=I+2*N
          DO 500 J=1,NT
          L=KRON*N+J                   $            MM=J/(NLP+1)
          ZF=VOL(I,3)                 $             YF=VOL(I,2)
          XF=VOL(I,1)+DL               $            ZS=ZP(J)
          YS=Y(J)
          R4=SQRT((ZF+ZS)**2+(YF-YS)**2+(XF-MM*(D+2.*DL))**2)
          R1=SQRT((ZF-ZS)**2+(YF-YS)**2+(XF-MM*(D+2.*DL))**2)
          R2=SQRT((ZF-ZS)**2+(YF+YS)**2+(XF-MM*(D+2.*DL))**2)
          R3=SQRT((ZF+ZS)**2+(YF+YS)**2+(XF-MM*(D+2.*DL))**2)
          G(K,L)=DSP*(U(R1)+U(R2)+U(R3)+U(R4))*(XF-MM*(D+2.*DL))
          IF(KRON.EQ.1)   GO TO 500
          G(K1,L)=DSP*((U(R1)+U(R4))*(YF-YS)+(U(R2)+U(R3))*(YF+YS))
          G(K2,L)=DSP*((U(R1)+U(R2))*(ZF-ZS)+(U (R3)+U(R4))*(ZF+ZS))
  500     CONTINUE
C***************************************************************************
C         THIS PART CALCULATES THE ELEMENTS OF G MATRIX.
C***************************************************************************
          DO 306 I = 1,KRON              $    DO 306 J = 1,KRON
```

```
      DO 306 M1 = 1,N                 $     K = (I - 1)*N + M1
      XO = VOL(M1,1)                  $     YO = VOL(M1,2)
      ZO = VOL(M1,3)                  $     DO 306 M2 = 1,N
      DELTAX = DELTAY = DELTAZ = VOL(M2,7)
      SIZE(1) = SIZE(2) = SIZE(3) = DELTAX
      START1 = GFACT* SIZE(1)         $     START2 = GFACT*SIZE(2)        12
      START3 = GFACT*SIZE(3)          $     ADD1 = DELTAX/GRID
      ADD2 = DELTAY/GRID              $     ADD3 = DELTAZ/GRID
      L = (J - 1)*N + M2              $     K1 = I
      K2 = J                          $     K4 = M2
      IF(J.EQ.1) GO TO 513            $     IF(J.EQ.2) GO TO 514
      G(K,L)=GMAT(Q1)+GMAT(Q2)-GMAT(Q3)-GMAT(Q4)
      GO TO 515
513   G(K,L)=GMAT(Q1)+GMAT(Q2)+GMAT(Q3)+GMAT(Q4)
      GO TO 515
514   G(K,L)=GMAT(Q1)-GMAT(Q2)-GMAT(Q3)+GMAT(Q4)
515   IF( NERR.EQ. 1) GO TO 999
306   CONTINUE                        $     GO TO 510                     14
510   PRINT155,FMEG,NX,NY,NZ,COMP,Q1,Q2,Q3,Q4
      IF(IFLAG.EQ.0) PRINT 188
      IF(IFLAG.EQ.1) PRINT 189
      IF(COMP.EQ.6HX,Y,Z.) PRINT 156
      IF(COMP.EQ.6HX-ONLY) PRINT 157
      CALL CMATPAC(G,MA,1,DLT,1.0E-100)     $      PTOT=0.0
      DO 307 M=1,N             $            EF1=CABS(G(M,MAP1))
      IF(KRON.EQ.1) GO TO 777
      J=M+N                    $            EF2=CABS(G(J,MAP1))
      K=J+N                    $            EF3=CABS(G(K,MAP1))
      PWR=0.5*VOL(M,6)*(EF1*EF1+EF2*EF2+EF3*EF3)
      PTOT=PTOT+PWR*VOL(M,4)
      PRINT 173,M,G(M,MAP1),EF1,G(J,MAP1),EF2,G(K,MAP1),EF3,PWR
      GO TO 307
777   PWR=0.5*VOL(M,6)*(EF1*EF1)
      PTOT=PTOT+PWR*VOL(M,4)
      PRINT 174,M,G(M,MAP1),EF1,PWR
307   CONTINUE
      PRINT 144
      DO 142 I=1,NT
      J=KRON*N+I
      CHARGE=G(J,MAP1)*4.*PI*EPS
      PRINT 141,I,CHARGE
142   CONTINUE
C*********************************************************************
C
C     READ AND WRITE FORMATS.
C
C
C*********************************************************************
700   FORMAT(5F10.4,2I3,2X,A3)
701   FORMAT(1H0,///,30X,*DISTANCE BETWEEN TWO ELECTRODES       =*,
     1F5.2,2X,*CM*,///,30X,*ELECTRODE-BODY GAP                  =*,
     2F6.3,2X,*CM*,///,30X,*APPLIED VOLTAGE                     =*,
     3F5.2,2X,*VOLTS*,///,30X,*UPPER ELECTRODE SIDE LENGTH         =
     4*,2X,F5.2,*CM*,///,30X,*LOWER ELECTRODE SIDE LENGTH         =*,
     52X,F5.2,*CM*,///,30X,*NUMBER OF SUBAREAS ON 1/4 OF THE UPPER ELECT
     6RODE =*,2X,I3,///,30X,*NUMBER OF SUBAREAS ON 1/4 OF THE LOWER ELEC
     7TRODE =*,2X,I3)
100   FORMAT(A6,4X,4A1,2X,F10.0)
101   FORMAT(3(I2,3X))
151   FORMAT(*1*,//,15X,*THE PARAMETERS OF EACH CELL AS READ IN*,
     1       1X,*ARE GIVEN BELOW IN CMS.*,//)
171   FORMAT(*-*,//,7X,*N*,8X,*AMX*,11X,*AMY*,11X,*AMZ*,10X,*DXCM*,
     1       10X,*DYCM*,10X,*DZCM*,//)
104   FORMAT(8F10.3)
153   FORMAT(*1*,//,15X,*X,Y,Z CORROSPOND TO CENTRAL LOCATION*,
     1       1X,*OF EACH CELL IN METERS*,//,7X,*N*,9X,*X*, 13X,*Y*,
     2       13X,*Z*,10X,*VOLUME*,10X,*EPS*,8X,*SIG(MHO/M)*,//)
172   FORMAT(*-*,4X,I3,1X,1P6E14.4)
155   FORMAT(1H1,//,45X,*( INDUCED ELECTRIC FIELDS IN QUADRANT 1 )*,
     1       //,33X,*FREQUENCY = *,F12.6,* MHZ,*,5X,*( NX = *,I2,5X
     2       *NY = *,I2,5X,*NZ = *,I2,* ) *,
     3      //,38X,* FIELD COMPONENTS = *,A6,5X,
     4       *QUADRANTS USED = *,A1,3(1X,A1))
188   FORMAT(1H0,//,55X,*GROUNDED POTENTIAL CASE*)
189   FORMAT(1H0,//,55X,*FLOATING POTENTIAL CASE*)
156  FORMAT(1H0 ,//,4X,*N*,5X ,*EXREAL* ,6X,*EXIMAG*,6X,*EX-ABS*,8X ,
     2*EYREAL*,6X,*EYIMAG* ,6X,*EY-ABS*,8X ,*EZREAL*,6X,*EZIMAG*,6X,
     3*EZ-ABS*,9X,*PWR*)
```

```
  157       FORMAT(1H0,//,38X,*N*,6X,*EXRAL*,6X,*EXIMAG*,6X,*EX-ABS*,6X,
        2   *PWR*,//)
  173      FORMAT(*--*,1X,I3 ,3X,3(E10.4,2X),2X ,3(E10.4 ,2X),2X,3(E10.4,2X)
        2  ,3X,E10.4)
  174       FORMAT(38X,I3,2X,4(E10.4,2X))
  144       FORMAT(1H1,//,20X,*CHARGE DENSITIES ON THE SUBAREAS OF ELECTROD
       1E (COULOMB/SQUARE METER)*,//,40X,*REAL*,10X,*IMAG*//)
  141       FORMAT(1H0,/,31X,I3,3X,E10.4,5X,E10.4)
  999       CONTINUE                 $                 END
```



```
            COMPLEX FUNCTION GMAT(QD)
            REAL MU
            DIMENSION U(3)
            COMPLEX TAUM2,FCTR1,FCTR2,EXPO,FUNC,TOTAL
            COMMON VOL(120,7),X0,Y0,Z0,M2,NERR
            COMMON/FIELD/SIZE(3),I,J,PI,EPS,MU,WVN,OMEG
            COMMON/GMTRF/UO(3),RO
            COMMON/BLKGMT/NDIV,GRID,PART,START1,START2,START3,
        1          ADD1,ADD2,ADD3,DENOM,REX1
            DVM2 = VOL(M2,4)              $     RLEP = VOL(M2,5) - 1.0
            SIG = VOL(M2,6)      $     TAUM2 = CMPLX(SIG, OMEG*EPS*RLEP)      282
            IF( QD.EQ.1H ) GO TO 55       $     CALL RFN(QD)
            IF(NERR.EQ.1) GO TO 55        $     IF(RO.EQ.0.) GO TO 54
            TOTAL = CMPLX(0. ,0.)         $     U1MIN = UO(1) + START1
            U2MIN = UO(2) + START2        $     U3MIN = UO(3) + START3        2
            U(3) = U3MIN                  $     DO 32 IZ = 1,NDIV
            U(1) = U1MIN                  $     DO 31 IX = 1,NDIV
            U(2) = U2MIN                  $     DO 30 IY = 1,NDIV
            R = SQRT( U(1)*U(1) + U(2)*U(2) + U(3)*U(3) )
            ALPHA = WVN * R
            FCTR2 = U(I)*U(J)*CMPLX( 3.0 - ALPHA*ALPHA, 3.0*ALPHA)/R**2
            FCTR1 = CEXP((0.,-1.)*ALPHA)/(ALPHA*ALPHA*ALPHA)
            IF(I.EQ.J) GO TO 52           $     FUNC = FCTR1 * FCTR2
            GO TO 53
  52        FUNC = FCTR1*(FCTR2 + CMPLX(-1. + ALPHA*ALPHA, -ALPHA))
  53        TOTAL = TOTAL + FUNC
  30        U(2) = U(2) + ADD2
  31        U(1) = U(1) + ADD1
  32        U(3) = U(3) + ADD3
            GMAT = (0.,-1.)*REX1*TAUM2*DVM2*TOTAL/DENOM       $  GO TO 99
  54        IF(I.EQ.J) GO TO 56
  55        GMAT= CMPLX(0.,0.)            $     GO TO 99
  56        A = ((3.*DVM2)/(4.*PI))**(1./3.)                                  304
            FCTR1 = (0.,-1.)*2.*OMEG*MU*TAUM2/(3.*WVN*WVN)
            EXPO = CEXP((0.,-1.)*WVN*A)
            FCTR2 = EXPO* CMPLX(1. ,WVN*A) - (1.,0.)
            GMAT = (FCTR1*FCTR2) - (1.,0.) - (TAUM2/((0.,3.)*OMEG*EPS))
  99        CONTINUE              $   RETURN    $  END
```

```
SUBROUTINE RFN         74/175   OPT=1   PMDMP                    FTN 4.8+552        07/06/82 .18.29.33        PAGE      1

               SUBROUTINE RFN(QD)
               COMMON VOL(120,7),XO,YO,ZO,IN,NERR
               COMMON/GMTRF/U(3),R
               IF(QD.EQ.1H1) GO TO 1           $     IF(QD.EQ.1H2) GO TO 2
               IF(QD.EQ.1H3) GO TO 3           $     IF(QD.EQ.1H4) GO TO 4
               GO TO 55
     1         U(1) = XO - VOL(IN,1)           $     U(2) = YO - VOL(IN,2)
               U(3) = ZO - VOL(IN,3)           $     GO TO 50
     2         U(1) = XO - VOL(IN,1)           $     U(2) = YO + VOL(IN,2)
               U(3) = ZO - VOL(IN,3)           $     GO TO 50
     3         U(1) = XO - VOL(IN,1)           $     U(2) = YO + VOL(IN,2)
               U(3) = ZO + VOL(IN,3)           $     GO TO 50
     4         U(1) = XO - VOL(IN,1)           $     U(2) = YO - VOL(IN,2)
               U(3) = ZO + VOL(IN,3)
    50         R=SQRT(U(1)*U(1)+U(2)*U(2)+U(3)*U(3))
               GO TO 99
    55         NERR=1
    99         CONTINUE     $      RETURN      $      END
```

```
SUBROUTINE CMATPAC     74/175   OPT=1   PMDMP                    FTN 4.8+552        07/06/82 .18.29.33        PAGE      1

               SUBROUTINE CMATPAC(A,N,M,DET,EP)

               COMPLEX A,B,DET,CONST,S
               DIMENSION A(120,121)

               DET = CMPLX(1.0 , 0.0)          $     NP1 = N + 1
               NPM = N + M                     $     NM1 = N - 1
     2         DO 4 J = 1,NM1                  $     C = CABS(A(J,J))
               JP1 = J + 1                     $     DO 5 I = JP1,N
               D = CABS(A(I,J))                $     IF( C-D )6,5,5
     6         DET = -DET                      $     DO 7 K = J,NPM
               B = A(I,K)                      $     A(I,K) = A(J,K)
     7         A(J,K) = B                      $     C = D
     5         CONTINUE                        $     IF(CABS(A(J,J))-EP)14,15,15
    15         DO 4 I = JP1,N                  $     CONST = A(I,J)/A(J,J)
               DO 4 K = JP1,NPM
     4         A(I,K) = A(I,K) - CONST*A(J,K)  $  IF(CABS(A(N,N))-EP)14,18,18
    14         DET = CMPLX(0. , 0.)    $  PRINT 30   $  RETURN
    18         CONTINUE                        $     DO 12 I = 1,N
               K = N - I + 1                   $     KP1 = K + 1
               DO 12 L = NP1,NPM               $     S = CMPLX(0. , 0.)
               IF( N - KP1 ) 12,19,19
    19         DO 13 J = KP1,N
    13         S = S + A(K,J) * A(J,L)
    12         A(K,L) = (A(K,L) - S)/A(K,K)
    30         FORMAT(1X,42HTHE DETERMINANT OF THE SYSTEM EQUALS ZERO./
          1           1X,36HTHE PROGRAM CANNOT HANDLE THIS CASE.//)
               RETURN                          $     END
```

```
FUNCTION SS            74/175   OPT=1   PMDMP                    FTN 4.8+552        07/06/82 .18.29.33        PAGE      1

               COMPLEX FUNCTION SS(R)
               COMMON/FIELD/SIZE(3),K1,K2,PI,EPS,MU,WVN,OMEG
               SS=CEXP(CMPLX(0.0,-WVN*R))/R
               RETURN          $         END
```

```
FUNCTION U             74/175   OPT=1   PMDMP                    FTN 4.8+552        07/06/82 .18.29.33        PAGE      1

               COMPLEX FUNCTION U(R)
               COMMON/FIELD/SIZE(3),K1,K2,PI,EPS,MU,WVN,OMEG
               U=(1.0+CMPLX(0.0 ,WVN*R))*CEXP(CMPLX(0.0,-WVN*R))/(R**3)
               RETURN          $         END
```

```
      SUBROUTINE SUM1(Y,X,N1,N2,A,B,M)
      DIMENSION Y(1),X(1)
      K=N1*N2
      DO 10 I=1,K
      K1=I-(I/N1)*N1
      IF(K1.EQ.0) GO TO 11
      X(I+M)=K1*A/N1-A/(2.*N1)
      GO TO 10
   11 X(I+M)=A-A/(2.*N1)
   10 CONTINUE
      S=B/(2.*N2)
      DO 20 I=1,N2
      DO 30 J=1,N1
      K2=(I-1)*N1+J
      Y(K2+M)=S
   30 CONTINUE
      S=S+B/N2
   20 CONTINUE
      RETURN
      END
```

```
DISTANCE BETWEEN TWO ELECTRODES      = 2.50  CM
ELECTRODE-BODY GAP                   =  .250  CM
APPLIED VOLTAGE                      = 2.00  VOLTS
UPPER ELECTRODE SIDE LENGTH          =   3.00CM
LOWER ELECTRODE SIDE LENGTH          =   2.00CM
NUMBER OF SUBAREAS ON 1/4 OF THE UPPER ELECTRODE =    4
NUMBER OF SUBAREAS ON 1/4 OF THE LOWER ELECTRODE =    9
```

THE PARAMETERS OF EACH CELL AS READ IN ARE GIVEN BELOW IN CMS.

N	AMX	AMY	AMZ	DXCM	DYCM	DZCM
1	1.0000E+00	1.0000E+00	1.0000E+00	1.0000E+00	1.0000E+00	1.0000E+00
2	1.0000E+00	2.0000E+00	1.0000E+00	1.0000E+00	1.0000E+00	1.0000E+00
3	1.0000E+00	1.0000E+00	2.0000E+00	1.0000E+00	1.0000E+00	1.0000E+00
4	1.0000E+00	2.0000E+00	2.0000E+00	1.0000E+00	1.0000E+00	1.0000E+00
5	2.0000E+00	1.0000E+00	1.0000E+00	1.0000E+00	1.0000E+00	1.0000E+00
6	2.0000E+00	2.0000E+00	1.0000E+00	1.0000E+00	1.0000E+00	1.0000E+00
7	2.0000E+00	1.0000E+00	2.0000E+00	1.0000E+00	1.0000E+00	1.0000E+00
8	2.0000E+00	2.0000E+00	2.0000E+00	1.0000E+00	1.0000E+00	1.0000E+00

X,Y,Z CORROSPOND TO CENTRAL LOCATION OF EACH CELL IN METERS

N	X	Y	Z	VOLUME	EPS	SIG(MHO/M)
1	5.0000E-03	5.0000E-03	5.0000E-03	1.0000E-06	8.0000E+01	5.0000E-01
2	5.0000E-03	1.5000E-02	5.0000E-03	1.0000E-06	8.0000E+01	5.0000E-01
3	5.0000E-03	5.0000E-03	1.5000E-02	1.0000E-06	8.0000E+01	5.0000E-01
4	5.0000E-03	1.5000E-02	1.5000E-02	1.0000E-06	8.0000E+01	5.0000E-01
5	1.5000E-02	5.0000E-03	5.0000E-03	1.0000E-06	8.0000E+01	5.0000E-01
6	1.5000E-02	1.5000E-02	5.0000E-03	1.0000E-06	8.0000E+01	5.0000E-01
7	1.5000E-02	5.0000E-03	1.5000E-02	1.0000E-06	8.0000E+01	5.0000E-01
8	1.5000E-02	1.5000E-02	1.5000E-02	1.0000E-06	8.0000E+01	5.0000E-01

(INDUCED ELECTRIC FIELDS IN QUADRANT 1)

FREQUENCY = 15.000000 MHZ. (NX = 2 NY = 2 NZ = 2)

FIELD COMPONENTS = X,Y,Z. QUADRANTS USED = 1 2 3 4

GROUNDED POTENTIAL CASE

N	EXREAL	EXIMAG	EX-ABS	EYREAL	EYIMAG	EY-ABS	EZREAL	EZIMAG	EZ-ABS	PWR
1	-.9330E-01	-.6291E+00	.6360E+00	.7867E-02	.5232E-01	.5291E-01	.7867E-02	.5232E-01	.5291E-01	.1025E+00
2	-.2321E-01	-.1711E+00	.1726E+00	.8556E-02	.5642E-01	.5707E-01	.3316E-02	.2320E-01	.2343E-01	.8402E-02
3	-.2321E-01	-.1711E+00	.1726E+00	.3316E-02	.2320E-01	.2343E-01	.8556E-02	.5642E-01	.5707E-01	.8402E-02
4	-.1209E-01	-.9065E-01	.9145E-01	.4775E-02	.3389E-01	.3422E-01	.4775E-02	.3389E-01	.3422E-01	.2677E-02
5	-.1227E+00	-.8462E+00	.8551E+00	.6601E-02	.5476E-01	.5516E-01	.6601E-02	.5476E-01	.5516E-01	.1943E+00
6	-.1947E-01	-.1455E+00	.1468E+00	.1139E-01	.9274E-01	.9344E-01	.3178E-02	.2577E-01	.2597E-01	.7739E-02
7	-.1947E-01	-.1455E+00	.1468E+00	.3178E-02	.2577E-01	.2597E-01	.1139E-01	.9274E-01	.9344E-01	.7739E-02
8	-.6867E-02	-.5249E-01	.5294E-01	.5378E-02	.4348E-01	.4382E-01	.5378E-02	.4348E-01	.4382E-01	.1660E-02

CHARGE DENSITIES ON THE SUBAREAS OF ELECTRODE (COULOMB/SQUARE METER)

	REAL	IMAG
1	-.3096E-08	.4374E-10
2	-.2967E-08	.4124E-10
3	-.1870E-08	.1128E-10
4	-.2967E-08	.4124E-10
5	-.2854E-08	.3912E-10
6	-.1804E-08	.1059E-10
7	-.1870E-08	.1128E-10
8	-.1804E-08	.1059E-10
9	-.1761E-08	.9075E-11
10	.6173E-08	-.4413E-10
11	.8251E-08	-.4321E-10
12	.8251E-08	-.4321E-10
13	.1021E-07	-.4214E-10

PART II

A USER'S GUIDE TO COMPUTER PROGRAM USED TO DETERMINE THE ELECTRIC FIELD INSIDE A BIOLOGICAL BODY INDUCED BY A CURRENT DISK APPLICATOR

Part II of Chapter VI describes the computer program used for calculating the electric field inside a biological body, maintained by a current disk placed on the surface of the body for the purpose of local heating. This program is a modified version of the computer program developed by Lee [18].

6.3 Formulation of the problem

The geometry of problem is shown in Figure 6.2 where a current disk of radius a is placed on the surface of a rotationally symmetric biological body. In order to calculate the induced electric field inside the body, the body is divided into a number of rings. Similary the area of the current disk is divided into a number of surface rings. The induced electric field at the center of each body ring can be obtained from the following equation which was derived in Chapter IV.

$$\begin{array}{cc} & N \\ N & \left[\begin{array}{ccc} & & \\ & M & \\ & & \end{array} \right] \end{array} \begin{bmatrix} E_1 \\ E_2 \\ \cdot \\ \cdot \\ E_N \end{bmatrix} = \begin{bmatrix} E_1^i \\ \cdot \\ \cdot \\ \cdot \\ E_N^i \end{bmatrix}$$

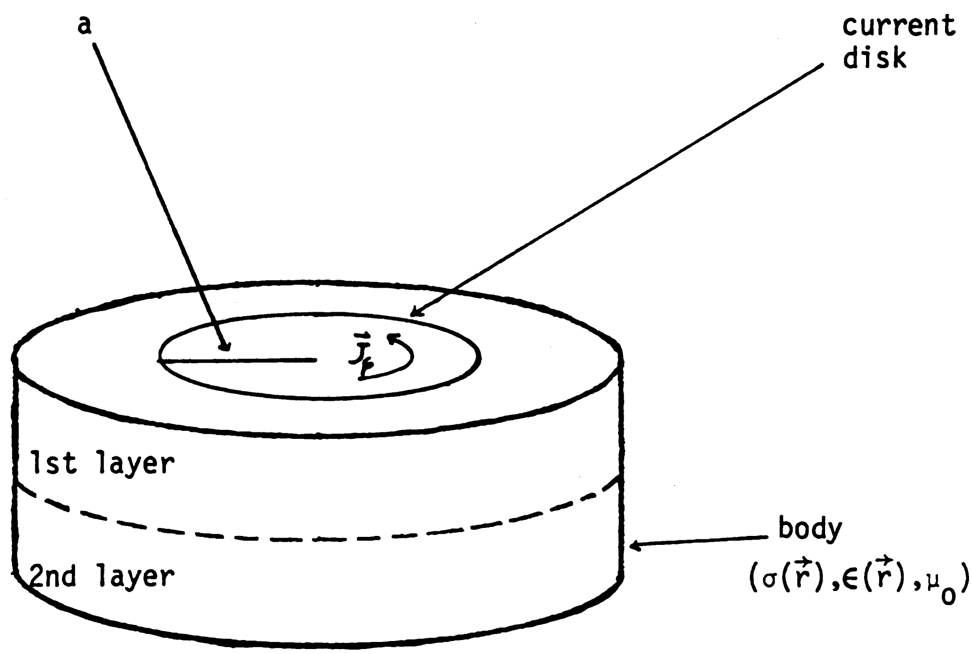

Figure 6.2. A circular current disk is placed on a body for the purpose of local heating.

where N is the nubmer of body rings, and

$$\begin{bmatrix} E_1^i \\ \cdot \\ \cdot \\ \cdot \\ \cdot \\ \cdot \\ \cdot \\ E_N^i \end{bmatrix} = \overset{N'}{\begin{bmatrix} \\ \\ & P & \\ \\ \\ \end{bmatrix}} \begin{bmatrix} K_1 \\ \cdot \\ \cdot \\ \cdot \\ K_N' \end{bmatrix}$$

with N' being the number of surface rings on the current disk. The elements of M and P matrices were defined in Chapter IV.

6.4 Description of the Computer Program.

The program "EDDY" uses the following complex functions and subroutines.

"LEEMAT" - Calculates the elements of [M] matrix

"HMAT" - Calculates the elements of [P] matrix

"FMMC" "FMMS" "FMNC" "FMNS" "F1" "F2" - are functions which determine the integrands of integrals H_{mn}, H_{mm}, $A_{m\nu}$.

"DCADRE" - is a subroutine for numerical integration called from the computer library.

"CMATP" - subroutine which solves linear algebric equations by using Gauss - Seidel method.

6.5 Structure of the input data files.

The structure of the data files and relating formats is presented in Table 6.2, and the informations on each data file are explained here.

<u>First data file</u> - contains one card with the following informations.

"N"- defines the total number of body rings.

"NPLAT"- specifies the number of rings on the surface of current disk.

"DIA" - the diameter of the disk in meter.

"FREINM"- specifies the operating frequency in MHz.

<u>Second data files</u> - reads the density of the currents on different rings on the disk.

<u>Third data file</u> - contains only one card which specifies the following variables.

"NPAR" - for the integrals H_{mm}, H_{mn}, $A_{m\nu}$, the integration interval 0^o and 180^o will be divided into "NPAR" subinterval in order to save the computational cost.

"AERR" - desired minimum absolute error for the numerical integration.

"RERR" - desired munimum relative error for the numerical integration.

<u>Fourth data file</u> - contains N cards each with the following information.

"XEND" "ZEND" correspond to the maximum boundaries (in cm) of a ring corss - section in the X- and Z-direction with reference to the origin.

"XAA" "ZBB" - are the codes for the dimensions of the ring cross-section in X- and Z- direction (in cm).

"REP" "SIG" - define the dielectric constant and conductivity (S/m) of each circular ring.

This concludes the specifications of theinput data for the program. A numerical example is presented in the next section.

Table 6.2. The symbolic names for the input variables and format specifications used in program "EDDY"/

File No.	Card No.	Column	Variable Name	Format
1	1	1-3	N	I3
		4-6	NPLAT	I3
		11-20	DIA	F10.4
		21-30	FREINM	F10.4
2	1		CD(I)	
			I = 1, NPLAT	NPLAT (F10.4)
3	1	1-5	NPAR	I5
		6-15	AERR	F10.5
		16-25	RERR	F10.5
4	1-N	1-12	XEND	F12.5
		13-24	ZEND	F12.5
		25-36	XAA	F12.5
		37-48	ZBB	F12.5
		49-50	REP	F12.5
		51-63	SIG	F13.6

6.6 An example to use the program

As an example, we consider a body of 2.cm height and 4 cm radius. The body is divided into two layers each containing 4 rings. The current disk is considered to be of 5. cm diameter and is divided into 5 concentric rings each having a current density of 200 Amp/m.
The sequential order of the input data files is as follows

File No.	Information on the file					
1	008005			0.05	100.0	
2	200.0		200.0	200.0	200.0	200.0
3	18.		0.0		0.01	
4.1	1.0	1.0	1.0	1.0	80.0	0.5
4.2	2.0	1.0	1.0	1.0	80.0	0.5
4.3	3.0	1.0	1.0	1.0	80.0	0.5
4.4	4.0	1.0	1.0	1.0	80.0	0.5
4.5	1.0	2.0	1.0	1.0	80.0	0.5
4.6	2.0	2.0	1.0	1.0	80.0	0.5
4.7	3.0	2.0	1.0	1.0	80.0	0.5
4.8	4.0	2.0	1.0	1.0	80.0	0.5

The following pages are devoted to numerical results and computer program listing.

```
*************************************************************************
C     THIS PROGRAM CALCULATES THE ELECTRIC FIELD INSIDE A ROTATIONALLY
C     SYMMETRIC BIOLOGICAL BODY INDUCED B Y A CURRENT DISK APPLICATOR.
*************************************************************************
      PROGRAM EDDY(INPUT,OUTPUT)
      DIMENSION XEND(90),ZEND(90),XAA(90),ZBB(90),B(90),PHA(90)
      COMPLEX LEE(90,91),EINC(90),DET,EIND(90)
      COMPLEX HFS(18,10)
      DIMENSION CD(10)
      REAL KO,MUO,MAG(90)
      COMMON/CONS1/FREQ,MUO,EPO,PI,OMEG,KO
      COMMON/PARA1/XCEN(90),ZCEN(90),A(90)
      COMMON/PARA2/SIG(90),REP(90)
      COMMON/PARA6/AREA(90)
      PI=3.1415926535
      MUO=4.0*PI*1.0E-07
      EPO=8.854E-12
      READ 1,N,NPLAT,DIA,FREINM
      READ 201,(CD(I),I=1,NPLAT)
      READ 2, NPAR,AERR,RERR
      PRINT 13
      DO 200 I=1,NPLAT
      RCEN=I*DIA/(2.*NPLAT)-DIA/(4.*NPLAT)
      R=RCEN*100.
      PRINT 14,I,R,CD(I)
  200 CONTINUE
      NP1=N+1
      FREQ=FREINM*1.0E+06
      OMEG=2.0*PI*FREQ
      RTMUEP=SQRT(MUO*EPO)
      KO=OMEG*RTMUEP
      DO 100 I=1,N
      READ 3, XEND(I),ZEND(I),XAA(I),ZBB(I),REP(I),SIG(I)
      XEND(I)=XEND(I)/100.
      ZEND(I)=ZEND(I)/100.
      XAA(I)=XAA(I)/100.
      ZBB(I)=ZBB(I)/100.
      AREA(I)=XAA(I)*ZBB(I)
      A(I)=XAA(I)/2.
      B(I)=ZBB(I)/2.
      XCEN(I)=XEND(I)-A(I)
      ZCEN(I)=ZEND(I)-B(I)
  100 CONTINUE
      PRINT 4
      DO 101 I=1,N
      PRINT 5, I,XEND(I),ZEND(I),XAA(I),ZBB(I),AREA(I)
  101 CONTINUE
      PRINT 6
      DO 102 I=1,N
      PRINT 7, I,XCEN(I),ZCEN(I),REP(I),SIG(I)
  102 CONTINUE
      CALL LEEMAT(N,NPAR,AERR,RERR,LEE)
      CALL HMAT(N,NPLAT,NPAR,DIA,AERR,RERR,HFS)
      PRINT 8
      DO 221 I=1,N
      EINC(I)=CMPLX(0.0,0.0)
      DO 222 J=1,NPLAT
      EINC(I)=EINC(I)+HFS(I,J)*CD(J)*DIA/(2.*NPLAT)
  222 CONTINUE
      LEE(I,NP1)=EINC(I)
      PRINT 9, I,EINC(I)
  221 CONTINUE
      CALL CMATP(LEE,N,1,DET,1.0E-50)
      PRINT 10, FREINM,NPAR,AERR,RERR
      DO 104 I=1,N
      EIND(I)=LEE(I,NP1)
      PRINT 11, I,LEE(I,NP1)
  104 CONTINUE
      CALL MAGPHA(EIND,N,MAG,PHA)
      PRINT 12
      DO 105 I=1,N
      PRINT 11, I,MAG(I),PHA(I)
  105 CONTINUE
  201 FORMAT(10F10.4)
    1 FORMAT(2I3,4X,2F10.4)
    2 FORMAT(I5,2F10.5)
    3 FORMAT(5F12.5,E13.6)
```

```
PROGRAM EDDY        74/175   OPT=1   PMUMP                    FTN 4.8+552        07/08/82 .17.16.06        PAGE     2

    4 FORMAT("1",10X,"THE EXTEND DIMENSION,AS WELL AS CRO-SEC AREA OF EA
     2CH RING ARE GIVEN BELOW IN METERS"/"-",10X,"N",7X,"XEND",11X,
     3"ZEND",7X,"X-DIMENSION",4X,"Z-DIMENSION",4X,"CRO-SEC AREA")
    5 FORMAT(1H0,8X,I3,5(2X,F13.6))
    6 FORMAT("1",10X,"THE CENTRAL POINT LOCATION AS WELL AS ELECTRICAL P
     2ROPERTIES OF EACH RING ARE GIVEN BELOW"/"-",10X,"N",2X,"XCEN( METE
     3RS)",2X,"ZCEN (METERS)",2X,"DIELEC.CONST.",2X,"CONDUC.(MHO/M)")
    7 FORMAT("0",9X,I3,4(2X,E13.6))
    8 FORMAT("1",10X,"THE IMPRESS ELECTRIC FIELD DUE TO INCIDENT MAGNETI
     2C FIELD (WITH UNIT INCIDENT ELECTRIC FIELD) IS AS FOLLOW"/"-",10X,
     3"N",10X,"IMPRESS ELECTRIC FIELD (VOLTS/METER)"/"-",24X,"REAL",22X,
     4"IMAG")
    9 FORMAT("0",8X,I3,13X,E13.6,4X,E13.6)
   10 FORMAT("1","THE INDUCED ELECTRIC FIELD IS IN AZIMUTHAL DIRECTION,
     2THE ESTIMATED VALUES AT CENTRAL OF EACH SUBAREA ARE GIVEN BELOW"/
     3"-","THE FREQUENCY BEING USED IS",F10.5,"MHZ,ZERO TO PI BEING DIVI
     4DED INTO",I5,"SUBINTERVALS DURING NUMERICAL INTEGRATIONS"/"-",10X,
     5"THE INTEGRATIONS INVOLVED RETAIN",F10.5,"ABSOLUTE ERROR",2X,
     6"AND/OR",F10.5,"RELATIVE ERROR"/"-",10X,"N",10X,"EINDUCED-REAL(VOL
     7TS/METER)",10X,"EINDUCED-IMAG(VOLTS/METER)")
   11 FORMAT("0",8X,I3,16X,E13.6,23X,E13.6)
   12 FORMAT(1H1,20X,*THE MAGNITUDES AND PHASES OF INDUCED E FIELDS ARE
     1GIVEN BELOW*,//,11X,*N*,10X,*EINDUCED-MAGN(VOLTS/METER)*,10X,
     2*(INDUCED-PHASE(IN DEGREES)*,/,)
13    FORMAT(1H0,///,30X,*AVERAGE RADIUS OF SURFACE RINGS ON THE DISK AN
     2D CURRENT DENSITY ON EACH RING*,///,42X,*N*,10X,*R(CM)*,4X,
     2*CURRENT DENSITY(AMP/METER)*,///,)
14    FORMAT(1H0,40X,I3,4X,F10.3,10X,F8.2)
      STOP
      END
```

```
SUBROUTINE HMAT     74/175   OPT=1   PMUMP                    FTN 4.8+552        07/08/82 .17.16.06        PAGE     1

C***** SUBROUTINE HMAT ***********************************************************
       SUBROUTINE HMAT(N,NPLAT,NPAR ,DIA ,AERR ,RERR ,HES )
       COMMON/CONS1/FREQ,MUO,EPO,PI,OMEG,KO
       COMPLEX HES(18,7)
       COMMON/PARA1/X(90),Z(90),A(90)
       COMMON/BLK1/XS,XF,ZF
       EXTERNAL F1,F2
       REAL MUO,KO
       DO 111 I=1,N
       XF=X(I)           $        ZF=Z(I)
       DO 111 J=1,NPLAT
       XS=J*DIA/(2.*NPLAT)-DIA/(4.*NPLAT)
       ALFA=0.0          $           BETA=PI/NPAR
       GAMA=BETA
       HES(I ,J)=CMPLX(0.0 ,0.0)
  15   HES(I,J)=HES(I,J )-CMPLX(0.0,1.0)*OMEG*MUO*XS*(DCADRE(F1,
     2 ALFA,GAMA,AERR,RERR,ERROR ,IER)-CMPLX(0.0,1.0)*DCADRE(F2,ALFA,
     3 GAMA,AERR,RERR,ERROR ,IER))/(2.*PI)
       ALFA=GAMA         $             GAMA=GAMA+BETA
       IF(GAMA.GT.PI) GO TO 111
       GO TO 15
 111   CONTINUE
       RETURN        $        END
```

```
C*****SUBROUTINE LEEMAT*************************************************************
      SUBROUTINE LEEMAT(N,NUM,AERR,RERR,LEE)
      EXTERNAL FMMC,FMMS,FMNC,FMNS
      COMPLEX LEE(90,91),KINTEG(90,90),TAU(90)
      REAL K0,MU0
      COMMON/CONST/FREQ,MU0,EP0,PI,OMEG,K0
      COMMON/PARA1/X(90),Z(90),A(90)
      COMMON/PARA2/SIG(90),EP(90)
      COMMON/PARA3/XM
      COMMON/PARA4/AM
      COMMON/PARA5/XN,ZN,ZM
      COMMON/PARA6/AREA(90)
      NP1=N+1
      DO 10 I=1,N
      DO 10 J=1,NP1
   10 LEE(I,J)=CMPLX(0.0,0.0)
      DELT=PI/NUM
      DO 20 I=1,N
      TAU(I)=SIG(I)+CMPLX(0.0,1.0)*OMEG*(EP(I)*EP0-EP0)
      XM=X(I)
      AM=A(I)
      SUMC=0.0
      SUMS=0.0
      ALPHA=0.0
      BETA=DELT
   15 SUMC=SUMC+DCADRE(FMMC,ALPHA,BETA,AERR,RERR,ERROR,IER)
      SUMS=SUMS+DCADRE(FMMS,ALPHA,BETA,AERR,RERR,ERROR,IER)
      ALPHA=BETA
      BETA=BETA+DELT
      IF(BETA.GT.PI+0.5*DELT) GO TO 20
      GO TO 15
   20 KINTEG(I,I)=(SUMC+CMPLX(0.0,1.0)*SUMS)*2.0*PI/AREA(I)
      DO 30 I=2,N
      IM1=I-1
      XM=X(I)
      ZM=Z(I)
      DO 30 J=1,IM1
      XN=X(J)
      ZN=Z(J)
      SUMC=0.0
      SUMS=0.0
      ALPHA=0.0
      BETA=DELT
   25 SUMC=SUMC+DCADRE(FMNC,ALPHA,BETA,AERR,RERR,ERROR,IER)
      SUMS=SUMS+DCADRE(FMNS,ALPHA,BETA,AERR,RERR,ERROR,IER)
      ALPHA=BETA
      BETA=BETA+DELT
      IF (BETA.GT.PI+0.5*DELT) GO TO 29
      GO TO 25
   29 KINTEG(I,J)=SUMC+CMPLX(0.0,1.0)*SUMS
   30 KINTEG(J,I)=KINTEG(I,J)
      DO 40 I=1,N
      DO 40 J=1,N
      IF (I.EQ.J) GO TO 35
      LEE(I,J)=CMPLX(0.0,1.0)*FREQ*MU0*AREA(J)*X(J)*TAU(J)*KINTEG(I,J)
      GO TO 40
   35 LEE(I,J)=1.0+CMPLX(0.0,1.0)*FREQ*MU0*AREA(J)*X(J)*TAU(J)*KINTEG(I,
     2J)
   40 CONTINUE
      RETURN
      END
```

```
SUBROUTINE CMATP       74/175   OPT=1   PMDMP                    FTN 4.8+552        07/08/82 .17.16.06        PAGE      1

        C*****SUBROUTINE CMATP*****************************************************************
                    SUBROUTINE CMATP(A,N,M,DET,EP)
        C
                    COMPLEX A,B,DET,CONST,S
                  DIMENSION A(90,91)
        C
                    DET = CMPLX(1.0 , 0.0)
                    NP1 = N + 1
                    NPM = N + M
                    NM1 = N - 1
          2         DO 4 J = 1,NM1
                    C = CABS(A(J,J))
                    JP1 = J + 1
                    DO 5 I = JP1,N
                    D = CABS(A(I,J))
                    IF( C-D )6,5,5
          6         DET = -DET
                    DO 7 K = J,NPM
                    B = A(I,K)
                    A(I,K) = A(J,K)
          7         A(J,K) = B
                    C = D
          5         CONTINUE
                    IF(CABS(A(J,J))-EP)14,15,15
         15         DO 4 I = JP1,N
                    CONST = A(I,J)/A(J,J)
                    DO 4 K = JP1,NPM
          4         A(I,K) = A(I,K) - CONST*A(J,K)
                    IF(CABS(A(N,N))-EP)14,18,18
         14         DET = CMPLX(0. , 0.)
                    PRINT 30
                    RETURN
         18         CONTINUE
                    DO 12 I = 1,N
                    K = N - I + 1
                    KP1 = K + 1
                    DO 12 L = NP1,NPM
                    S = CMPLX(0. , 0.)
                    IF( N - KP1 ) 12,19,19
         19         DO 13 J = KP1,N
         13         S = S + A(K,J) * A(J,L)
         12         A(K,L) = (A(K,L) - S)/A(K,K)
         30         FORMAT(1X,42HTHE DETERMINANT OF THE SYSTEM EQUALS ZERO./
               1            1X,36HTHE PROGRAM CANNOT HANDLE THIS CASE.//)
                    RETURN
                    END
```

```
FUNCTION F1            74/175   OPT=1   PMDMP                    FTN 4.8+552        07/08/82 .17.15.06        PAGE      1

        C***** FUNCTION F1 ********************************************************************
                   FUNCTION F1(PHI)
                   COMMON/CONS1/FREQ,MU0,EP0,PI,OMEG,K0
                   COMMON/BLK1/XS,XF,ZF
                   REAL MU0,K0
                   R=SQRT(XS**2+XF**2+ZF**2-2.*XF*XS*COS(PHI))
                   F1=COS(K0*R)*COS(PHI)/R
                   RETURN     *        END
```

```
FUNCTION F2          74/175   OPT=1   PMDMP                 FTN 4.8+552        07/08/82 .17.15.06        PAGE    1

C***** FUNCTION F2 *****************************************************************
             FUNCTION F2(PHI)
             COMMON/CONS1/FREQ,MU0,EP0,PI,OMEG,K0
             COMMON/BLK1/XS,XF,ZF
             REAL MU0,K0
             R=SQRT(XS**2+XF**2+ZF**2-2.*XF*XS*COS(PHI))
             F2=SIN(K0*R)*COS(PHI)/R
             RETURN                END

FUNCTION FMNS        74/175   OPT=1   PMDMP                 FTN 4.8+552        07/08/82 .17.16.06        PAGE    1

C*****FUNCTION FMNS*****************************************************************
           FUNCTION FMNS(T)
           REAL K0,MU0
           COMMON/CONS1/FREQ,MU0,EP0,PI,OMEG,K0
           COMMON/PARA3/XM
           COMMON/PARA5/XN,ZN,ZM
           ROOT=SQRT(XM*XM+XN*XN-2.*XM*XN*COS(T)+(ZM-ZN)*(ZM-ZN))
           FMNS=-COS(T)*SIN(K0*ROOT)/ROOT
           RETURN
           END

FUNCTION FMMC        74/175   OPT=1   PMDMP                 FTN 4.8+552        07/08/82 .17.16.06        PAGE    1

C*****FUNCTION FMMC*****************************************************************
           FUNCTION FMMC(T)
           REAL K0,MU0
           COMMON/CONS1/FREQ,MU0,EP0,PI,OMEG,K0
           COMMON/PARA3/XM
           COMMON/PARA4/AM
           ALPHAM=2.0*AM/SQRT(PI)
           F1=2.0*XM*XM*(1.0-COS(T))
           F2=SQRT(F1)
           ROOT=SQRT(F1+ALPHAM*ALPHAM)-F2
           FMMC=COS(T)*COS(K0*F2)*ROOT
           RETURN
           END

FUNCTION FMNC        74/175   OPT=1   PMDMP                 FTN 4.8+552        07/08/82 .17.16.06        PAGE    1

C*****FUNCTION FMNC*****************************************************************
           FUNCTION FMNC(T)
           REAL K0,MU0
           COMMON/CONS1/FREQ,MU0,EP0,PI,OMEG,K0
           COMMON/PARA3/XM
           COMMON/PARA5/XN,ZN,ZM
           ROOT=SQRT(XM*XM+XN*XN-2.*XM*XN*COS(T)+(ZM-ZN)*(ZM-ZN))
           FMNC=COS(T)*COS(K0*ROOT)/ROOT
           RETURN
           END

FUNCTION FMMS        74/175   OPT=1   PMDMP                 FTN 4.8+552        07/08/82 .17.16.06        PAGE    1

C*****FUNCTION FMMS*****************************************************************
           FUNCTION FMMS(T)
           REAL K0,MU0
           COMMON/CONS1/FREQ,MU0,EP0,PI,OMEG,K0
           COMMON/PARA3/XM
           COMMON/PARA4/AM
           ALPHAM=2.0*AM/SQRT(PI)
           F1=2.0*XM*XM*(1.0-COS(T))
           F2=SQRT(F1)
           ROOT=SQRT(F1+ALPHAM*ALPHAM)-F2
           FMMS=-COS(T)*SIN(K0*F2)*ROOT
           RETURN
           END
```

```
C*****SUBROUTINE MAGPHA*************************************************************
      SUBROUTINE MAGPHA(EIND,N,MAG,PHA)
      COMPLEX EIND(90)
      REAL IM(90),MAG(90)
      DIMENSION RE(90),PHA(90)
      DO 10 I=1,N
      MAG(I)=CABS(EIND(I))
      RE(I)=REAL(EIND(I))
      IM(I)=AIMAG(EIND(I))
      PHA(I)=ATAN2(IM(I),RE(I))
      PHA(I)=PHA(I)*57.29577951
   10 CONTINUE
      RETURN
      END
```

AVERAGE RADIUS OF SURFACE RINGS ON THE DISK AND CURRENT DENSITY ON EACH RING

N	R(CM)	CURRENT DENSITY(AMP/METER)
1	.250	200.00
2	.750	200.00
3	1.250	200.00
4	1.750	200.00
5	2.250	200.00

THE EXTEND,DIMENSION,AS WELL AS CRO-SEC AREA OF EACH RING ARE GIVEN BELOW IN METERS

N	XEND	ZEND	X-DIMENSION	Z-DIMENSION	CRO-SEC AREA
1	.010000	.010000	.010000	.010000	.000100
2	.020000	.010000	.010000	.010000	.000100
3	.030000	.010000	.010000	.010000	.000100
4	.040000	.010000	.010000	.010000	.000100
5	.010000	.020000	.010000	.010000	.000100
6	.020000	.020000	.010000	.010000	.000100
7	.030000	.020000	.010000	.010000	.000100
8	.040000	.020000	.010000	.010000	.000100

THE CENTRAL POINT LOCATION AS WELL AS ELECTRICAL PROPERTIES OF EACH RING ARE GIVEN BELOW

N	XCEN(METERS)	ZCEN (METERS)	DIELEC.CONST.	CONDUC.(MHO/M)
1	.500000E-02	.500000E-02	.100000E+03	.500000E+00
2	.150000E-01	.500000E-02	.100000E+03	.500000E+00
3	.250000E-01	.500000E-02	.100000E+03	.500000E+00
4	.350000E-01	.500000E-02	.100000E+03	.500000E+00
5	.500000E-02	.150000E-01	.100000E+03	.500000E+00
6	.150000E-01	.150000E-01	.100000E+03	.500000E+00
7	.250000E-01	.150000E-01	.100000E+03	.500000E+00
8	.350000E-01	.150000E-01	.100000E+03	.500000E+00

THE IMPRESS ELECTRIC FIELD DUE TO INCIDENT MAGNETIC FIELD (WITH UNIT INCIDENT ELECTRIC FIELD) IS AS FOLLOW

N	IMPRESS ELECTRIC FIELD (VOLTS/METER) REAL	IMAG
1	-.312268E-02	-.241543E+03
2	-.936720E-02	-.472353E+03
3	-.156093E-01	-.361658E+03
4	-.218472E-01	-.180906E+03
5	-.312240E-02	-.812584E+02
6	-.936638E-02	-.184114E+03
7	-.156079E-01	-.180707E+03
8	-.218453E-01	-.129951E+03

THE INDUCED ELECTRIC FIELD IS IN AZIMUTHAL DIRECTION, THE ESTIMATED VALUES AT CENTRAL OF EACH SUBAREA ARE GIVEN BELOW

THE FREQUENCY BEING USED IS 100.00000MHZ,ZERO TO PI BEING DIVIDED INTO 18SUBINTERVALS DURING NUMERICAL INTEGRATIONS

THE INTEGRATIONS INVOLVED RETAIN 0.00000ABSOLUTE ERROR AND/OR .01000RELATIVE ERROR

N	EINDUCED-REAL(VOLTS/METER)	EINDUCED-IMAG(VOLTS/METER)
1	-.478527E+01	-.246506E+03
2	-.113365E+02	-.484053E+03
3	-.120886E+02	-.373977E+03
4	-.924112E+01	-.190229E+03
5	-.366765E+01	-.849999E+02
6	-.910857E+01	-.193374E+03
7	-.104169E+02	-.191221E+03
8	-.852015E+01	-.138493E+03

THE MAGNITUDES AND PHASES OF INDUCED E FIELDS ARE GIVEN BELOW

N	EINDUCED-MAGN(VOLTS/METER)	EINDUCED-PHASE(IN DEGREES)
1	.246553E+03	-.911121E+02
2	.484186E+03	-.913416E+02
3	.374172E+03	-.918514E+02
4	.190454E+03	-.927812E+02
5	.850790E+02	-.924707E+02
6	.193588E+03	-.926968E+02
7	.191505E+03	-.931181E+02
8	.138755E+03	-.935204E+02

CHAPTER VII

SUMMARY

A numerical method is developed in Chapter II for determining the electric charge densities on the surfaces of two squares, parallel electrodes of arbitrary dimensions and spacing, energized by a HF voltage. The denisty of electric charge is calculated numerically by the moment-method technique for several cases, and the accurate value for capacitance between two electrodes is evaluated. The induced charge is calculated for both floating and grounded excitations, and significantly different distributions are observed. As expected, the charge densities are nearly uniform near the center of the electrodes with their increase with the well-known singularity near the edges.

Based on the calculated charge density the components of electric field at various points in free space are calculated for a variety of cases. It is noted that for two electrodes of equal size, separated by a distance small compared to the dimensions of the electrodes, the electric field between electrodes is uniform. In the case of two electrodes of different sizes, the electric field is mostly concentrated near the smaller electrode.

In the next two chapters the problem of local heating of a biological body with HF electric and magnetic fields is discussed. This study was motivated by the fact that HF electromagnetic radiation has been utilized to heat tumor-bearing biological bodies for the purpose of hyperthermia cancer therapy.

A pair of energized electrodes can be used to induce heating in biological bodies. This problem is analysed theoretically in Chapter III. Two coupled integral equations for the unknowns total electric field inside body and charge density on the electrodes are established and solved numerically for different cases. The distribution of specific absorption rate (SAR) of energy in the body is calculated for both homogeneous and heterogeneous bodies. From numerical results it is observed that power is absorbed mainly in that part of the body located between electrodes. For a body with an embedded tumor, the magnitude of absorbed power at the location of tumor is a function of tumor conductivity; less conductive tumors absorb more power than those with higher conductivity.

In Chapter IV the shortcoming of a capacitor plate applicator, relating to overheating of the fat layer in biological bodies, is discussed. This difficulty can be eliminated by using a current disk applicator.

The problem of a current disk applicator is analyzed theoretically in Chapter IV. The electric field induced inside a biological body, having rotational symmetry, by a current disk placed on the surface of that body is calculated. Numerical results are presented for several cases.

It is found that the induced electric field is strong near the surface of the body, in the vicinity of current disk, with approximately equal amplitudes in fat and muscle layers near the interface. The intensity of induced electric field decreases rapidly in the direction away from the disk. This suggests that the current disk applicators are more effective on tumors located near the surface of the body. For tumors located deep inside the body capacitor plate applicators are perferable.

It is possible to synthesize the voltage distribution on a capacitor plate applicator and the current distribution on a current disk applicator in order to obtain a localized heating pattern inside a biological body. The theoretical procedures are presented in Chapters III and IV, respectively.

To confirm the accuracy of the theory, a series of experiments was conducted where the electric field induced inside a simulated biological body by different applicators was measured and was compared with the theoretical values. In each case a good agreement between theory and experiment was observed.

BIBLIOGRAPHY

BIBLIOGRAPHY

1. H.D. Suit and M. Schayder "Hyerthermia: Potential as an antitumor agent," Cancer, 34, 1, 122-129, 1974.

2. J. Overgaad, "Combined adriamycin and hyperthermia treatment of a murine mammary carcinoma in vivo ," Cancer Research 36, 3077-3081, 1976.

3. J.E. Robinson, M.J. Wizenberg and W.A. McGready, "Radiation and hyperthermal response of normal tissue in situ," Radiology, 113, 1, 195-198, 1974.

4. H.H. Leveen, S. Wapnick, V. Piccone, G. Falk and N. Ahmed, "Tumor eradication by radiofrequency therapy," JAMA, 230, 29, 2198-2200, May 17, 1976.

5. J.A.G. Holt, "Effects of 434 MHz electromagnetic waves on human cancer," Presented at 1977 International symposium on biological effects of electromagnetic waves, Airlie, Virginia, October 30 - November 4, 1977.

6. P. Antich, N. Tokita, J. Kim and E. Hahn, "Selective heating of cutaneous human tumors," Presented at 1977 International Microwave symposioum, San Diego, California, June 21-23, 1977.

7. W.T. Jaines, R.U. Thomas, K. Noell, L.S. Miller and K.T. Woodward, "Techniques and results of using microwaves and X-rays for the treatment of tumors in man," Presented at 1977 International Symposioum on biological effects of electromagnetic waves, Airlie, Virginia, October 30 - November 4, 1977.

8. J.A. Dickson "Destruction of solid tumors by heating with radiofrequency energy," presented at 1977 International symposioum on biological effects of electromagnetic waves, Airlie, Virginia, October 30 - November 4, 1977.

9. J.B. Marmor, N. Hahn and G.M. Hahn "Tumor cure and cell survival after localized radio-frequency heating" Cancer Research, 37, 879-883, March 1977.

10. R. Baker, V. Smith, L. Kobe, T. Phillips, "A system for developing microwave induced hyperthermia in small animals" Presented at 1977 International Microwave Symposioum, San Diego, California, June 21-23, 1977.

11. A. Cheung, D.McCulloch, J. Robinson and G. Samaras, "Bolusing techniques for batch microwave irradiation of tumors in far field," Presented at 1977 International Microwave Symosioum, San Diego, California, June 21-23, 1977.

12. C.C. Johnson, H. Plenk and C.H. Durney, "A 915 MHz exposure system for hyperthermia treatment of cancer," Presented at 1977 International Symposioum on biological effects of electromagnetic waves, Airlie, Virginia, October 30 - Novermber 4, 1977.

13. S.B. Field and J.W. Hand "The response of pig skin to combined X-irradiation and microwave heating," Presented at 1977 International symposioum on biological effects of electromagnetic waves, Airlie, Virginia, October 30 - November 4, 1977.

14. Harrington, R.F. Field Computation by Moment Methods, Ch. 1, Macmillan, 1968.

15. Van Bladel, J., "Some remarks on Green's dyadic for infinite space," IRE Trans. Antennas Propagat., Vol. AP-9, PP. 563-566 November 1961.

16. K.M. Chen, "Interaction of electromagnetic fields with biological bodies" Research Topics in Electomagnetic Wave Theory, Edited by J.A. Kong, Chapter 13, pp. 290-347, John Wiley and Sons, 1981.

17. R.S. Elliott, W.H. Harrison and F.K. Storm, "Hyperthermia: Electromagnetic Heating of Deep-Seated Tumors," IEEE Transaction on biomedical engineering, Vol. BME-29, No. 1, pp. 61-64 January 1982.

18. J.H. Lee, "Induced electromagnetic fields in conducting bodies by magnetic fields and microwave," Ph.D. Dissertation, Mich. State Univ. East Lansing, MI 1977.

19. K.M. Chen, S. Rukspollmuang, D.P. Nyquist, "Measurment of Induced Electric Fields in a Phantom Model of Man" To appear in Radio Science, 1982.

20. "The Radio Amateurs Handbook" published by the American Radio Relay League, 1981.

21. W.L. Weeks, "Antenna Engineering", pp. 167-179, McGraw-Hall, 1968.

22. E.C. Jordan, "Electromagnetic Waves and Radiating Systems", Ch. 11, Prentice-Hall, Inc. 1950.

23. G.S. Smith "Analysis of Miniture Electric Field Probes with Resistive Transmission Lines", IEEE Transaction on Microwave theory and techniques, Vol. MTT-29, No. 11, pp. 1213-1224, November 1981.